EVALUATION OF THE GEOTHERMAL ENERGY POTENTIAL OF THE OLKARIA FIELD KENYA, BASED ON GEOCHEMICAL DATA - A NUMERICAL MODEL

Submitted by

RUTH NELIMA WAMALWA

I80/96007/2014

DEPARTMENT OF GEOLOGY, SCHOOL OF PHYSICAL SCIENCES

UNIVERSITY OF NAIROBI

A THESIS SUBMITTED IN FULFILMENT OF THE REQUIREMENTS FOR THE DEGREE OF DOCTOR OF PHILOSOPHY IN THE DEPARTMENT OF GEOLOGY (APPLIED GEOCHEMISTRY) OF THE UNIVERSITY OF NAIROBI

DECEMBER, 2017

DECLARATION

I declare that this thesis is my original work and has not been submitted elsewhere for examination, award of a degree or publication. Where other people's work or my own work has been used, this has been properly acknowledged and reference in accordance with the University of Nairobi's requirements.

Signature……..Date…….

Ms. Wamalwa Ruth,

I80/96007/2014

Department of Geology,

School of Physical Sciences,

University of Nairobi.

This thesis has been submitted with our approval as University supervisors

Signature……..Date…….

Prof. Christopher Nyamai,

Department of Geology,

University of Nairobi.

Signature……..Date…….

Dr. Willis Ambusso,

School of Pure and Applied Sciences,

Kenyatta University.

Signature……..Date…….

Dr. Josephat Mulwa,

Department of Geology,

University of Nairobi.

ACKNOWLEDGEMENT

Completion of this work is attributed to support received from various sources which I wish to sincerely thank. First and foremost to my Almighty God for his grace, faithfulness and guidance that enabled me to cope with challenges of academic life.

Sincere gratitude to my supervisors Prof. Nyamai, Dr. Ambusso and Dr. Mulwa for their continuous guidance throughout the research and to the entire University of Nairobi fraternity.

I am greatly indebted to the Kenya Electricity Generating Company LTD (KenGen) for supporting my entire study through finances, lab facilities and permission to use the archived data.

Last but not least my husband Edwin Wabomba, children Larissa and Ivanna, mother Mary Wamalwa, brothers Sam, Godwin, Joel, Philip and Peter, sisters Janepher and Esther for their support for their love, support and encouragement.

ABSTRACT

The Olkaria geothermal field is located in the Kenyan Rift valley, about 120 km from Nairobi. It is surrounded by further geothermal prospects, such as Suswa, Longonot and Eburru. Exploration of the Olkaria geothermal resource started in 1956. Upon realization of resource potential deep drilling commenced in 1973. A feasibility study in 1976 indicated that development of the geothermal resource was feasible and consequently the construction of a three unit power plant of 15 Mwe each at Olkaria 1 build in 1981, 1982 and 1985 respectively (Ouma, 2010). Subsequent years saw numerous expansions with additional power plants being installed in Olkaria. These include a binary plant at Olkaria South West (Olkaria III) in 2000, with a capacity of 110 Megawatts (MW), a condensing plant at Olkaria North East (Olkaria II) in 2003, with a capacity of 105 MW and another binary plant at Olkaria North West (Oserian) in 2004, with a capacity of 2 MW. In the year 2014 additional 280 Mw was commissioned from the Olkaria East and the Olkaria-Domes fields.

Evaluation of the reservoir response to exploitation has always focused on the measured pressure, temperature, total flow from wells and enthalpy. Though geochemical data is also of essence, the data had remained scattered i.e. reporting done on individual wells other than on the field integrating all the wells. This research therefore aimed at numerically modeling the geochemical data of the Olkaria area in order to determine its potential with major focus in the changes in concentration of chemical species of Cl, B, Li, gas and solute geothermometers amid drilling of additional wells which are deeper, reinjection and performance of the existing wells in the Olkaria East and the Olkaria-Domes fields. The Cl, B and Li are used as natural tracers to indicate the source of the fluids whereas the gas and solute geothermometers were used to show the geo-conditions of the reservoir.

The research was a computer-based numerical model which would ultimately be used to predict the reservoir response to different exploitation scenarios. It considered sampling of all the wells in the fields of interest that is 52 wells; 16 in the Olkaria domes and 36 in the EPF that gave a total of 152 samples. The new data was used to verify the methods of sampling and analysis of

the data contained in the database. The representative fluid (both brine and steam) samples from the wells were collected from the weir box and webre separator respectively.

The result of the model estimates reservoir temperatures at about 300^{o}C. Deep wells like OW-5 has highest temperatures of about 320^{o}C due to the deepening effect whereas shallow wells like OW-22 had the lowest temperatures of less than 240^{o}C. OW-5 has the high values of chloride and silica concentrations of 950 ppm and 700 ppm respectively and thus thought to be tapping from deep, high temperature and pressure reservoirs. On production capacities, the result of this study reveals that the potential of the fields is depended on the reinjection strategy to be implemented. Without reinjection, for example, OW-5 will sustain production to 2028, 2025 for OW-19, OW-16 till 2022 and lastly OW-22 in 2019. Minimal reinjection translates to low pressure support for the field leading to the well on the periphery of the field receiving higher amounts of cooler fluids rendering them unproductive.

With regard to well depths, deep drilled wells have the ability to sustain a given production regime for a longer period compared to shallow wells. This arises from the fact that deep wells tap from high temperature and pressure reservoirs of about 300°C and 200 bars which are suitable for geothermal resources. The silica scaling evaluation indicates that the wells have varying minimum separation temperatures. Deeper wells have the highest potential for scaling compared to the shallow ones as they have tapped from high temperature and silica content reservoirs. The gas species are not in equilibrium with the mineral assemblages due to processes of boiling, condensation, and mixing. The East production field had the smallest gas concentrations estimated to be about at 52 bars arising from degassing and near surface boiling

The study recommends independent studies firstly, on the cause of measured high N_2 gas of about 80mmol/kg in the central part of the EPF especially in well OW-5 which is also a deeper well. Secondly, a study be done to evaluate the effects of the accelerated drilling on the physical and chemical characteristics of the wells. Finally, tracer dilution studies to determine the connectivity of the reinjection wells. This will be to ensure targeted reinjection that minimizes early breakthrough in to the producing reservoirs.

TABLE OF CONTENTS

List of tables

List of figures

List of published papers

List of appendices

LIST OF ACRONYMS, SYMBOLS AND ABBREVIATIONS

ARGeo- African Rift Valley Geothermal Development Facility

As- Arsenic

ASL- Above Sea Level

B- Boron

B- Boron

BASICA- Basic programming

$CaCO_3$ –Calcium carbonate

CBE- Charge Balance Error

CH_{4-} Methane

CI- Convergence Index

Cl- Chloride

CO_2- Carbon dioxide

CONVER-Convergence

CYCIT- Cycle Iteration

DELV- type- Deliverability type

DOE- United States Department of Energy

EGS- Enhanced Geothermal System

EI- Equation Index

EOS- Equation of State

EPF- East Production Field

F-Fluoride

GOGA- Greater Olkaria Geothermal Area

GoK- Government of Kenya

H_2-Hydrogen

H_2S- Hydrogen sulfide

IAEA- International Atomic Energy Agency

IFDM- Integral finite difference method

ITCZ- Inter-tropical convergence zone

ITER- Iteration

K- Potassium

KPLC- Kenya Power and Lighting Company

KWS- Kenya Wild Life Service

Li- Lithium

LINEQ-Linear Equation

Mg- Magnesium

MULTI- Multiple

MW- Megawatts

N_{2-} Nitrogen

Na- Sodium

NER-Element Index

NH_3- Ammonia

NH_4OH- Ammonium hydroxide

OD- Olkaria Domes

OW- Olkaria Well

QU-Quotient

RMF- Risk Mitigation Facility

ROGs - Reactive Organic Gas

SiO_2 –Silica

SO_4^{2-}- Sulfate

SSC- Sulfide Stress Cracking

TDS- Total Dissolved Solids

TOGs - Total Organic Gases

TSC- Time step counter

U.S. EPA- United States Environmental Protection Agency

UNDP- United Nations Development Programme

US- United States

WATCH- Water Chemistry programme

WEC- World Energy Council

CHAPTER ONE

1.0 INTRODUCTION

1.1 Background of Study

Exploration of the Olkaria geothermal resource started in 1956. Upon realization of resource potential deep drilling commenced in 1973. A feasibility study in 1976 indicated that development of the geothermal resource was feasible and consequently the construction of a three unit power plant of 15 Mwe each at Olkaria 1 build in 1981, 1982 and 1985 respectively (Ouma, 2010). Subsequent years saw numerous developments of geothermal power plants being installed in Olkaria. These include a binary cycle plant at Olkaria South West (Olkaria III) in 2000, with a capacity of 110 Megawatts (MW), a condensing plant at Olkaria North East (Olkaria II) in 2003, with a capacity of 105 MW, another binary plant at Olkaria North West (Oserian) in 2004, with a capacity of 2 MW, Olkaria 1 additional unit and Olkaria IV plants commissioned in 2014, with a capacity of 140MW each. The power plants are served with steam from a total of 100 wells (Wanyonyi, 2014).

The Olkaria East Production Field (EPF), serving the Olkaria I power plant has been under steam exploitation since 1981. It is supplied with steam from twenty five (25) wells and two other wells, OW-6 and OW-3 are being used for reinjection. Olkaria-Domes geothermal field was yet to be connected at the time of this study. This development translates into large volumes of steam being extracted and hence causing changes and processes that influence fluid composition and thermodynamics in the process. The processes ought to be understood for prudent reservoir management.

1.2 The Proposed Research

1.2.1 Statement of the Research Problem

Geochemical monitoring is important in evaluating a geothermal reservoir response to exploitation (Osato *et al.*, 1998) amid programmes of reinjection, drilling of additional wells that

are deeper, deepening of initially shallow wells and varying levels of performance of existing wells; a typical case of Olkaria geothermal area. Such parameters have a direct influence on the reservoir temperatures, pressure, fluid interactions that account for concentration of elements which, in turn, dictates a field's performance. This is understood through the use of principles of geochemistry, e.g. the presence of dilution as indicated by changes in chloride and boron concentration and geo-indicators which reflect specific environments of equilibrium, e.g. Na and K geothermometers.

Potential of a geothermal field can be reduced with increased chances of scaling and corrosion in the wellbore of production and reinjection wells. Scaling, which plugs wells, is dependent on the SiO_2, $CaCO_3$ and SO_4^{2-} concentrations in the well fluids with varying temperature and pressure conditions. The pH, salts and H_2S concentrations, on the other hand, cause erosion and corrosion problems that mostly lead to collapsing of the wells. Thus, geochemical monitoring and geochemical data simulation is as important as down-hole temperature and pressure logging and down hole data simulation. This has led to recent development multi parallel simulating programs (TOUGHREACT V2.0-OMP) which handles fluid-rock interaction (Tianfu et al. 2014).

Despite the importance of geochemistry in geothermal exploitation, geochemical data in Olkaria Geothermal field remained scattered with reporting done on individual wells rather than the whole field. Integrated geochemical studies would assist in determining the change in the field's behavior due to extraction or drilling of more wells that are likely to reduce pressure and cause excessive boiling. In addition, there exists no documented time analysis to predict future response of the reservoir. There was need to investigate the chances of scaling and corrosion based on the fluid and gas geochemistry considering that the geothermal project is a long-term one with varied attempts to maximize production. Such assessment assists in determining the response of the field to steam extraction for power generation and addition of production wells within Olkaria 1, 2 and Olkaria Domes. This assessment is important bearing in mind that plans of expansion are in the implementation stage, and that the need to bridge the knowledge gap was necessary so as to enable the making of informed decisions that can avert eminent crises.

1.2.2 Scope of Research

The main objective of this research was to determine the future potential of the Olkaria geothermal field based on geochemical data amid reinjection programmes, deepening of existing wells and drilling of deeper wells and varied levels of performance of connected wells. This is in recognition that there is an ambitious plan to increase productivity by four folds so as to secure clean energy for the Kenya's rapidly growing population. This will see the generation capacity, currently at 202MW, increasing to 1054MW by 2018. This expansion is capital intensive; for example the 140MW project in the EPF, now in the implementation stage, has cost the Kenyan taxpayer and the company over 100 M USD. This calls for need for the company to be certain that the field has the capability to sustain the earmarked increase in the production load, foresee challenges of production due to corrosion, dissolution and scaling so as to set up a comprehensive maintenance schedule.

The research considered only two fields; these are the Olkaria East Field (EPF) and the Olkaria-Domes. The geochemical elements were categorized into two i.e. chemically inert tracers that once added to the fluid, tend to remain unchanged like chloride and boron, and chemically reactive tracers i.e. geo-indicators which reflect specific environments of equilibrium (e.g. Na, K as geothermometers) and chances of scaling and corrosion. Reinjection programmes were assessed according to the duration of injection, flow rate in the reinjection wells, chemistry of fluids at reinjection and noted chemical changes of fluids in the wells. The idea on deepening of wells, both existing and new wells, were categorized into two i.e. performance of the wells before and after deepening and the effects of deepening on the performance of other wells in the field as not all the existing wells were deepened. Levels of performance of existing wells were compared with performance of the wells in the field with increased number of new wells and retiring of non-commercial wells.

The realization of this study was vital as it enabled an understanding of the productivity and likely challenges during the exploitation of the Olkaria geothermal field in line with the expansion programmes. The study made use of the geochemical data that has been collected for over a decade but has remained scattered. The results are also to be a start of using numerical

modeling use in geochemical studies in Olkaria geothermal project as it has all along been used in reservoir studies entailing temperature, pressures and enthalpies studies alone.

1.2.3 Objective of the Study

To evaluate the Geothermal Energy potential of the Olkaria geothermal area based on the geochemical data.

1.2.3.1 Specific Objectives of the Study

1. To evaluate the potential of the Olkaria- East and Olkaria-Domes fields based on the changes in concentration of Cl, B, Li, gas and solute geothermometers due to reinjection and performance of the existing wells.
2. To evaluate the changes in concentration of chemical species of Cl, B, Li, gas and solute geothermometers amid drilling of additional wells which are deeper and deepening of the existing shallow wells so as to predict future potential of the Olkaria East and the Olkaria-Domes fields.
3. To evaluate the potential of scaling, dissolution and corrosion in the Olkaria- East and Olkaria-Domes fields based on the variation in concentration of SiO_2, SO_4^{2-}, $CaCO_3$ and pH.

1.2.3.2 Research Questions

The research seeks to answer the following questions:

Based on the geochemical data of the wells within the Olkaria Geothermal Area,

1. Is there a risk of reduced energy potential of the East Production Field (EPF) and the Olkaria- Domes field due to dilution and other geochemical related changes arising from reinjection?

2. Is there a chance of increased energy potential of the EPF and the Olkaria-Domes due to the deepening of wells that has led to striking of deeper reservoirs with different chemical characteristics?

3. Does the performance of existing wells impact on the performance of the newly drilled wells and vice versa especially in regard to the chemistry of the already developed EPF and the yet to be developed Olkaria- Domes?

4. Is there a risk of scaling, dissolution and corrosion in the Olkaria- East and Olkaria-Domes fields based on the variation in concentration of SiO_2, SO_4^{2-}, $CaCO_3$ and pH?

1.2.3.3 Expected Inputs

In order to realize the objectives, the research considered the following inputs:

1. Surface and corresponding subsurface concentration of chemical elements i.e. Na, Ca, Cl, B, Mg, Li, SiO_2, $CaCO_3$, K and gases i.e. H_2S, CH_4 and CO_2.

2. Calculated reservoir temperatures as given by the solute geothermometers calculated from the Na, K ratio and gas geothermometers from the gas concentrations.

3. Calculated concentrations of gases at separation pressures used during power plant operations.

4. Calculated amorphous silica temperatures to determine chances of scaling

1.2.3.4 Justification and Significance of the Research

There is an ambitious plan to expand the Olkaria geothermal project to almost four times its current generation capacity. Though geochemical data had been collected routinely since the inception of the project in early 1980s, the data has remained scattered with many incidences seeing geochemistry of the wells being reported separately. The analysis of integrated data from a whole geothermal field and interpretation is of significance to realize the reservoir response to the over two decade exploitation and challenges of production through the exploitation history and then model for future responses that will consider the earmarked projects. In addition, the success will enable the adoption of numerical modeling technique in geochemistry that can be applied in Olkaria.

1.2.3.5 Expected Outputs

At the end of the study, the research will provide the following:

1. Graph of time dependent simulations and distribution maps of geothermal related chemical concentrations of Cl, gas and solute geothermometers and enthalpies of the wells at different scenarios of operation so as to indicate the performance of the field.
2. Graph of time dependent simulations and distribution maps of the concentrations of SiO_2, SO_4, $CaCO_3$ and pH at different scenarios of operation that will indicate possibilities of corrosion, dissolution and scaling.
3. Graph of time dependent simulations and distribution maps of the calculated separation pressures of gases to determine pressure changes in the reservoir.

1.3 The Study Area

1.3.1 Location and Description of the Study Area

The Greater Olkaria geothermal area (GOGA) is located in the central sector of the Kenya Rift Valley to the south of Lake Naivasha and 120 km northwest of Nairobi (Figure 1.1).

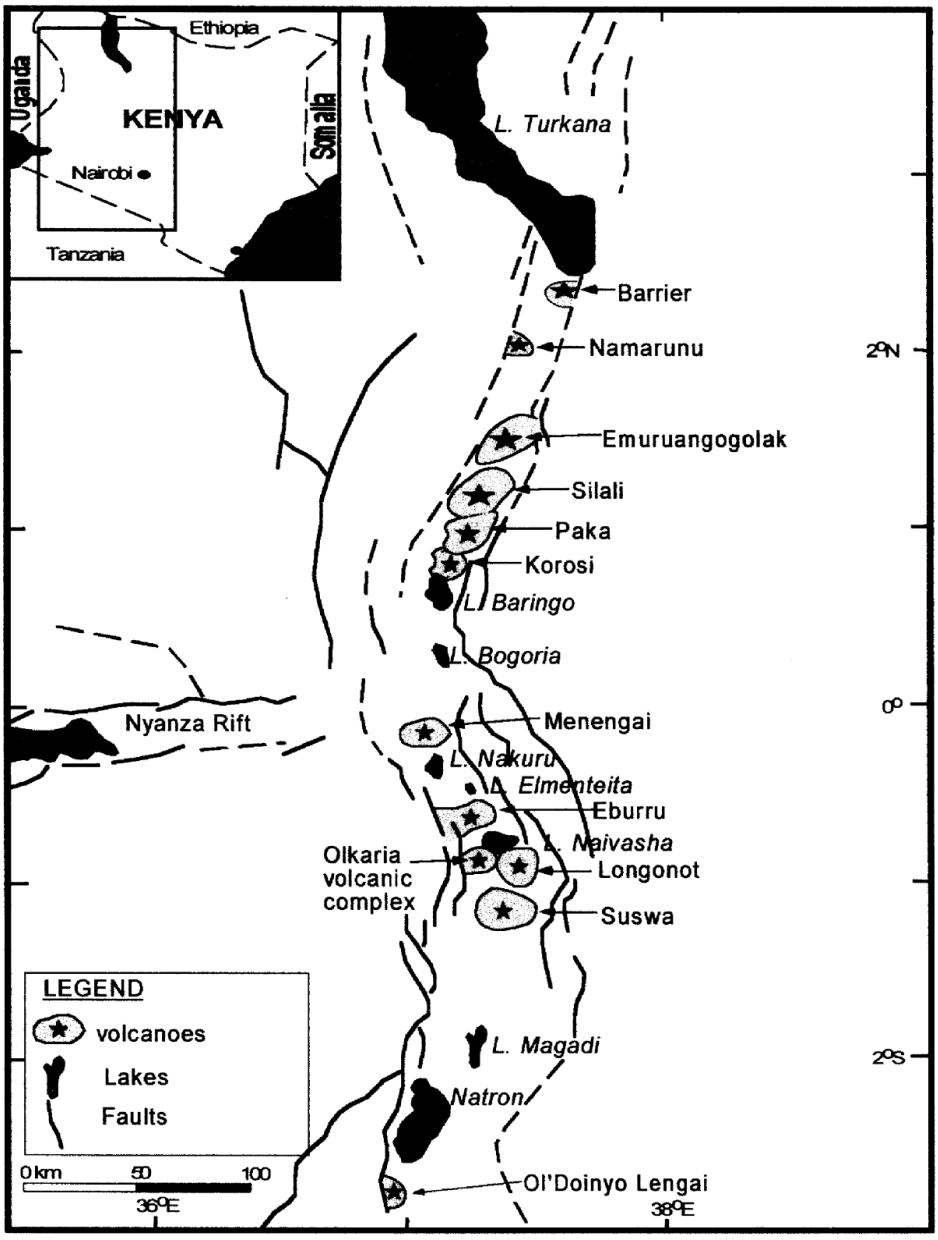

Figure 1.1: Map of the Kenya rift faults showing location of the Olkaria volcanic complex and the major Quaternary central volcanoes (KenGen, 1999).

This geothermal area covers approximately 140 km^2 and it is divided into seven fields, namely: Olkaria East, Olkaria Northeast, Olkaria Central, Olkaria Northwest, Olkaria Southwest, Olkaria Southeast, and Olkaria Domes (Fig. 1.2). The fields are in different stages of exploitation. The completely explored fields are Olkaria East, Olkaria Northeast and Olkaria Southwest while

Olkaria- Domes is the most recent of them all where exploitation for power production has not yet started.

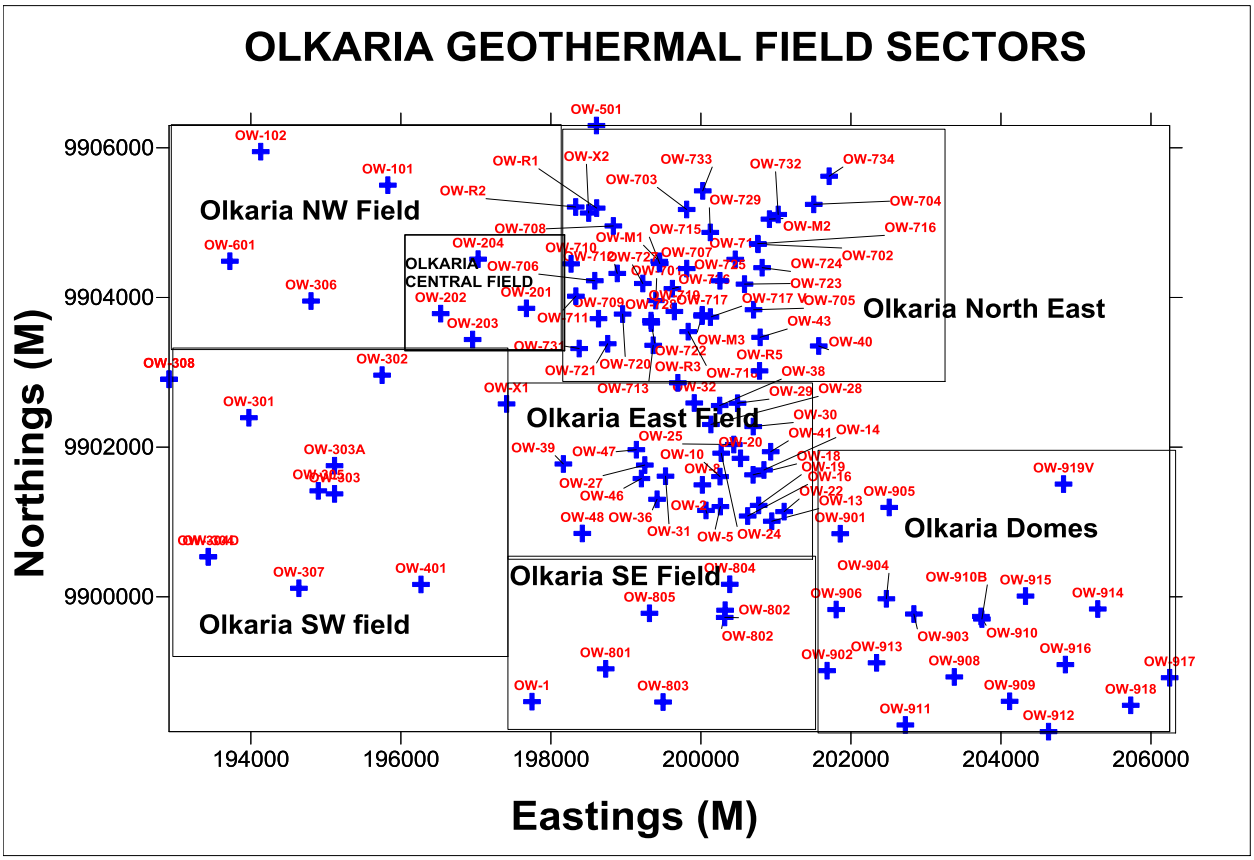

Figure 1.2 Geothermal fields within the Greater Olkaria geothermal area (KenGen, 1999).

1.3.2 Climate of the Olkaria Area and its Environs

Climatic features of the project area and its environs are closely related to altitude changes and variations induced by the local topography (Sombroek *et al.* 1982). Sombroek *et al*., (1982) add that the entire floor of the rift valley experiences higher temperature than the highlands; therefore, Olkaria being in the Rift Valley at approximately 2000m above sea level (asl), has a mean monthly range between 18-19.4^{o}C (Table 1.1). The mean maximum temperatures range between 24.6-28.3°C. With that, July is the coldest month while February is the hottest.

Table1.1: Temperature and precipitation variations in Naivasha in 2012 (Kenya Meteorological Department, 2012)

	Temperature			Precipitation
Months	Normal	Warmest	Coldest	Normal
January	18	25.5	10.5	4
February	18.8	26.7	10.9	4
March	19.4	26.8	12.1	8
April	19.2	25	13.4	15
May	17.8	23.5	12.1	13
June	16.3	22.5	10	5
July	15.6	22	9.2	3
August	15.9	22.7	9.1	4
September	17.3	25	9.7	4
October	18.5	25.7	11.3	7
November	18.4	24	12.7	14
December	18.1	24.4	11.7	9

The area around Olkaria has been classified as Agro-climatic zone V i.e. semi-arid (Sombroek *et al*., 1982). The monthly distribution of rainfall in the basin is governed by the movement of Inter-tropical convergence zone (ITCZ) (Sombroek op. cit). This has resulted in a bimodal pattern of rainfall distribution with long rains in March, April and May while short rains are received in the months of October and November. Rainfall, however, is normally lower, recording an average of 634mm annually. According to Kollikho and Kubo (2001), this reflects the general trend in that the floor of the Rift Valley has lower rainfall than the flanking highlands. Kollikho and Kubo (2001), adds that this area experiences a double rain shadow effects from the West and East flanking escarpments i.e. the Mau and Aberdare Range/ Kinangop respectively besides experiencing evaporation that exceeds precipitation almost throughout the year. It ranges from approximately 1700mm per year at the lake to approximately 1000mm per year on higher grounds. This combined together with the very porous nature of soils accounts for the arid nature of the land.

The relationship between the Olkaria geothermal field and the regional hydrogeology is explained by the isotopic studies done by (Darling et al, 1990). It is considered for some time that the currently-producing Olkaria East well field might be obtaining at least some of its

water from Naivasha. The lake is suspected to have significant subsurface leakage (Sikes, 1935). The leakage to occur in both northerly and southerly directions. According to Darling et al, (1990) the stable isotopic techniques show that lake water appeared to be detectable in wells drilled in the Olkaria and Eburru geothermal fields to the southwest and northwest of the lake, respectively . The reservoir fluid could be explained by a 2:l mixture of lake water with unmodified meteoric recharge from the rift wall area. Darling et al, (1990) further added that well OW-706 seems to be too far to the west side of the lake water plume to show a result significantly different from the main well field, but OW-705 and OW-703 show the anticipated northerly increase.

1.3.3 Geochemistry application in geothermal resource exploitation

Geochemistry, given in terms of concentrations of various chemical constituents in both brine and steam discharged from geothermal wells is vital. Various chemical constituents in both brine and steam discharged from geothermal wells, provide valuable quantitative information that can be used to monitor the reservoir condition and changes in response to steam exploitation (Stapleton, 2002). Ideally, this is done by grouping the elements into two i.e. tracer/conservative elements to trace the origin of the fluids and geo-indicators to reflect the specific environments of equilibrium. The reduction in the concentration of conservative elements will signify dilution occurring in the reservoir leading to cooling. The geo-indicators like Sodium, Silica and Potassium which are chemically reactive reflect specific environments of equilibrium. They are therefore used in the determination of reservoir temperatures. Such studies apart from being used directly in reservoir modeling and simulations also assist with calibration of the other reservoir models as trends in physical and chemical parameters change (Wessel and Smith, 2010).

The Olkaria field has a unique chemistry in the sense that it is low in dissolved solids compared to other drilled high-temperature geothermal fields in the world (Muna, 1982). For example, chloride concentrations in water at the weir box range between 50 and 1100 ppm, being lowest in well OW-34 and highest in well OW-10 (Muna, 1982), with a general trend that water from wells in Olkaria East and Northeast tend to be highest in chloride. In the Olkaria West field the solute concentrations are quite low (100–200 ppm) except in well OW-305, which discharges water similar to that of wells in the Olkaria East and Olkaria Northeast fields (Wambugu, 1995).

Wambugu (1995) notes that well OW-305 is probably tapping the up-flow fluid for Olkaria West field, while other wells are probably discharging fluid which has been diluted by either steam condensate or shallow groundwater.

The alkalinity of the Olkaria wells is moderate (pH 8.1-9.9 as measured at 20^{o}C) and are relatively high in bicarbonate, with concentrations between 90-13000ppm of HCO_3^-. The high bicarbonate is considered to be a consequence of CO_2 supply to the geothermal fluid and subsequent reaction between the carbonic acid and minerals rocks, which act like bases, thus converting some of the carbon dioxide to bicarbonate (Karingithi, 1993, 1996). There is however variations with Olkaria West field having discharge with distinctly high carbon dioxide concentration. According to Karingithi (1996), the source of the CO_2 is considered to be predominantly from the magma heat source of the geothermal system.

On the other hand, temperature reversals are evident in some wells, like OW-201. According to Arnórsson *et al*., (1990), these reversals imply recharge of cold water encroaching the field from the surface or laterally. Such recharge causes steam condensation and reaction of the acid condensate is probably the process which leads to the formation of bicarbonate water rather than CO_2 gas evolution from hot geothermal fluid. It is evident that the geochemistry of the Olkaria area is complex and its use in determining potential of this geothermal field entails studying them corroboratively though some can still be informative when studied independently (Ármannsson and Ólafsson, 2006 and Axelsson, 2008).

It is notable that chemical changes have occurred in the reservoir especially EPF arising from various production activities and development of adjacent fields as noted by various researches e.g. the field optimization report (Mannvit, 2011). Throughout, these changes in various elements had been assessed individually and within a given time and their results presented in plots of chemical constituents with time and on individual wells with no documented integrated modeling of data. This research, therefore, seeks to numerically model the geochemical data of the Olkaria geothermal area linking with various processes of development. Emphasis is on the EPF and Olkaria- Domes fields' area so as to determine their future potential. Reinjection

processes, drilling of new wells, deepening of the wells as well as performance of existing wells have been considered as key influences on the chemistry of the fluids.

1.3.4 Chemistry of the Fluids and the Energy Potential of a Field

The evaluation of the potential of a field considers changes in concentrations of elements through time hence can help determine the presence or absence of dilution or cooling effects in the deep wells (Ármannsson and Ólafsson, 2006). For example high chloride content indicate minimum dilution or recharge from high chloride source whereas low reservoir chloride concentrations indicate dilution of the reservoir fluids by either steam condensate or shallow groundwater. This may act to cool the well hence reducing the productivity. In relating with silica temperatures, D'Amore and Arnórsson (2000) added that wells that have a decline in the chloride content accompanied with a drop in silica temperatures have a high risk of blockage due to silica scaling. According to Opondo (2007), these chemical changes might have led to the blockage of OW-34 after being in production for ten years since 1992.

Corroboratively, chloride, sulfate and carbonate relationship is expressed in a ternary diagram which classifies thermal water based on the relative concentrations of the three major anions Cl^-, SO_4^{2-} and HCO_3^- (Giggenbach, 1991). Giggenbach (1991) adds that the water is classified into mature, peripheral, steam-heated and volcanic waters respectively besides this diagram providing an initial indication of mixing relationships. Chloride-rich waters, the most desired waters in geothermal setting, are associated with high temperatures and characterized by high productive wells. High SO_4^{2-} steam-heated waters are usually encountered over the more elevated parts of a field. High HCO_3^- charged fluids occur at lower temperature, are undesirable in geothermal setting, and are thought to be fluids that have travelled for a distance underground (Truesdell *et al.*, 1987).

On the other hand, the use of the relationship between chloride (Cl), lithium (Li) and boron (B) contents in a geothermal field recognizes that Lithium (Li) is only used as a tracer. This enables it to be used as a reference for evaluating the possible origin of Cl and B (Xiang *et al.*, 2000). The Boron content in thermal fluids reflects maturity of a geothermal system which has stable chemistry (Karingithi, 2000). However due to its volatility it is expelled during the early heating

up stages. In such a case, fluids from older hydrothermal systems can be expected to be depleted in Boron while the reverse holds for younger hydrothermal systems. In reservoir temperature determination, Cl occurs as HCl and B as H_3BO_3 in high temperatures (above 350^oC) domains (Stefánsson and Arnórsson, 2000). Both are volatile and can be mobilized by high-temperature steam. They are, therefore, quite likely to have been introduced with the magmatic vapor invoked above to lead to the formation of deep acid brine responsible for rock dissolution (Karingithi, 2000). Though this can be confusing when estimating the temperatures, it can be a way to estimate the lifespan of a field right from the beginning as nearness to magma source means a stable heat source. At low temperatures (below 200^oC) the acidity of HCl increases rapidly, and is soon converted to the less volatile NaCl through water-rock interaction reactions. B remains in volatile form to be carried in the vapor phase.

1.3.5 Chemistry of Fluids in the Estimation of the Future Challenges of Production in Geothermal Fields

Production in geothermal fields can be hampered by many fluid chemistry dependent factors among them corrosion, scaling (either silica or calcite), dissolution due to SO_4 and low pH.

a) Chemistry of the Geothermal Fluids and Scaling

Geothermal waters are saturated with silica and are frequently close to saturation with calcite, calcium sulfate and calcium fluoride (Tole *et al.*, 1993). According to Stapleton (2002), the rate of scaling is normally aggravated with variation in temperature and pressure that causes in equilibrium. Calcite and silica deposits are the most frequent scale formations with calcite deposition mostly happening at depths of flushing (Moller *et al*., 2004).

b) Silica Scaling

Silica related scaling is one of the most difficult scales occurring in geothermal operation (Opondo, 2008 and Pang and Ármannsson, 2006). Silica is found virtually in all geothermal brine and its concentration is directly proportional to the temperature of the brine. As brine flows through the well to the surface, the brine cools, silica solubility decreases correspondingly and the brine phase becomes over saturated. This is further augmented when pressure drops in the flash vessel during steam flashes. Under these conditions, silica precipitates as either amorphous

silica or it will react with available cations (e.g. Fe, Mg, Ca, Zn) and form co-precipitated silica deposits. Precipitation of amorphous silica, however, mostly occurs in the plant equipment and wells leading to porosity losses in both production and injection well formations. According to Opondo and Ofwona (2003), this form of silica was responsible for the blockage of OW-34 well after being in production for less than ten years.

In high-temperature hydrothermal systems like Olkaria, the formation is frequently in near equilibrium with quartz (Opondo, 2007). Opondo, (2007) further adds that since the solubility of pure silica minerals decrease rapidly with decreasing temperature, large amounts of quartz would be expected to precipitate as the brines in these systems are cooled upon production and energy extraction. However, quartz rarely precipitates because of the slow kinetics involved in this reaction.

In the up flow of the geothermal system e.g. in the NE field of the GOGA, reservoir temperatures are about 250^{o}C. The boiling accompanying these temperatures causes the concentrations of aqueous solutes to increase in proportion to the steam fraction (Núñez *et al.,* 2005). This also causes the pH of the water to increase because of the weak acids dissolved in the water, CO_2 and H_2S, which then become transferred into the steam phase (Núñez *et al.,* 2005). For example, in the Aluto-Langano Geothermal Field, Ethiopia, silica scaling in the new wells drilled has been estimated using a water speciation programme (WATCH). From the results, H_4SiO_4 is not the only aqueous silica species in natural waters. H_4SiO_4 being a weak acid, it dissociates at high pH to yield $H_3SiO_4^-$ (Mekuria et al, 1987). According to Teklemariam (2000), boiling the fluids causes the activity of silica to decrease and finally precipitate as amorphous silica thus explaining why this field has high risk of silica scaling.

CHAPTER TWO

2.0 LITERATURE REVIEW

2.1 Geology and Geological Structures of the Olkaria Geothermal Area

2.1.1 Surface Geology of the Olkaria Geothermal Area

The Olkaria geothermal area is generally covered by young Quaternary ejecta believed to have originated from Longonot and Suswa volcanoes (Macdonald *et al.* 1987). Altered and warm grounds are extensive, with the present geothermal manifestations showing a close association with the dominant N-S structures in Olkaria central and ENE-WSW Olkaria fault zone; a very key influence on recharge of the reservoir. The main rock units are pyroclastics, trachytes, tuffs, rhyolites and basalts (Clarke *et al*., 1990) (Fig. 2.1). The tuffs occur as thin layers intercalating other rock units and are either vitric or lithic tuffs. The former type is glassy and pumiceous with secondary silica infilling the pumiceous vesicles whereas the latter is mainly made up of the lithics of basaltic and trychytic lavas cemented in ashy matrix with calcite deposition. Rhyolites are glassy and have low phenocryst content and show low angle flow banding. Omenda (1998) added that this rock is not so much affected by hydrothermal alteration that may weaken its internal structure. Basalts are porphyritic with plagioclase feldspars and olivines, the groundmass consisting of tiny lathlike plagioclase feldspars. Vesicles are rare with calcite, sometimes epidote and clays infilling the vugs. The textures characterizing these rocks have the quality to hinder free flow within that is the cap rock for the reservoir. The sequences overlying the crystalline basement are about 3.5km thick based on seismic velocities (Simiyu and Keller, 1997).

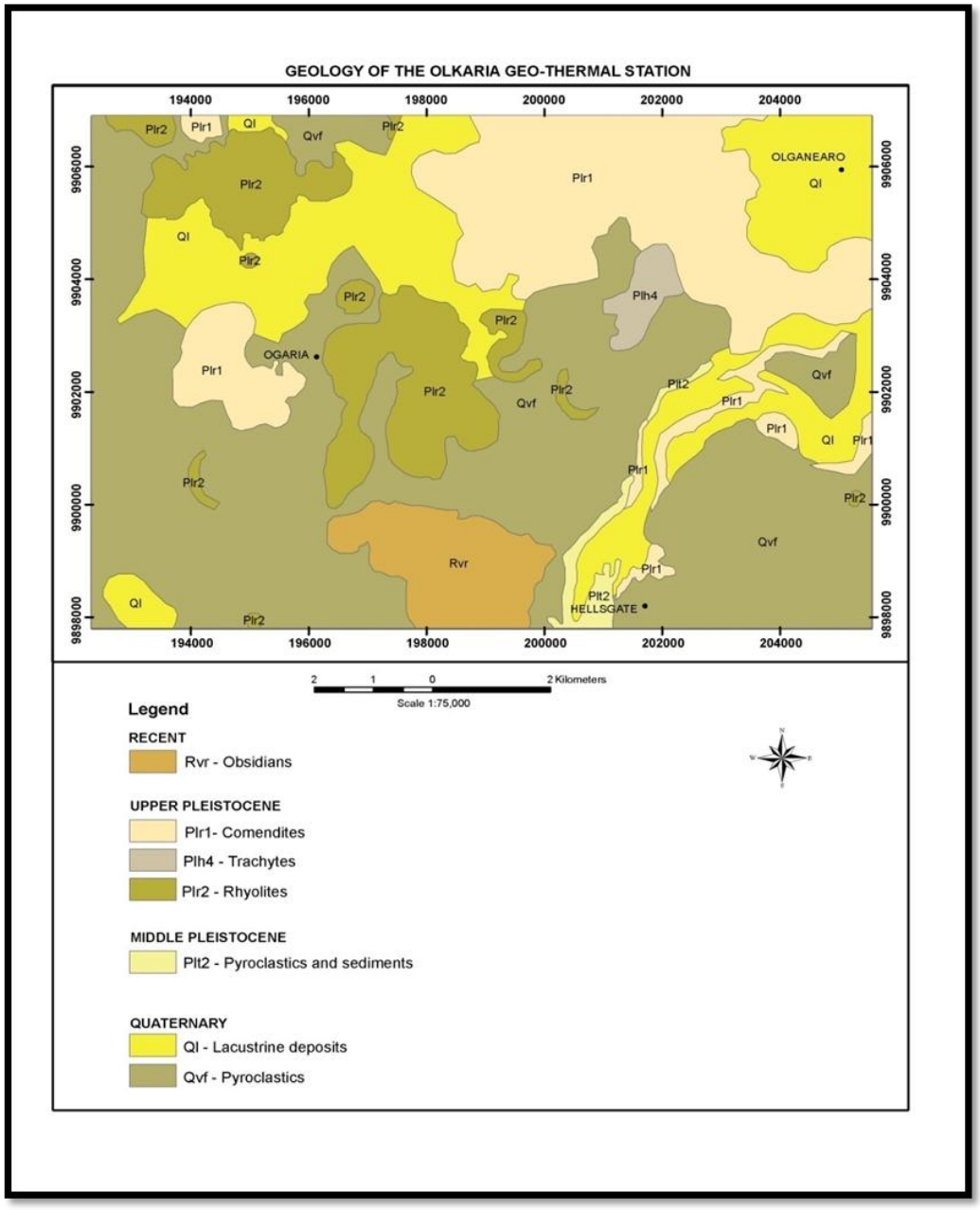

Figure 2.1: The geology of the Olkaria geothermal area (Source: Clarke *et al.*, 1990).

2.1.2 Subsurface Geology of the Olkaria Area

The subsurface geology of the Olkaria geothermal field can be divided into five broad lithostratigraphic groups based on age, tectono-stratigraphy, and lithology (Muchemi, 1992). The formations are The Mau Tuffs, Plateau Trachytes, Olkaria Basalts, Upper Olkaria Volcanics and minor intrusive (Muchemi, 1992; Omenda, 1998). A structural N-S running boundary passes

through the Olkaria Hill that divides the Greater Olkaria area into east and west stratigraphic zones. The geothermal reservoir to the east of the Ol Olbutot Fracture Zone is hosted within the Pleistocene Plateau Trachytes while in the west it is within the Pliocene Mau Tuffs.

The basement rock comprise of amphibolite and schists of the Mozambiquan group (Shackleton, 1986, Mosley, 1993 and Smith and Mosley, 1993). Corelation of data from seismics, gravity and geological indicate that the depth to the basement is about 5-6 km in central Kenya rift (Simiyu *et al*., 1995, Simiyu and Keller, 1997). The same study also detects the presence of a high-density magmatic intrusion into this basement (Baker and Wohlenberg, 1971, Baker *et al*., 1971, and Simiyu, 2010).

The Pre-Mau formation, on the other hand, outcrops on the rift scarps in the parts of the southern Kenya rift (Omenda, 2000). Omenda (2000) added that they comprise of trachytes, basalts and ignimbrites and are of unknown thickness and are directly overlain by the Mau tuffs of pleistocene. Mau tuffs are the oldest rocks in the GOGA. They are common on the west of the Olkaria Hill (Omenda 1994 and 1998) and vary in texture from consolidated to ignimbritic. These formation form the main geothermal reservoir rocks in the Olkaria west field as observed from drill chippings.

Plateau trachytes occurring in wells in the Olkaria area from about 1000 m to more than 2600 m in depth (Ogoso-Odongo, 1986; Omenda, 1994 and 1998). They occur in the area to the east of Olkaria Hill thought to have a graben that existed prior to their eruptions (Omenda, 1994 and 1998). The Olkaria basalts comprise of basalt flows, minor pyroclastics and trachytes (Clarke *et al.,* 1990). They vary in thickness from 100 m to 500 m and act as cap-rock for the Olkaria geothermal system (Haukwa, 1984, Ambusso and Ouma, 1991 and Omenda, 1998). The Upper Olkaria formation consists of comendite lavas and their pyroclastic equivalents (Clarke *et al*., 1990 and Omenda, 1998). These rocks occur from surface to a depth of about 500 m. also in existence are the youngest of the lavas i.e. Ololbutot comendite, which, dates to about 180±50 years (Clarke op cit). Their vents are structurally controlled with most of the centers occurring along N-S faults/fractures and a ring structure.

2.1.3 Hydrothermal Minerals in the Olkaria Geothermal Area

The minerals are as from the study on rocks penetrated by wells drilled in the Olkaria geothermal system. They include kaolinite, biotite, hydrobiotite, vermiculite, chlorite, chlorite-illite, illite, smectite, epidote, calcite, quartz, fluorite, anhydrite, Fe-oxides, prehnite, wairakite, stilbite, pyrite, adularia, albite, sphene, leucoxene, actinolite, garnet and talc (Muchemi, 1992 and Omenda, 1998). Secondary minerals comprise of clay minerals, fluorite, anhydrite**,** calcite, pyrite and iron oxides. Smectite and chlorite prevail in the East above 1000m a.s.l. (Leach and Muchemi, 1987). At depths below 1000m a.s.l., inter-layered chlorite-biotite and biotite dominate. Epidote has been observed to be closely associated with basalts and is abundant in the eastern fields compared to the western fields.

2.1.4 Structures in the Greater Olkaria Volcanic Complex

The major structures in the Greater Olkaria volcanic complex are the ring structure, the Ol'Njorowa gorge, the ENE-WSW Olkaria fault and N-S, NNE-SSW, NW-SE and WNW-ESE trending faults (Fig. 2.2).

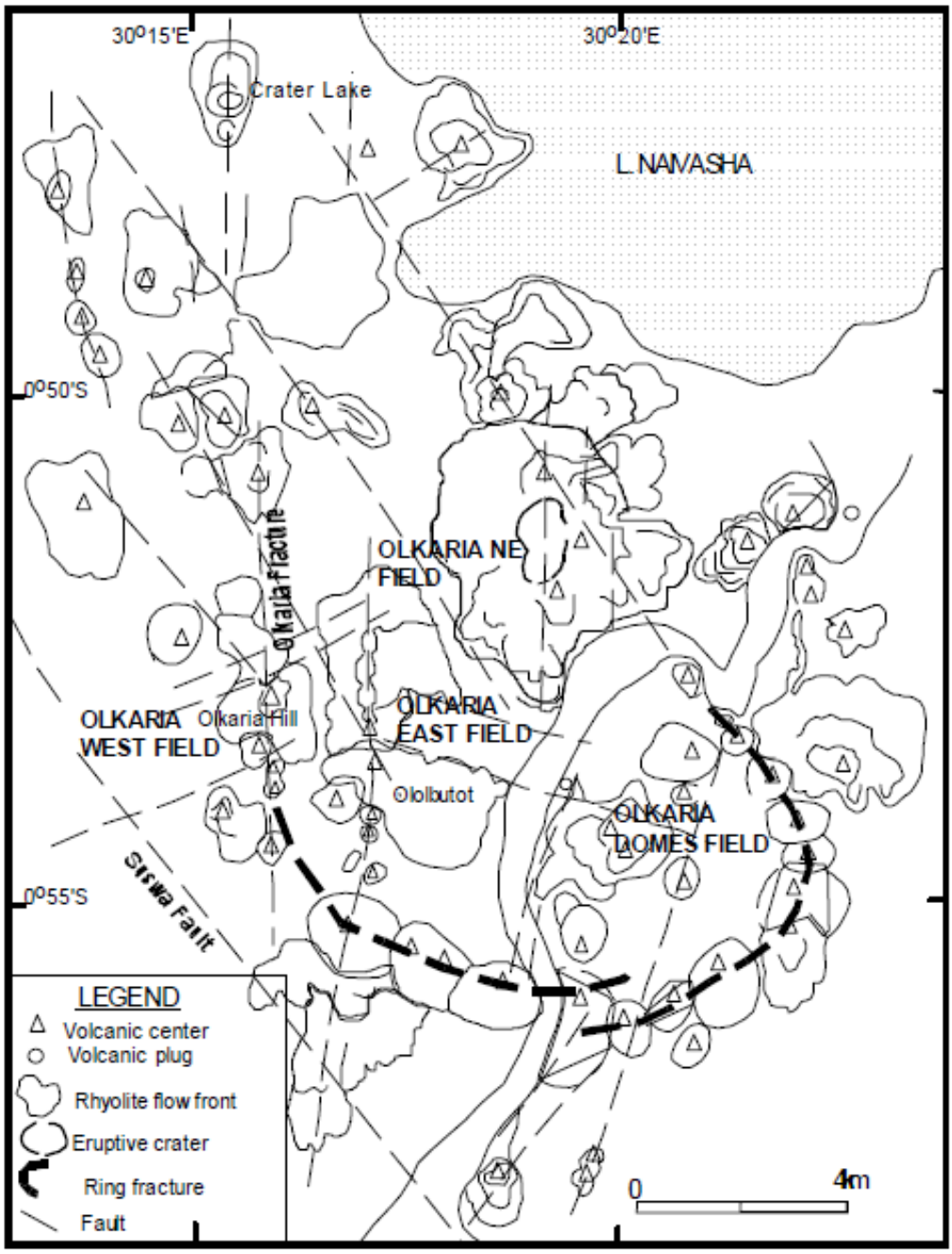

Figure 2.2: Structural map of Greater Olkaria geothermal area (modified from Muchemi (1992) and Mungania (1992)).

The faults are more prominent in the East, Northeast and Olkaria West fields but are scarce in the Olkaria Domes area, possibly due to the thick pyroclastics cover. The NW-SE and WNW-ESE faults are thought to be the oldest and are associated with the development of the rift. The most

prominent of these faults is the Gorge Farm fault, which bounds the geothermal fields in the northeastern part and extends to the Olkaria Domes area. The most recent structures are the N-S and the NNE-SSW faults.

2.2 Use of Geochemistry as a Study tool in geothermal systems

Geochemistry is one of the most useful tools of studying changes in geothermal reservoirs in response to production load. It creates an understanding of the reservoir recharge, pressure drawdown, temperatures and scaling, dissolution or corrosion tendencies caused by chemical changes arising from the impacts of injection, drilling of additional wells, deepening of wells and various levels of performance of existing wells (Capasso *et al*., 2001, Fournier, 1999 and Giggenbach, 1991). In this case, geochemistry makes use of geochemical methods which include classifications of natural water, geothermometry, mixing models, mineral-solution equilibria and interpretation of monitored chemical components (Capasso *et al*., 2001). Prediction on future performance can be achieved through projections of the geochemical data.

Geothermal resources exploitation in Olkaria started in the early 1980s. Geochemical studies have been based on changes in solute concentration, chemical and gas geothermometry which have manifested numerous physical changes. The data in the EPF wells show large data scatters and irregularities (Opondo, 2008). This is partly due to high-enthalpy production from 2-phase conditions and multiple feed zones. Examples of these zones are those lying along or very close to the liquid-vapor saturation curve such that it takes only very small shifts of temperature or pressure to generate or collapse the steam phase (West JEC, 2009). In spite of this, some small trends over extended time are apparent. For example, the pattern of Cl and gases increasing then decreasing over time, in most wells, are evident and can be attributed to boiling in the two-phase zone of the reservoir, which concentrates Cl, causing gases to increase as liquid dominated zones are boiled off. Subsequent decrease in gases then occurs as a portion of re-supply coming to greater depth where gases are lower. It is also observed that there is a rise in alkalinity / Cl ratio in some wells and a decline in some. According to Giggenbach (1991), this shift can be attributed to changes in production zones and infiltration from above the reservoir or from the sides. However, none of these shifts is large enough to merit a conclusion of major changes to

have occurred in the reservoir so far but integrated modeling is needed for conclusions concerning future changes.

2.3 Re-injection Activities in the Olkaria Geothermal Area

The start of re-injection programmes led to significant changes in the geochemistry of the wells. Re-injected hot brines from wells OW-27, 31 and 33 into well OW 3 could have reached the production aquifers of the wells 2, 5, 8 and 32. This has been revealed in the reduction in the solutes concentration in the later compared to periods before reinjection; with OW-32 having a steady decline in enthalpy since 2010 to date. Well OW-5 has since recovered as the monitoring in June 2001 indicated an increase in the chloride concentration. This has been attributed to the deepening of the well such that it started tapping from the chloride rich part of the reservoir (Ofwona, 2010). The cold reinjection in OW-12 affected wells 15, 18 and 19 (Ouma, 2010) in a way that OW-15 gave a lot of water with very low concentration of chemical elements than it was in the period before injection but its steam output was stable. OW-18 declined in steam output but the enthalpy remained high and high concentration of elements possibly due to low water content. OW-19 continued with its initial trend of increment in steam and water production i.e. slightly affected by the reinjection.

2.4 Effects of Drilling Depths on Chemistry in the Olkaria Geothermal Area

The newly drilled and connected well in the EPF i.e. OW-35A, 36A, 37A, 38, 38A, 39A, 41, 42A 44, 44A and 44B depict deep liquid Cl concentrations and high Na/K temperatures. The wells on the margin of the EPF are generally characterized by relatively high Cl concentrations and high Na/K temperatures. This appears inconsistent with the pattern of deep Cl concentrations and Na/K temperatures in the older EPF wells that were highest in center of the field and declined towards the margins (Opondo, 2007). This distribution was interpreted to indicate an up flow of deep, hot and Cl rich water at the center of the EPF. The apparent discrepancy between the older and newer data may be due to the differences in the drilling depths (Ofwona, 2010) i.e. the older wells are generally between 1000m and 2000m deep, whereas the newer wells are generally around 3000 m deep. The high observed Cl concentration and Na/K temperatures observed in the recently drilled wells on the periphery of the EPF does therefore indicate that the

postulated deep, hot and higher geothermal water is accessible by deeper drilling all around and presumably inside the EPF (Ofwona, 2010 and Ouma, 2010).

2.5 Challenges of Production in the Olkaria Geothermal Area

With regard to silica scaling, corrosion and impacts of non-condensable gases, there has been no major challenge in the Olkaria geothermal area. According to Opondo (2008), this is attributed to the fact that the production wells that have existed are relatively shallow with reservoir temperatures ranging from about 240 to about 250°C. As such, boiling of the two phase fluid down to about 160°C is not sufficient enough to produce supersaturated liquid with respect to silica and therefore the low risk of silica scaling. Furthermore, many of the old production wells were sunk into a steam dominated aquifer, with no risk of scaling (Opondo, 2008). The exception is in OW-34 (Opondo, 2007) which had high enthalpy and high chloride content with silica super saturation due to extensive depressurization boiling. These trends however need not to be relied upon as wells drilled in recent years planned for future expansion in the EPF and the Domes areas are deeper and hotter. These high enthalpy wells are of concern, especially with regard to silica scaling, as was indeed the case for well OW-34.

Evaluation of gases concentration in three wells in the Domes field, the East and Northeast production fields (West JEC, 2009) found that their concentrations are on average highest in the Domes well fluids, intermediate in Northeast production field well fluids and lowest in East production field well fluids. This distribution is considered to be the primary cause of a similar zonation of HCO_3/Cl among the well fluids from the three fields (depth also considered). In addition, their enthalpy-Cl study imply a similar deep origin for the fluids of all three well fields, and thus the different gas concentrations in each (along with related anion differences) appear to be the result of separate processes in each area (West JEC, 2009). West JEC (2009) considered three options such that the first one was that the CO_2 gets added at great depth to Northeast production field and Domes waters as a result of volcanic degassing below these areas, with less input of deep CO_2 to the East production field. The second option was that the deepest CO_2 is similar in all three areas, but waters of the East production field lost CO_2 during the onset of deep boiling such that the CO_2 escapes to fumaroles which lie west and south of the East production field and lastly, the cap-rock conditions in the Northeast production field and Domes

are somewhat more restrictive than in the East production field, leading to more entrapment at shallower levels of CO_2 that has been released by deep boiling. Though all the options may hold, it was prudent for an integrated approach in handling the changes between the ions, gases and enthalpies for a concrete conclusion; a fact that was missing in the West JEC findings.

2.6 Application of Geothermometry in Geothermal resources exploitation

Geothermometers are usually applied in geothermal wells to infer reservoir temperatures during exploration and exploitation (Arnórsson, 2000). The most commonly used are silica concentrations, cation ratios (mainly Na/K) and gas ratios.

2.6.1 Silica geothermometers

The silica geothermometers evaluate the reservoir temperatures from the silica concentration of natural water in equilibrium with either quartz or chalcedony (Arnórsson, 2000). The silica geothermometer equations used to calculate the temperature of a reservoir are as follows:

$$-55.3+0.2659S-5.3954*10^{-4}S^2+5.5132*10^{-7}S^3+74.360\log S \quad \text{.....2.1}$$

2.6.2 Cation geothermometers

The use of these geothermometers is based on the partitioning of sodium and potassium between aluminosilicates and aqueous solutions and is strongly temperature dependent described by the reaction below:

$$T^oC = 1319/1.699 + \log (Na/K) - 273.15 \quad \text{.....2.2}$$

2.6.3 Gas geothermometers

These geothermometers are based on gas equilibria and works on an assumption that the gas is in equilibrium with the thermal water and the bedrock. The concentrations and ratios of many gas species are sensitive functions of the reservoir temperature (D'Amore, 1991). They are described by the reactions below:

$$T°_{CO_2}C = -44.1+269.25Q-76.88Q^2+9.52Q^3 \quad \text{.....2.3}$$

$$T°_{H_2S}C=246.7+44.81Q \quad \text{.....2.4}$$

$$T°_{H_2}C=277.2+20.99Q \quad \text{.....2.5}$$

Where T is temperature in degrees celcius and Q is gas concentration in mmol/100kg of steam.

CHAPTER THREE

3.0 GENERIC MODEL

3.1 Simulation Grid System

The grid is meant to represent the geothermal system in three dimensions (Fig.3.1). The study considered an updated conceptual model of the Olkaria Geothermal field after Mannvit (2011) and was constrained on the following basis:

1. The need to define individual grid blocks for known sinks and sources due to production
2. Location of faults or aquifers controlling fluid flow within the geothermal system
3. Lithologic units that show significant differences in hydrologic properties i.e. porosity, permeability or thermal properties
4. The need to control numerical dispersion particularly in the calculated temperature, pressure and chemical elements distribution

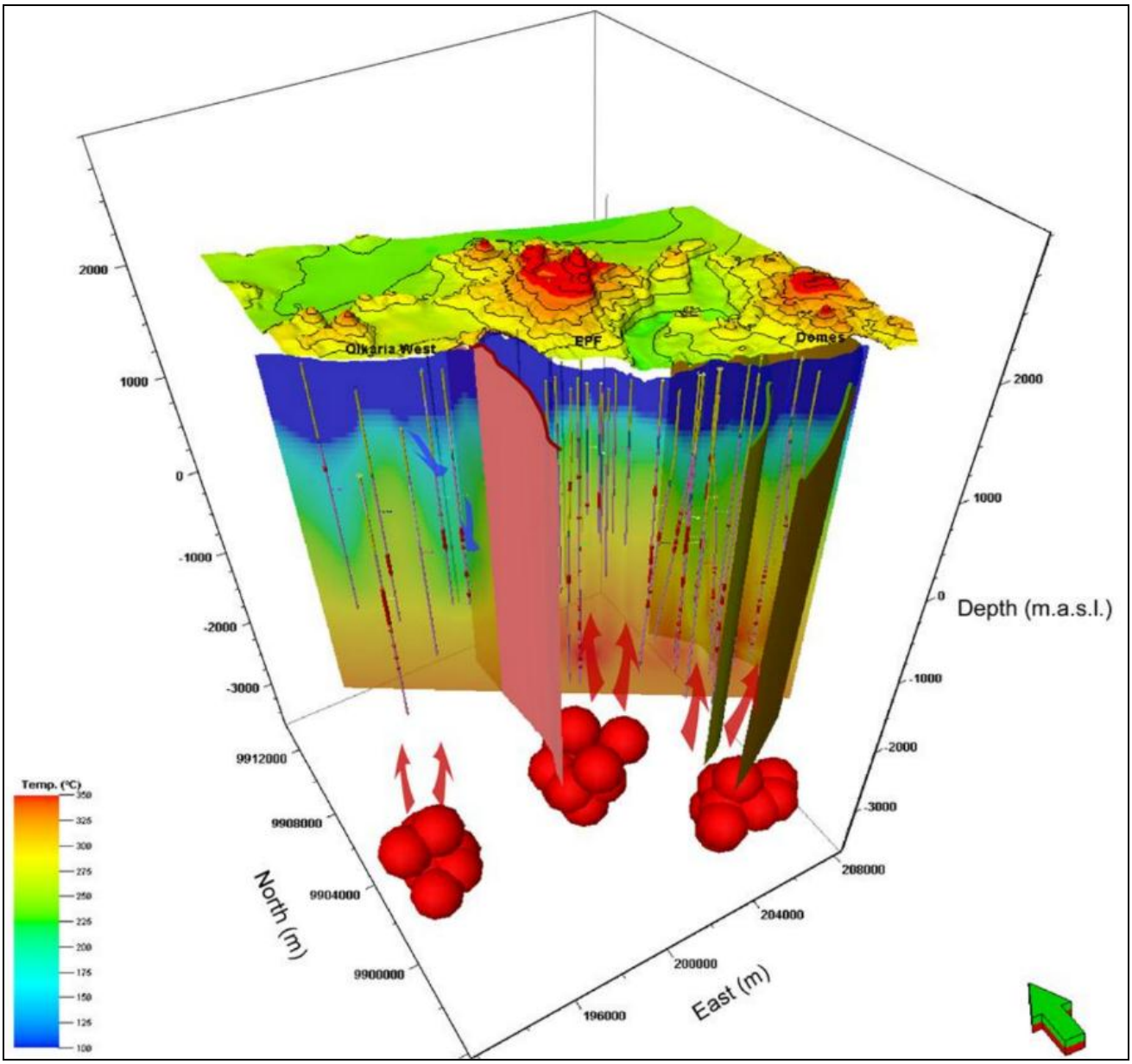

Figure 3.1: Olkaria Geothermal Field Conceptual Model (Source: Mannvit, 2011).

The resultant simulation grid (Fig. 3.2) with Olkaria wells is oriented in a NW-SE direction and includes a total area of 40km^2.

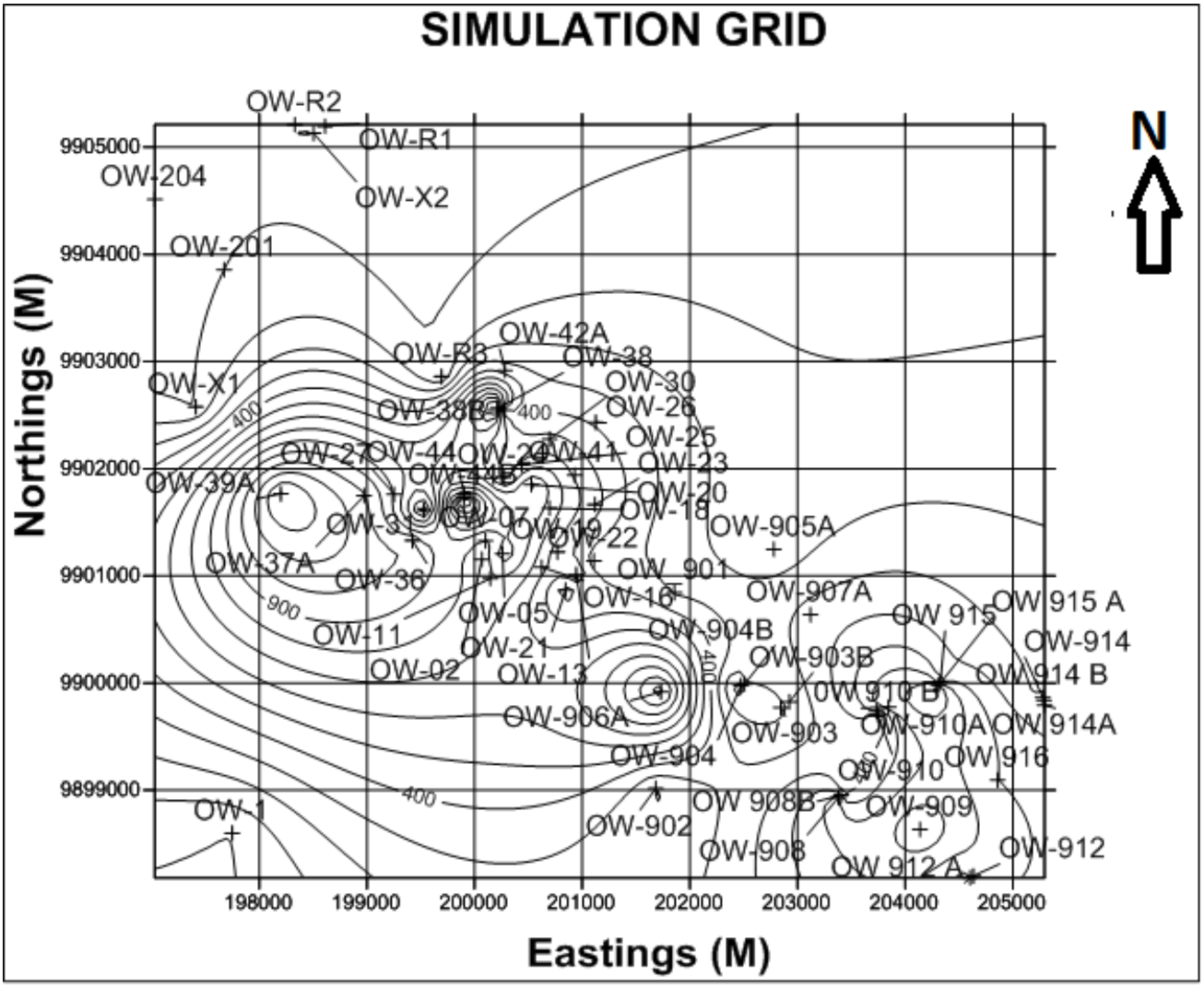

Figure 3.2: Simulation Grid of the Study area; the contours represent elevation.

The grid is rectangular in outline and measures 8km long and 7km wide. The simulation area covers the Olkaria East and Olkaria Domes fields plus an area margin of 1 km, which is required to ensure a reasonable representation of the overall framework of the geothermal system and to reduce the effects of boundary conditions.

In the vertical dimensions, the grid extends from an elevation of +2000m asl (above sea level) to 0m (sea level) for the Olkaria East production field and -1000m bsl for the Olkaria Domes. The uppermost layer is a temperature-pressure boundary with a thickness of 500m hence not included in the simulation. Beneath this, is considered to be the reservoir depth, of about 2500m divided into 5 layers. There are 50 grid blocks in each of the 5 layers, thus giving a total of 250 blocks in the entire model.

The boundary conditions applied to the initial state model are as follows:

1. The bottom layer in the model allows for conductive heat transfer from the rock that underlies the field.
2. The sides of the model are closed to fluid flow except at known recharge and discharge sites.
3. The model contains constant temperature boundaries to represent the regional temperature gradients.

3.1.1 Initial State Model

For each grid block in the model, rock properties were assigned to reflect the different factors that contribute to the heterogeneity of any given geologic unit like hydrothermal alteration and zones of enhanced fracturing. These rock properties, locations of upflow and outflow zones, upflow mass rates and Cl contents were continuously adjusted until a fit to the temperature distribution and pressure in the initial state of the reservoir was achieved.

3.1.1.1 Material Balance Computation

It was given by the following mathematical and numerical formulae respectively (Bodvarsson and Witherspoon, 1989):

$$\delta m/\delta t = \delta/\delta t \int dm = \delta/\delta t \int_v \rho dv \quad \text{.....3.1}$$

where m is the total mass flow,

t is time,

v is volume

$$V\Phi C\{(\underline{P_j^{n+1}-P_j^n})/\Delta t\}=\kappa/\mu*\Sigma\,(p^{n+1}-p_j^{n+1})/\Delta^x_{ki}\,\delta s_{ki}+q_{ki},\ldots\ldots \quad 3.2$$

$$P_j^{n+1} = P_j^n + \{\Delta t/\, V\Phi C\}\,\Sigma\,(p_k^n-p_j)^{\,n}/\,\Delta x_{ki}\delta s+q_{ki}\,, \quad 3.3$$

where P is the reservoir pressures at different times, i.e. P_j^n is the initial pressures, whereas P_j^{n+1} is the subsequent measured pressures,

s is the surface area,

κ/μ is transmissivity,

VΦ is the total mass flow,

C is the concentration of chemical elements in the reservoir fluids.

The permeability was allowed to range from $1.0x10^{-2}$ m^2 to $5.0x10^{-5}$ m^2 to essentially represent horizontal and vertical permeability respectively (Appendix 1). According to Pruess *et al* (1999) the intrinsic permeability of a geothermal field is relatively low except where it is fractured.

3.1.1.2 Chemical Computation

The chemical computation used the Bodvarsson and Witherspoon, (1989) formulas as shown:

$$V\Phi\,(\delta C)/\,\delta t = D\nabla^2 C+q\nabla C+KC, \quad 3.4$$

where VΦ is the total mass flow,

C is the concentration of elements in the reservoir fluids,

D is the diffusion factor,

q is the flow,

K is the advection factor,

t is time,

$$(C_j^{n+1}-C_j^n)/\,\Delta t = D\{(C_j^{n+1}-C_j^n)/V\Phi C\Delta x_{ij}\}\delta s+q_i\{(C_j^{n+1}-C_j^n)/\,V\Phi C\}\,\delta s_i\,, \quad 3.5$$

Where C_j^n is the initial concentration of the elements,

C_j^{n+1} is subsequent concentration of the element,

t is time,

D is the diffusion factor,

VΦ is the total mass flow,

C is the concentration of elements in the reservoir fluids,

δs is the initial surface area,

δs_i is the current surface area,

q_i is the flow.

$$C_j^{n+1} = C_j^n + D\Delta t / V\Phi \{(C_j^{n+1} - C_j^n)/\Delta x_{ij}\}\delta s_i + q_i \{(C_j^{n+1} - C_j^n)/ V\Phi C\} \delta s_{ij}, \quad \text{.....3.6}$$

Where C_j^n is the initial concentration of the elements,

C_j^{n+1} is the subsequent concentration of the element,

t is time,

D is the diffusion factor,

VΦ is the total mass flow,

C is the concentration of elements in the reservoir fluids,

δs is the initial surface area,

δs_i is the current surface area,

q_i is the flow,

where

$$q_i = -\kappa/\mu\ (p_j - p_i), \quad \text{.....3.7}$$

where q is the flow,

κ/μ is transmissivity,

p_i is initial pressure,

p_j is the current pressure.

The data inputs and the model were allowed to run until a quasi state condition (when the graphs level out) was achieved. This was achieved by varying the time steps (Appendix 1). Assuming production in the center grid i.e. grid block 24, the results of various grid blocks were evaluated from drawn graphs of concentration against time at each time step (Fig. 3.3).

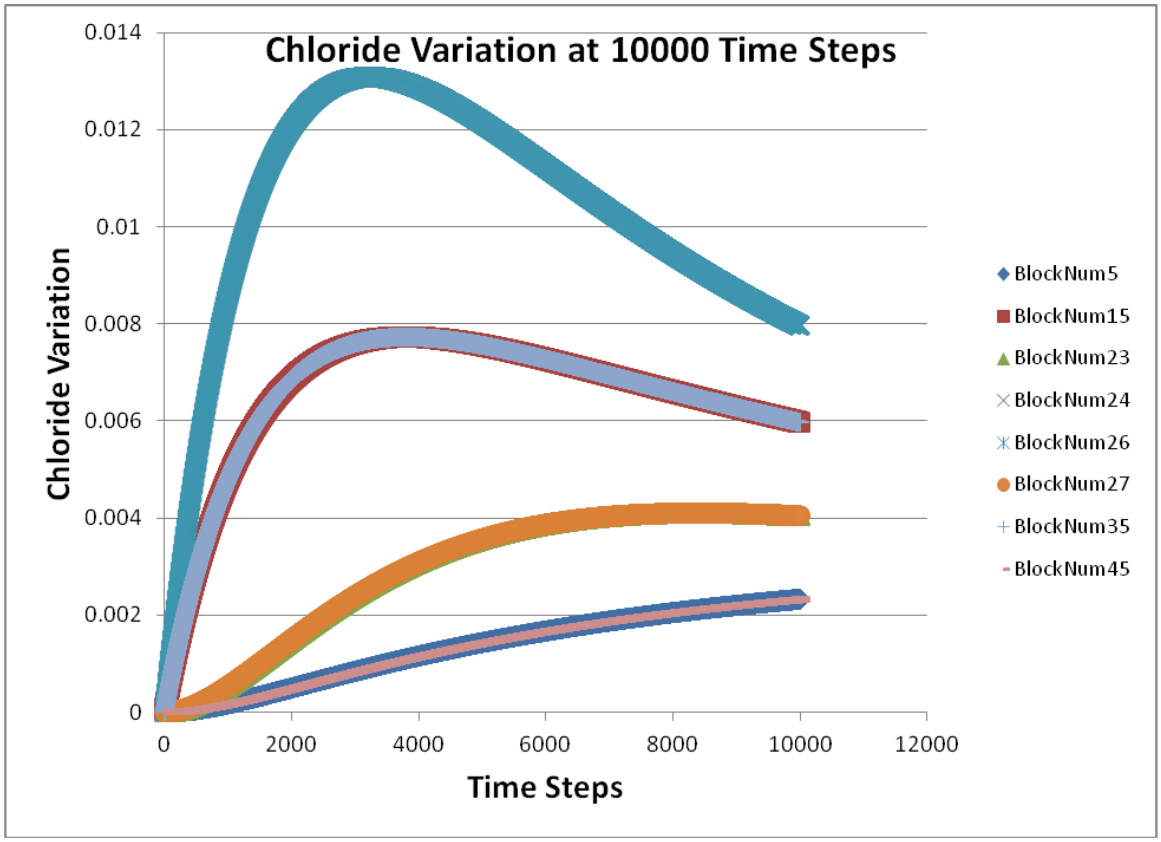

a) Graphs for Chloride Variations at 10,000 time steps

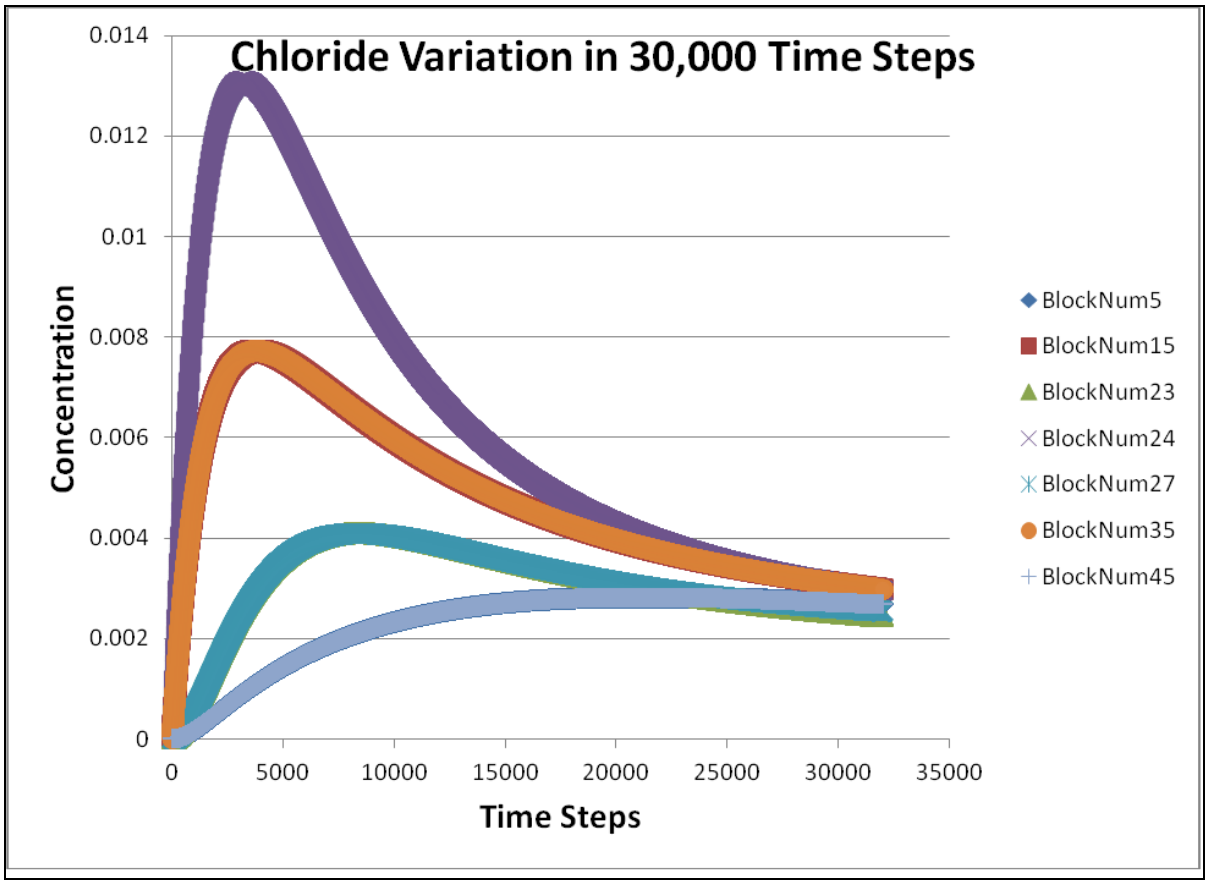

b) Graphs for Chloride Variations at 30,000 time steps

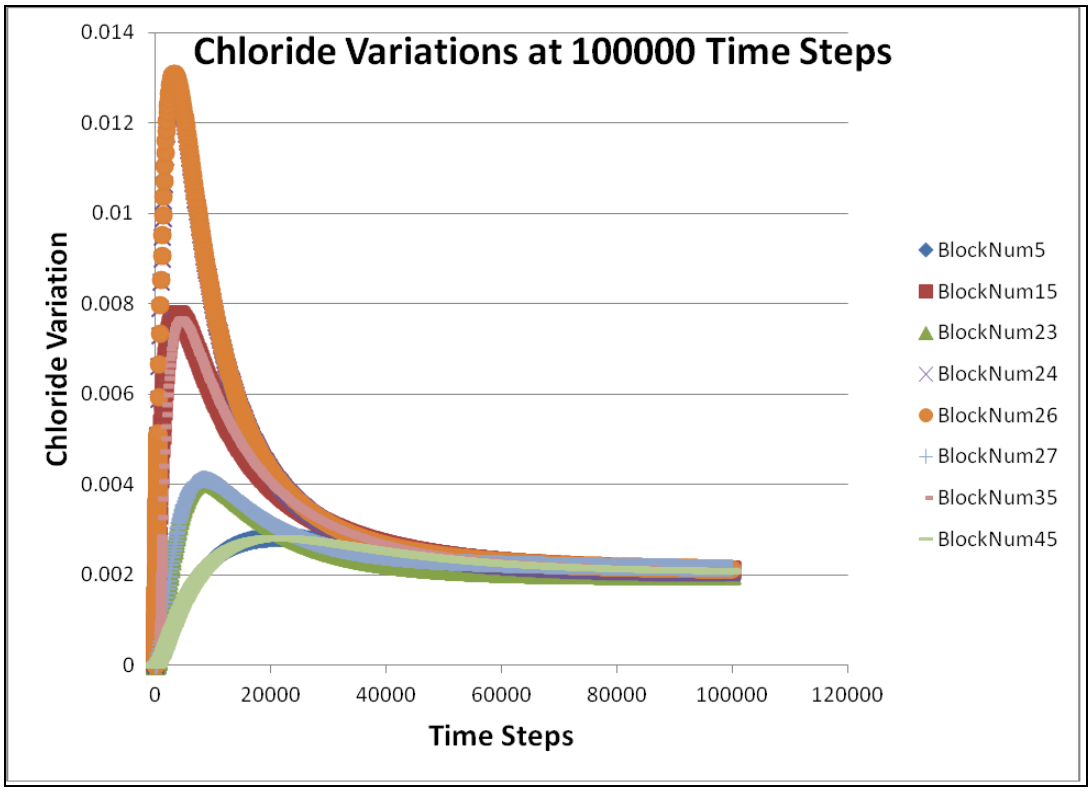

c) Graphs for Chloride Variations at 100,000 time steps

Figure 3.3: Graphs for Chloride Variations at Different time steps. The time steps are in seconds.

Once the initial state of the model was achieved, the final distributions of temperature, pressure and Chloride concentrations, as computed by the model, were compared to the observed distributions. In case the calculated and observed distributions matched within a chosen tolerance, the model was assumed to be a representative quantitative model of the initial state of the system. If not, the input parameters were modified further and the model re-run.

In the final match, flow to the system was assumed to be in grid block 37 in well OW-901 (where the Olonjoruwa gorge acts as the major recharge feature to the system). Final check on the validity of the initial state matching was achieved by comparing plotted graphs of chloride concentrations calculated by the model with the measured concentrations from wells' discharge fluids. The figures agree on an initial chloride concentration of about 350 ppm.

3.1.2 Historical Matching of the Chemical data

Here, the production history data collected from the available wells was used to further verify and calibrate the initial state model. The first step in this case was to assign the location of production, injection and observed wells for which data is available. The grid blocks that are used to represent the wells are assigned basing on completion intervals and inferred permeable zones. It is however notable that due to insufficient pressure monitoring data, the study considered the 1 bar/year draw down in Olkaria I as had been indicated from the 2001 to 2011 monitoring data.

3.1.3 Fore Casting of the Chemical data

In forecasting, it was assumed that the wells supplying the Olkaria I power plant in the EPF and those designed to serve the Olkaria IV plant in the Olkaria Domes (OD) as of 2012 would continue to be used without modification, no change in the production and reinjection scheme. In therefore starting to run the forecast model, the starting conditions of the reservoir i.e. pressure, temperature, steam saturation and elements concentration for each matrix and grid block were set equal to the value at the end of the history match run.

CHAPTER 4

4.0 MATERIALS AND METHODS

4.1 Overview of the Materials and Methodological Approach

This research was a computer-based numerical model which ultimately used to predict the reservoir response to different exploitation scenarios. The executable programme was written in C sharp as this language is versatile, terse and relatively low-level, extremely portable and easily entrenched in the UNIX environment. The model was split into three stages namely:

I. Natural State model
II. Model calibration with production history
III. Forecasting stage

4.1.1 Natural State Model

The goal of developing natural state models was to determine the validity of both fields (EPF and Olkaria-Domes) geochemical models, hence describing their undisturbed state and to quantify the natural mass flow within the system; not considering periods of reinjection (Bodvarsson and Witherspoon, 1989). This was done by matching the chemistry of the wells before exploitation, observed temperatures and pressures at sampling and the calculated enthalpy. At this stage, an initial and rough estimate of these parameters distribution, i.e. fluid chemistry, permeability and magnitude of heat source (as given by the sampling temperatures) and mass sources were obtained (Appendix 1). The result from the natural state simulations did not only serve as the initial conditions for the history match stage that follows in the modeling process but also was used to compare the match with the measured formation temperature and pressure.

4.1.1.1 Initial Conditions

From the natural state simulation, the initial conditions were generated by the domain using the set icon script, in which chemistry of the fluids was specified at the top of the domain. The values used correspond to the monthly and daily average chemical concentrations in production wells and discharging wells in the GOGA, respectively (Appendix 2). This helped in the

generation of fluid chemistry at the center of all layers to be used in the script. After that, fluid chemistry in the top layer of the domain was specified. To estimate it, the groundwater table maps of the area were used as described by (Thorarinsson and Bjorgvinnsdottir, 1980).

4.1.2 Model Calibration with Production History

This was done for the Olkaria East Field (EPF). The goal of the production history model was to refine the initial formation parameter distribution throughout the reservoir, i.e. changes in the chemistry with continued steam extraction, distribution and magnitude of heat (temperatures at fluids sampling), pressure conditions and enthalpies. This was done by matching the available production data of the chemistry of the wells, sampling pressure, temperatures and calculated enthalpies of the wells. At this point, the various scenarios, i.e. chemistry variation with reinjection, deepening of wells and different levels of performance were created such that performance with these variations could be determined. According to Wessel and Smith (2010), this stage of the modeling process is crucial and it is likely that the amount of changes done to the model here are significantly larger compared to the natural state model in order to improve the match with observed data. When an acceptable match is obtained, it is assumed that the parameters estimated are representative of the actual parameters present in the reservoir and, therefore, forecast modeling is commenced.

4.1.2.3 Computation Parameters

The history period simulations for the EPF was run for 47 years, starting from 1983 up to 2030 and the calculated system response obtained every year and compared to the measured response. In order for the results to be easily compared, geochemical isomaps were generated for every year as modeling progressed. The default Levenberg-Marquardt optimization algorithm of the model was used, with an initial Levenberg parameter of 0.001 and a Marquardt parameter of 10. The Jacobian matrix was calculated using forward differences.

4.1.3 Forecasting Stage

The forecast results were obtained for future production of the field based on the chemistry, sampling pressure and temperature conditions, enthalpy and natural mass flow within the system. The challenges of production were based on the chemistry changes and pressure- temperature

declines and enthalpy using coupled reservoir simulation, as well as a comparison with the corresponding results defining wells as constant well bottom pressure (DELV-type). This was done for data from both fields (EPF and the Olkaria-Domes) at different scenarios. For each scenario the model was run with and without reinjection of brine with forecasting period running for 18 years as follows.

Scenario 1: Current production in each of the fields with the existing injection rates, depth and performance of the wells.

Scenario 2: Current production of the EPF and 140 MW expansion of production at Olkaria I with the proposed injection in the selected wells, new depths and performance of existing wells.

Scenario 3: Production with the 140 MW expansion of production at Olkaria IV with the proposed injection in the selected wells, new depths and performance of existing wells.

Scenario 4: Current production (now in both fields) and 140 MW expansions of production at Olkaria I in the EPF and 140 MW productions at Olkaria IV in the Olkaria-Domes field.

This research was carried out by using a computer-based numerical model that utilized the already collected geochemical data of the GOGA since its inception from 1983 to 2011 and the newly collected data of 2012. The numerical model was obtained after writing a code in C sharp programming language (Appendix 1). The code had a massively parallel (MP) version, designed for multiple simulations of multi-components in porous and fractured media.

4.1.4 Desk Top Studies

This was done to verify the source of the data, methods of sample analysis used, calculation involved to achieve certain parameters like the enthalpies and the quality of the data. The geochemical data was from fifty two (52) wells from the Olkaria East field and the Olkaria Domes areas. The chemical compositions have been calculated from analysis of discharged water- and steam-phases i.e. samples analyzed for pH, TDS, Conductivity, Cl, B, Na, Li, SiO_2, K, Mg, SO_4^{2-} and gases including CO_2, F, H_2S, CH_4, H_2 and N_2. The discharge enthalpies were

calculated using the Russel James method (Bodvarsson and Witherspoon, 1989). Under this method, values for critical lip pressure and water flow from an atmospheric silencer are used.

4.1.5: Field Work and Laboratory Analysis

4.1.5.1 Well Sampling

The research considered sampling of 52 wells in the fields of interest that is; 16 in the Olkaria domes and 36 in the EPF that would give a total of 152 samples. The new data was used to verify the methods of sampling and analysis of the data contained in the database. The representative fluid (both brine and steam) samples from the wells was collected from the weir box and webre separator respectively. The separator in this case was connected on the steam flow line and left to flush and warm for at least 10 minutes. It was then closed and the sampling pressure recorded using a pressure gauge installed on the separator. The sampling temperature were measured using a thermocouple.The geothermal steam and liquid separated completely by adjusting the outlet of the sampling valves. The brine sample from the weirbox was collected using a jug and its samples treated the same way as separated samples.

The samples were then grouped into untreated and treated at the source in accordance with guidlines in Sampling Method for Geothermal Fluids and Gases (Ólafsson, 1988). Silica sample was diluted in the ratio 1:10. Sample for SO_4^{2-} analysis was preserved by precipitation of $ZnSO_4$, which is done by addition of 1ml of zinc acetate to 100ml of the sample. Gas phase was collected into two evacuated sampling bulbs containing 25% NaOH solution from steam outlet valve. This was meant to ensure a quality of data right from the point of collection.

4.1.5.2 Chemical Analysis

The analysis for the different chemical components was done at the KenGen Geochemical Laboratory at Olkaria in accordance with IAEA,Vienna, (2005) laboratory procedures. The Instrumental methods used are indicated on Appendix 2.

4.1.5.3 Chemical Data Quality

This was done by ensuring that the intruments to be used are calibarted according to the Manufacturers and the Kenya Bureau of Standards requirements. Before any analysis was done, the instruments were calibrated against a reference sample analyzed at the KenGen laboratory and results compared to those obtained from other laboratories so that corrections can be made where necessary. The running of reference samples was a good way to check the consistency of any analytical method and this was done for every batch of samples. If the results for the reference sample differed from the values expected, the batch was reanalysed. After analysis, the charge balance error (CBE), i.e. the balance between cations and anions in a sample, was calculated also as a measure to determine the quality of the data sets using the formula:

$$CBE(\%)=\sum Z_{cation}M_{cation}-\sum Z_{anion}M_{anion}/\sum Z_{cation}M_{cation}+\sum Z_{anion}M_{anion} *100\% \text{ ,..............4.1}$$

where Z is the charge of an ion i, and M is molar concentration (mol/kg).

For a good data set, CBE should be within 95% confidence limit.

4.1.5.4 Chemical Data Analysis

4.1.5.4.1 Deep Fluid Composition

This was in recognition that the surface composition is not equal to the deep liquid concentration and was done in two- phase samples. In this case, having sampling pressure (Ps) and sampling temperature (Ts) measured at sampling point. The Ps was to give the enthalpy of liquid and vapor phases at sampling conditions (h^l and h^v; from steam tables). The enthalpy of the deep liquid h^{dl} was then calculated from the equation by Fournier (1999) as follows:

$$h^{dl} = X\, h^v + (1 - X)\, h^l \text{ ,……………………………………………. 4.2}$$

where X is the steam fraction given as:

$$X = (h^{dl} - h^l) / (h^v - h^l) \text{ ,..4.3}$$

Amount of element *i* in deep fluid m_i^{dl} was then computed by:

$$m_i^{dl} = m_i^v X + m_i^l (1 - X) \text{ ,……………………………………..4.4}$$

where m_i^l represents the amount of element *i* in the liquid phase

and m_i^v is the amount of element *i* in the vapor phase.

It was, however, notable that this formula was only used to compute the concentrations of all dissolved constituents in the deep fluid (except pH). pH of deep fluid was computed by

speciation calculations where the concentration of all weak acids was taken into account as well as their dissociation constants.

4.1.5.4.2 Non Condensable Gases Determination

The individual gas concentration, i.e. CO_2, CH_4, H_2S, O_2, N_2 and H_2, was converted from mmol/100 moles of steam to mg/kg and subsequently to mmol/kg using the following formula:

$$\text{mmol/kg} = \frac{\text{mmoles /100moles steam}}{1.8} * \text{RMM} \quad \text{.....4.5}$$

where, RMM is the relative molecular mass of the gas of interest.

The concentrations were then converted to %weight by dividing the mg/kg by 10000 and their totals taken to represent all gases in the steam by percentage weight i.e. Total Non-Condensable Gases (TNCGs). The NCG was then calculated to the pressure of interest i.e. separation pressure as used in Olkaria from the sampling pressure using the formula:

$$C_2 = \frac{C_1 X_1}{X_2} \quad \text{.....4.6}$$

where C_2 is the concentration of gas at pressure of interest (pa), C_1 is the concentration of gas at sampling pressure, X_1 is fraction of steam at pressures of sampling (ps) and x_2 is the fraction of steam at pressure of interest (pa)

X is the steam fraction and this was calculated based on the total enthalpy of fluid of a well, from the following formula:

$$X = \frac{h_l^T - h_l^{pa}}{h_v^{ps} - h_l^{pa}} \quad \text{..... 4.7}$$

where h_l^T is the total enthalpy of the well as measured, h_l^{pa} is the enthalpy of saturated liquid at the pressure of interest (pa) in bar absolute (bar-a) and h_v^{ps} is the enthalpy of saturated steam at the pressure of sampling in bar absolute (bar-a).

4.1.5.4.3 Chemical Geothermometers Calculations

The chemical geothermometers comprised the solute and gas geothermometer functions and were used to estimate the reservoir temperatures.

a) Solute geothermometer functions

1. The silica geothermometer by Fournier and Potter (1982) was used,

$$TQtz= -53.5+0.11236S-0.5559*10^{-4}S^{2}+0.1772*10^{-7}S^{3}+88.390\log S$$,…… 4.8

where S represents silica concentration as SiO_2 in ppm.

2. The Na/K geothermometer adopted formula by Arnorsson *et al*, (1983)

$$TNaK=1319/1.699+\text{Log}\ (Na/K)-273.15$$,……………………………………..4.9

where the concentration of Na and K is in ppm.

b) Gas geothermometer functions

The gas geothermometers functions of Arnorsson and Gunnlaugsson (1985) was used with gas concentrations in log (mmol/kg) given as follows:

$$CO_2t\ (^{o}C) = -44.1+ 269.25Q - 76.88Q^{2} + 9.52Q^{3}$$,...4.10

where Q is the logarithm of the carbon dioxide gas concentration

4.1.5.4.4 Evaluation of Amorphous Silica Scaling Potential

Geothermal solutions in high temperature geothermal systems are generally in equilibrium with quartz. Silica scaling mostly occurs when the fluid becomes supersaturated due to conductive cooling or boiling. Amorphous silica compared to quartz is the most dominant mineral contributing to silica scaling. Therefore, to determine the saturation temperatures of amorphous silica, the steam fraction (X) from the reservoir (at temperatures given by the chemical geothermometers) to the weir box was computed then used to calculate the deep liquid concentration of silica using the formula:

$$SiO_2(ppm) = m^{i}\ (1-X)$$,..4.11

where m^{i}=concentration of SiO_2 in liquid phase (Fournier, 1999).

This was followed by stepwise boiling at interval of 10°C from the reservoir to weir box conditions so as to determine solubility of amorphous silica (am.SiO_2) at specific steam fractions using the formulae:

amorphous.SiO_2: $\log SiO_2 = 4.52 - 731/T$ (K) ,..... 4.12

where T is temperatures in Kelvin (Fournier, 1999).

4.1.6 Numerical Data Analysis

4.1.6.1 Modeling procedure

The procedure started with the continuous space and time variables discretizations. The continuous space discretizations avoided reference to a global positioning system and thus made applicable to both regular and irregular discretizations.

The discretizations gave time dependent linear equations which had chemistry of the grid blocks set as unknown. Time steps were automatically adjusted during the simulations. This was an efficient solution of multiphase flow problems (Sato *et al*., 1998). The accuracy of the model was tested by comparing with the observed field data.

4.1.6.2 Assumptions of the Model

The model assumes that we were dealing with a porous media which allowed for free flow of the reservoir fluids. This flow is, however, highly controlled by structures in that the NW-SE and WNW-ESE faults are thought to be the oldest fault system and they link the parallel rift basins to the main extensional zone (Pruess *et al,* 1999). These faults bring in high temperature and Cl rich waters. Gorge Farm fault, bounding the geothermal fields in the north eastern part and extending to Olkaria Domes area is the most prominent of these faults. The most recent structures are the N-S (Ololbutot eruptive fissure) and the NNE-SSW faults (Mungania, 1999). The faults within the Ol Njorowa gorge act to carry cool, less mineralized water.

4.1.6.3 Program Structure and Execution

The coding of the model was structured around two large arrays. These are the primary chemical properties of the grid blocks and thermo physical properties defining flow and transport equations (Fig. 4.1).

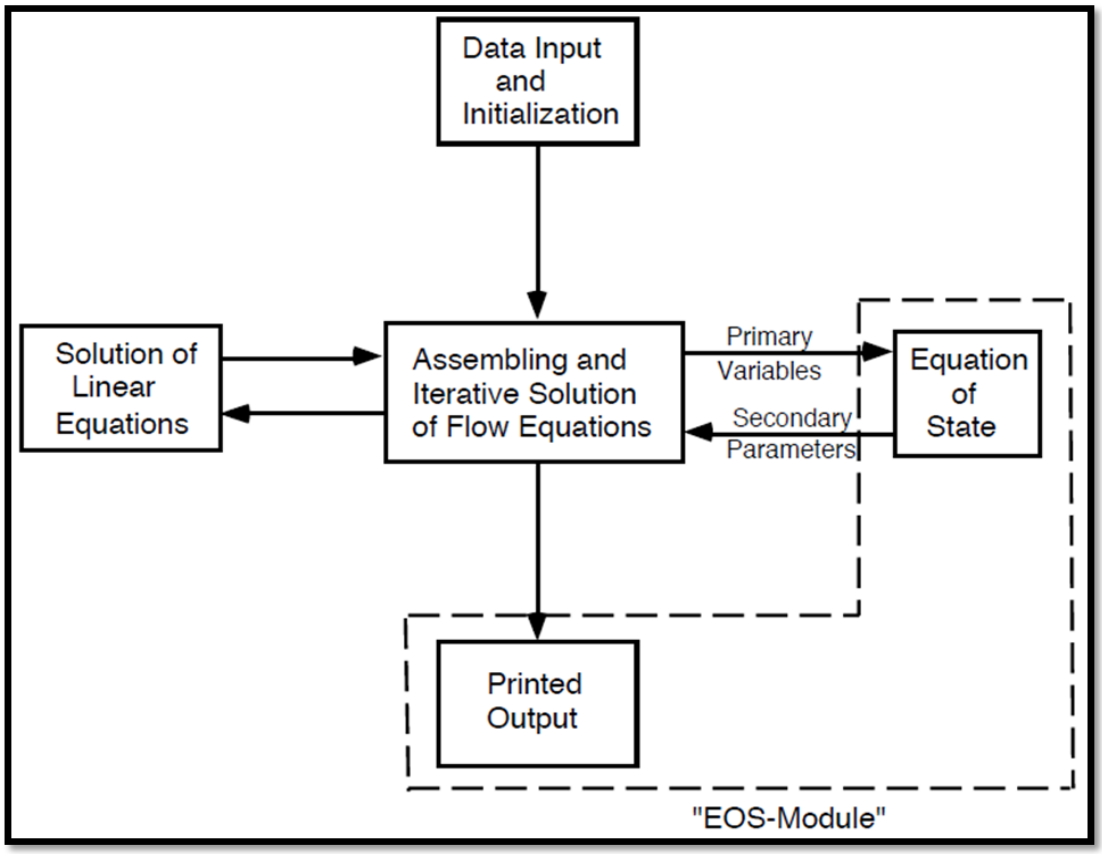

Figure 4.1: The Model structure (Modified from White *et al.,* 2003).

The initialization runs are normally by subroutines INPUT and OUTFILE (White *et al.,* 2003). In our case, the data was directly provided from the flash disk in to the INPUT file. These runs also generated a number of grid blocks with time sequence being governed by cycle interaction (CI). The first time step had all the thermo physical properties being initialized.

4.2 Methodology of evaluation of factors controlling the concentration of non condensable gases and their possible impact on the performance of wells in the Olkaria

4.2.1 Sampling, analysis and data quality

This was done as described in chapters 4.1.5.2 and 4.1.5.3.

4.2.2 Data analysis

The chemical data was first run through SOLVEQ to determine the equilibrium state of the system and then through Chiller considering the processes like boiling, mixing and condensation that characterize most high temperature geothermal fields (Reeds et al., 2012a). Their effect on the gases generation is by looking at the resulting recalculated gas pressures.

4.2.3 Equilibrium evaluation

The equilibrium constants were determined using mineral assemblages that potentially controlled the concentrations of non condensable gases in the reservoirs using reactions as shown in Table 1 and temperature equations for the equilibrium constants in Table 2. These included thermodynamic data on oxide and silicate minerals as given by Holland and Powell (1998) whereas sulfide minerals were as reported by Robie and Hemingway (1995).

Activities of end-members in the epidote (epidote and clinozoisite), garnet (grossular and andradite) and prehnite (Al-prehnite and Fe-prehnite) solid solutions were used. The values were 0.8 and 0.2 for Epidote and clinozoisite, respectively, as well as for Al and Fe-prehnite. Grossular had 0.3 and 0.2 for andradite.

4.2.4 Evaluation of gas concentrations versus the reservoir processes

a. Gas concentrations as a result of boiling and condensing processes

The calculations were done according to Reed et al. (2012a and b). This was by inputting the reservoir temperatures as recorded from SOLVEQ run. CHILLER (CHIM) was run at the specified reservoir temperatures TEMP and a set limit SLIM so that no temperature increments take place. The fluid pressures (PFLUID) in the pickup file was set lower than the saturation pressures while the temperature increments (STEP INCREM) for temperatures were set to -10 (decreasing temperatures). It must be noted that the oversaturated minerals as read out in SOLVEQ were suppressed to minimize their masking of the convergence of the equations. CHIM was then allowed to execute. The programme equilibrated with the gas phase and started boiling following STEP INCREM temperature drop and adjusted PFLUID. To ensure that the boiling remained isoenthalpic, the starting total enthalpy SENTH was set at zero, CHIM sets

SENTH equal to the current total enthalpy ENTH. From the output (CHIMOUT.DAT, at full equilibration), the gas saturation was determined.

b. Fluid-fluid mixing ('Coolbrew' calculations)

The study first considered the mixing of aqueous solution into a high temperature reservoir with enthalpy constraint scenario (Reed et al. 2012b). CHIM computed an enthalpy balance between the boiling solution and the mixer solution. The change of composition of the system (TOTAL MOLES was calculated as TOTAL MOLES + STEP INCREM * MIXER TOTAL MOLES) while the total current enthalpy of the system was also changed from ENTH to ENTH + STEP INCREM * MIXER TOTAL MOLES * ENTHW (enthalpy of the mixer solution). The mixing first resulted in the condensation of the gas phase at a constant temperature. Just like in the boiling evaluation, oversaturated minerals as read out in SOLVEQ were suppressed. According to Reeds et al., (2012b) once all the gas phase were condensed, CHIM proceeded in computing fluid-fluid mixing and temperature change by setting TEMPC to a non-zero value. This allowed CHIM to titrate a mixer solution of composition given by mixer total moles into the current solution of composition given by total moles. The composition of the mixer solution was in moles, except for water, mixer total moles, which were in kilograms.

c. Water- rock interaction (MINSOLV option)

The water-rock interaction option in CHIM option was enabled with MINSOLV being set to a non-zero value and allowing SiO_2, Fe_2O_3, FeO, MgO, CaO, Na_2O, FeS and NaCl as the reactants. The CHIM then read the names and amounts of reactants in the CHIMRUN file and their stoichiometries CHIM from the MINOX data file (Reeds et al., 2012b). At the start of a reaction calculation, the total mixer was set to zero while the composition of the system changed from TOTAL MOLES to TOTAL MOLES + STEP INCREM * WTPC * 0.01 * spec/mwox, where spec is the molar amount of a given component species in the reactant NOMOX, and mwox is the molecular weight of reactant NOMOX. For increments in moles, total moles are changed to TOTAL MOLES + STEP INCREM*WTPC*0.01*spec. The procedure in a, b and c above are as summarized in Fig 4.2 below.

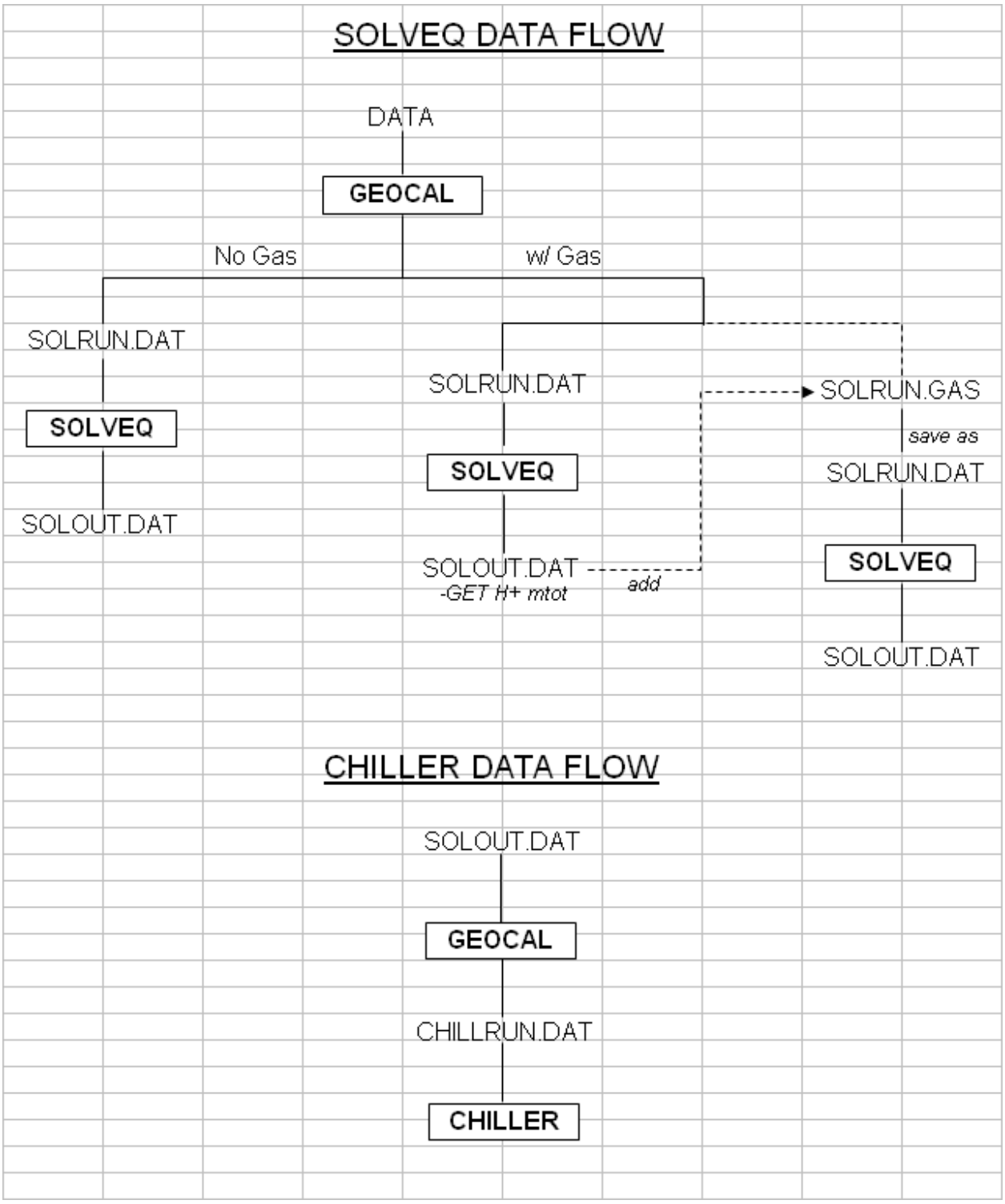

Figure 4.2: Flow chart summarizing the analysis of data in solveq and chiller programmes (modified from Reeds et al., 2012b).

4.2.5 Evaluation of depth of gas breakout or bubble point

Gas breakout or two-phase conditions occurs at the depth at which the gas pressure plus water pressure exceeds the total pressure i.e. bubble point depth (Haizlip et al., 2012). In this case the gas pressure is given in the output files of CHIM programme whereas the water pressures were estimated using steam tables as follows:

$$P_{liq} = P_{water}@\text{sat } T \quad \ldots\ldots 4.13$$

$$P_{tot} = P_{gas} + P_{liq} \quad \ldots\ldots 4.14$$

The temperatures values were taken from the SOLVEQ output files and were assigned to the major feed zones as determined from the downhole temperature and pressure profiles of each well.

CHAPTER 5

5.0 RESULTS AND DISCUSSIONS

Sub-chapter 5.1: Evaluation of the factors controlling concentration of non-condensable gases and their possible impact on the performance of geothermal systems

Evaluation of gas concentrations in Olkaria geothermal field revealed that on average, gases are highest in the Domes, intermediate in Northeast production field and lowest in East production field (West JEC, 2009). West JEC (2009) considered three factors for the variations: (i) CO_2 gets added at great depth to Northeast production field and Domes waters as a result of volcanic degassing below these areas, with less input of deep CO_2 to the East production field; (ii) CO_2 addition at depth is similar in all three areas, but waters of the East production field lost CO_2 during the onset of boiling in the reservoir such that the CO_2 escapes to fumaroles which lie west and south of the East production field; (iii) cap-rock conditions in the Northeast production field and Domes are somewhat more restrictive than in the East production field, leading to more entrapment at shallower levels of CO_2 that has been released by boiling. Gases, in particular CO_2, H_2S, H_2 and CH_4, are natural components of volcanic geothermal systems like Olkaria (Kenya), Mahanagdong (Philippines) and Nesjavellir, Hellisheidi and Krafla (Iceland) (Arnórsson et al., 2010 and Angcoy, 2010).

The gas concentration in systems that are unexploited is generally controlled by temperature dependent equilibria with various mineral buffers (Giroud and Arnórsson, 2005). This results in variation in gas concentration with temperature. Giroud and Arnórsson (2005) also stated that for geothermal systems with average reservoir temperatures of between 230-300 °C, as at Olkaria, their CO_2 buffer is considered to be clinozoisite, prehnite, quartz and calcite whereas that of H_2S buffer to be pyrite, pyrrhotite, epidote and prehnite. In highly saline waters, the H_2S mineral buffer consists of pyrite, magnetite and hematite. The gas ratios like in the case of H_2S/H_2 activity ratio correspond to pyrite/pyrrhotite and pyrite/magnetite ratios that are generally under saturated compared to these minerals individually.

The gases are among the factors that affect the reservoir pressure in the deep liquid-dominated geothermal reservoirs (Haizlip et al., 2012). Haizlip et al. (2012) further added that under static conditions, pressure in most producing aquifers around the world ranges between 130 to 230 bars at depths between 1700 to 2800m. The temperatures in these depths range between 219 to 242 $^{\circ}$C. The effect of the gas pressures on a well performance is evaluated in terms of the gas breakout pressure i.e. the pressure below which the fluids begin to transform into two-phase. According to Haizlip et al. (2012) gas breakout pressure is the sum of the gas pressure and water pressure at the reservoir temperature. In most cases, due to pressure drop, thermal fluids start to boil leading to degassing of CO_2 while fluids rise in a wellbore. In bicarbonate type of waters, this leads to the fluid becoming saturated with calcite as a reaction between CO_2 and calcium.

For a field that is under utilization like Olkaria, changes in the amount of gases in the fluids being discharged with time provide valuable information about the response of the reservoir to the production load (Karingithi, 2002). This is in respect with processes such as cold recharge resulting to fluid-fluid mixing, volcanic degassing and enhanced boiling (Gudmundsson and Arnórsson, 2002; Armannsson, 2003). In this study, an evaluation of reaction processes controlling the concentration of prevalent reactive gases in Olkaria well discharges is determined. The procedure involves first the determination of the equilibrium state between fluids and rocks using the software package SOLVEQ followed by determination of reaction processes in aqueous-mineral-gas systems using the software package CHILLER (Reed et al., 2012a, b). The software packages SOLVEQ/CHILLER, have been preferred due to its applicability for studying multiphase systems (Bienkowski et al., 2003). This issue is relevant for the long-term release of gases from geothermal power plants. This is with the purpose of predicting possible decline in gas emissions. Then the results are evaluated against the measured pressures through the downhole temperature and pressure surveys to determine if there are chances of gas breakout occurrence. The study comprises samples from 4 producing wells of 3 fields out of 7 in the Olkaria geothermal area (Table 5.1).

Table 5.1: Geochemical data from selected Olkaria wells

	OW-44	OW-724A	OW-914	OW-915
WHP (bar-g)	14	10	11	11.58
SP (bar-g)	14	9	10	10
pH at 20°C	7.91	9.43	9.91	9.93
Enthalpy (KJ/Kg)	2500	1698	2111	2034
Cond (μΩ/cm)	6130	2770	7482	2690
TDS (ppm)	3064	1660	3742	1345
SiO_2 (ppm)	487	610	636	682
B (ppm)	14.41	3.783	2.37	3.17
Cl (ppm)	1203	452.7	431.54	480.64
F (ppm)	79	35.8	244.28	187.41
SO_4 (ppm)	143.1	201.6	68.5	16.1
CO_2 (ppm)	88.22	321.86	1520.6	246.62
H_2S (ppm)	0.15	7.14	6.3	17.88
Li (ppm)	1.83	1.42	2.547	0.671
Na (ppm)	827	508.7	1455	653.5
K (ppm)	245.9	70.95	445.9	189.8
Ca (ppm)	1.266	2.159	0.01	2.672
Mg (ppm)	0.54	0.033	1.282	0.047
Fe (ppm)	1.37	0.265	1.35	1.35
CO_2 (mmol/100moles.H_2O)	88.4	261.3	498.1	329.8
H_2S (mmol/100moles.H_2O)	10.26	4.66	0.91	5.03
CH_4 (mmol/100moles.H_2O)	0.29	0.03	0.61	0.25
H_2 (mmol/100moles.H_2O)	12.91	9.62	12.26	19.5
N_2 (mmol/100moles.H_2O)	21.21	12.15	18.05	2.58
O_2 (mmol/100moles.H_2O)	0	0	0	0.35

WHP = well head pressure

SP = sampling pressures

The results are categorized into two parts. Part one presents the evaluation of the equilibrium states of the fluids in the wells considered whereas part 2 details the processes leading to gas evolution.

5.1.1 The equilibrium state of the fluids

The log gas concentration vs temperature curves (Figures 5.1, 5.2 and 5.3) are defined by equations 5, 6, 7 and 8 (see tables 5.2 and 5.3).

Table 5.2: Reaction equations for the equilibrium constants (Arnórsson et al., 2010)

1 H_2S =	1/3pyrite + 1/3pyrrohtite + 2/3prehnite + 2/3H_2O_l = 2/3 epidote + H_2S_{aq}
2 H_2S =	2/3grossular + 1/3pyrite + 1/3pyrrohtite + 2/3quartz + 4/3H_2O = 2/3epidote + 2/3wollastonite +H_2S_{aq}
3 H_2S =	2grossular + 1/4pyrite + 1/2magnetite +2quartz +2H_2O = 2epidote + 2wollastonite +H_2S_{aq}
4 H_2S =	1/4 pyrite + 1/2pyrrohtite + H_2O = 1/4 magnetite + H_2S_{aq}
5 H_2 =	4/3pyrrohtite + 2/3prehnite + 2/3 H_2O = 2/3epidote + 2/3pyrite + $H_{2,aq}$
6 H_2 =	2/3grossular + 4/3pyrrohtite + 2/3quartz + 4/3H_2O_l = 2/3epidote + 2/3wollastonite + 2/3 pyrite +$H_{2,aq}$
7 H_2 =	6grossular + 2magnetite + 6quartz + 4H_2O = 6epidote + 6wollastonite + $H_{2,aq}$
8 H_2 =	3/2pyrrohtite + H_2O = 3/4pyrite + 1/4magnetite + $H_{2,aq}$
9 CO_2 =	clinozoisite + calcite + 3/2quartz + H_2O = 3/2prehnite + $CO_{2,aq}$
10 CO_2 =	2/5clinozoisite + calcite + 3/5quartz = 3/5grossular + 1/5 H_2O + $CO_{2,aq}$

Table 5.3: Log K-temperature equations for the reactions given in Table 5.2 above (Arnórsson et al., 2010)

1 log [H_2S]	13.608 +592324/T^2-9346.7/T -0.043552T +0.000029164T^2+5.139logT
2 log [H_2S]	13.659 +555082/T^2 -9256.6/T -0.043608T +0.000028613T^2 +5.148logT
3 log [H_2S]	-0.836 -216659/T^2 -2847.3/T +0.008524T -0.000002366T^2+0.152logT
4 log [H_2S]	13.589 +590215/T^2 -9024.5/T -0.044882T+0.000029780T^2+5.068logT
5 log [H_2]	-1.640 -124524/T^2 -777.19/T -0.0005501T +0.000007756T^2 -0.565logT
6 log [H_2]	-1.544 -151109/T^2-752.389/T -0.0005868T +0.000007080T^2 -0.532logT
7 log [H_2]	1.444 -273812/T^2 -3962.1/T +0.002401T +0.000001304T^2 +0.979logT
8 log [H_2]	-1.654 -95456.8/T^2 -621.84/T -0.001257T +0.000007569T^2 –0.600logT
9 log [CO_2]	-0.890 +7251.5/T^2 -1710.6/T+0.004188T +0.000002683T2 -0.064logT
10 log [CO_2]	-1.449 -40536/T^2 -2135.9/T +0.0065639T +0.000002725T2 -0.193logT

T = Temperature in kelvin

The plotted results show that the study wells closely correlate with mineral assemblages in equation 5 which are pyrrohtite, prehnite, epidote and pyrite and 8 with Magnetite, pyrite and pyrrohtite (see Table 5.3). OW-914 appears to be in near equilibrium as it plots close to the equation curve followed by OW-44. OW-915 and OW-724A appear to be non equilibrium as they plot far from the top most equation curve number 5. These results agree with those by Arnórsson et al., (2010) where some wells in the field plotted close to the mineral assemblages in 5 and 8 indicating equilibrium with the minerals while others were scattered hence showing non-equilibrium. The gas concentration is low, ranging between -2.0 moles/kg in OW-915 and -2.5 moles/kg in OW-914, which closely corresponds to a range between -3 moles/kg to -5.5 moles/kg by (Arnórsson et al., 2010).

The log H_2S vs temperature graph has mineral curves for 1, 2, 3 and 4 (Figure 5.2). The temperature in the wells varied between 300 °C and 330 °C. This is in the exception of OW-724A that plots at 250 °C. OW-724A seems to be in equilibrium with mineral assemblage in

equation 1 which comprise pyrite, pyrrohtite, prehnite and epidote and 4 which has pyrite, pyrrohtite and magnetite. OW-44, on the other hand, with mineral assemblages grossular, pyrite, pyrrohtite, quartz, epidote and wollstonite for equation 2 and grossular, pyrite , magnetite, quartz , epidote, wollastonite for equation 3. OW-915 and OW-914 seems to be in non-equilibrium with the mineral assemblage. The results still hold for Arnórsson et al., (2010) with the exception of OW-914 which seemed depleted with H_2S an indication of steam loss and, therefore, gas loss.

The log CO_2 graph (Figure 5.3) is defined by two mineral assemblages 9 and 10. Two wells, i.e. OW-914 and OW-915, are in equilibrium with mineral assemblages in equation 10. OW-44 plots way below mineral assemblage in equation 9 whereas OW-724A plots above the mineral assemblage in equation 10. This is an indication that OW-724A and OW-44 are in non-equilibrium. The values of concentration also give OW-44 to be having the smallest amount of gas whereas OW-914 has the highest amount. The findings concur with Arnórsson et al., (2010) where the Domes Sector had the highest CO_2 concentration whose likely cause was the high evolution from hot geothermal fluids.

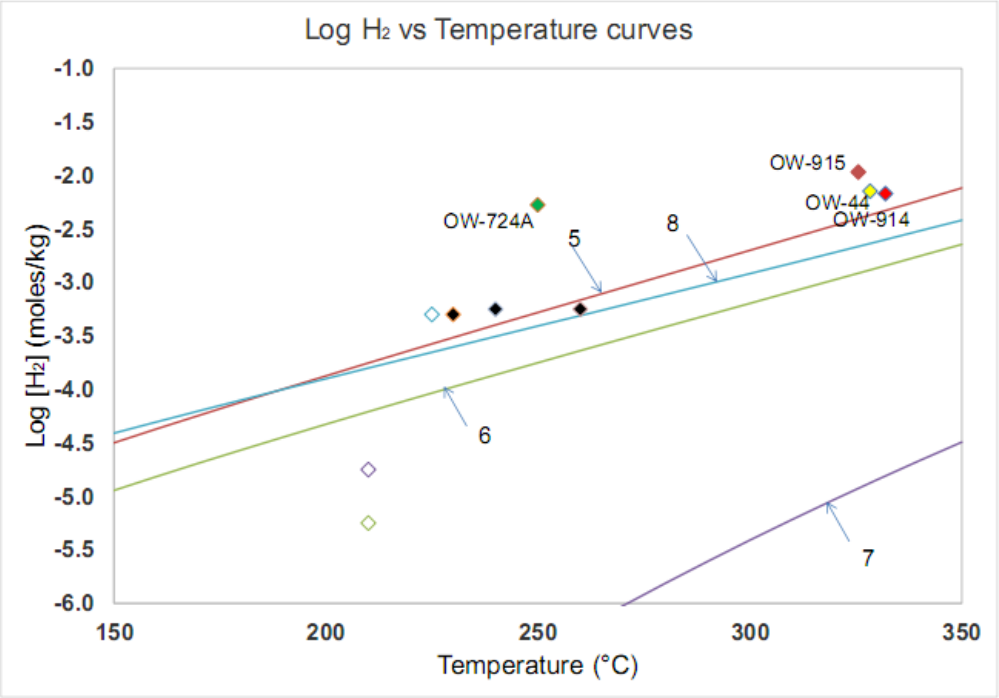

Figure 5.1: H_2 content in wells OW-44, OW-724A, OW-914 and OW-915. White and black symbols are Arnórsson et al., (2010) data from Olkaria Domes and Olkaria Central field respectively. The numbers on the curves refer to the reactions in Table 5.2

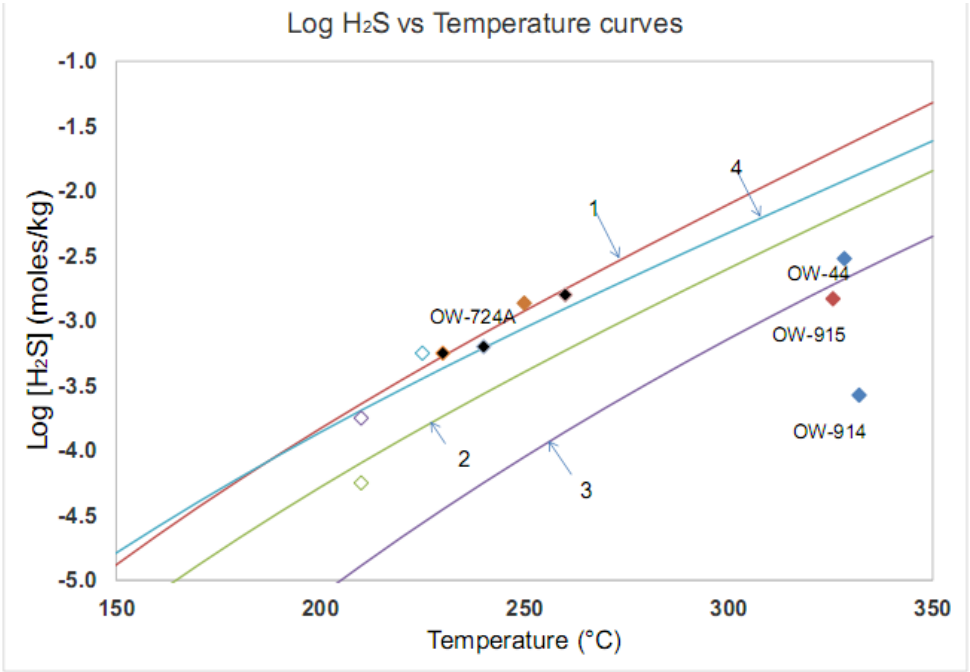

Figure 5.2: H_2S content in wells OW-44, OW-724A, OW-914 and OW-915. White and black symbols are Arnórsson et al., (2010) data from Olkaria Domes and Olkaria Central field respectively. The numbers on the curves refer to the reactions in Table 5.2

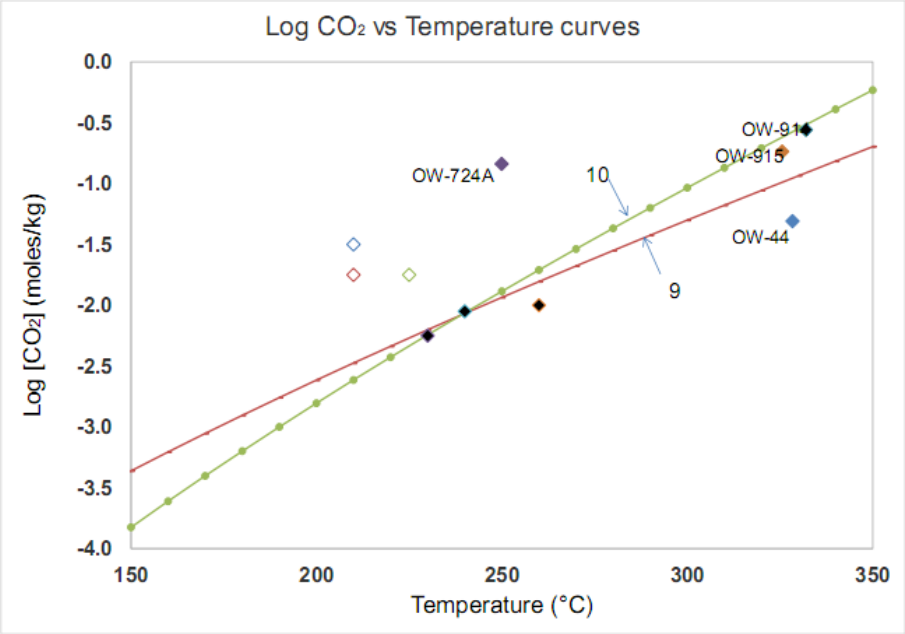

Figure 5.3: CO_2 content in wells OW-44, OW-724A, OW-914 and OW-915. White and black symbols are Arnórsson et al., (2010) data from Olkaria Domes and Olkaria Central field respectively. The numbers on the curves refer to the reactions in Table 5.2

5.1.2 Gas concentrations and the reservoir processes in the wells

The reservoir processes considered were boiling, fluid-fluid mixing and titration (Figure 5.4, 5.5, 5.6 and 5.7).

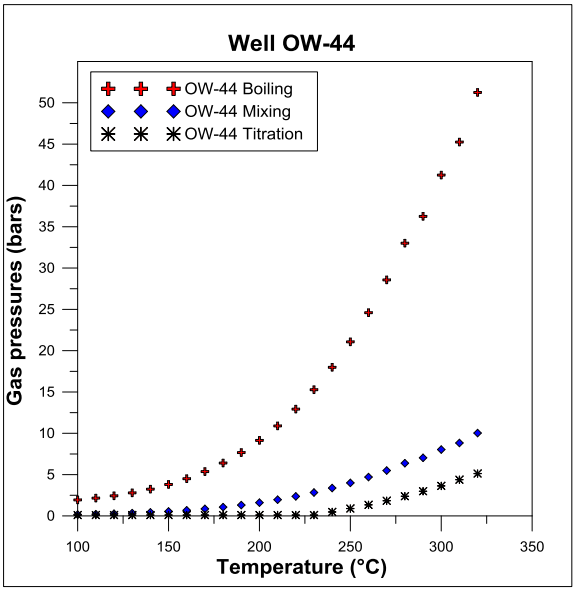

Figure 5.4: Gas pressures against the reservoir processes in OW-44

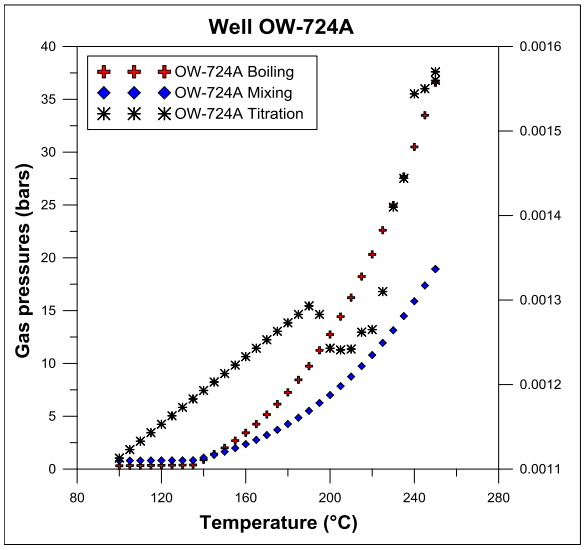

Figure 5.5: Gas pressures against the reservoir processes in OW-724A. The titration curve has been plotted on the secondary axis

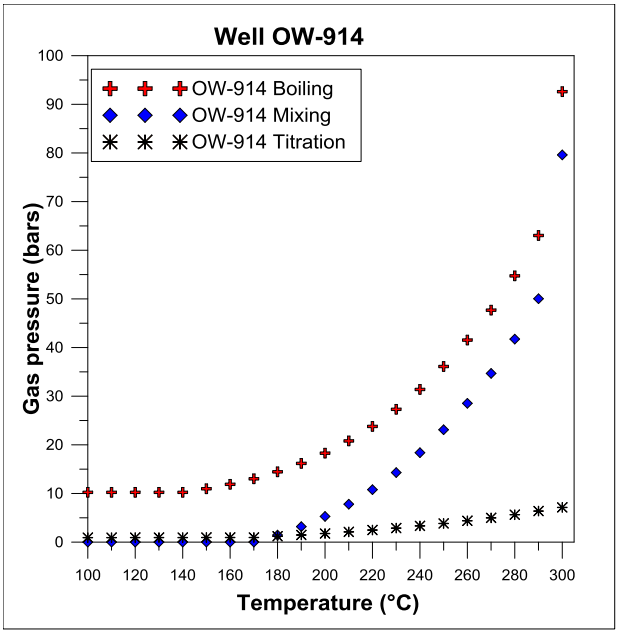

Figure 5.6: Gas pressures against the reservoir processes in OW-914

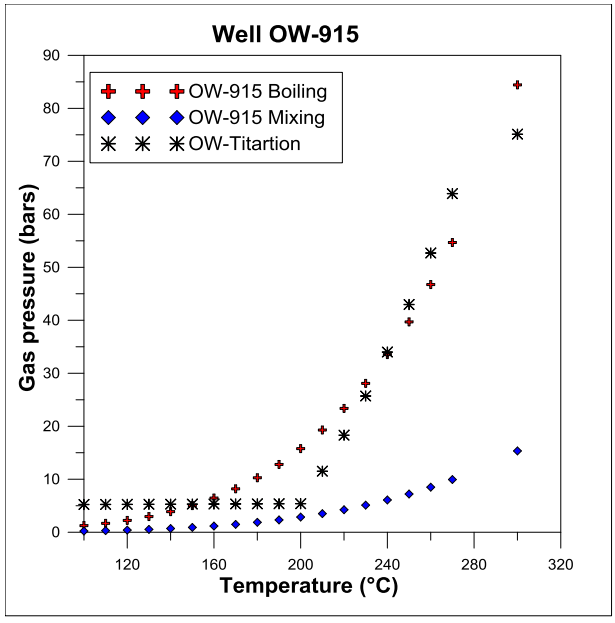

Figure 5.7: Gas pressures against the reservoir processes in OW-915

The plots for OW-44 indicate that boiling is the lead contributor to non-condensable gas evolution. The gas pressures increased steadily with temperatures, steadily rising from 2.4 and 50 bars. The mixing process comes in second. Unlike the boiling process, the curve remained leveled up to about 200°C before starting to increase. The curve on titration has almost similar trend but lesser values ranging between 0 and 2.4 bars (Figure 5.4).

OW-724A, just like OW-44 has boiling processes immensely contributing to gas generation (Figure 5.5). The graph begins with no change in the gas pressures between 100 °C and 120 °C at a gas pressure value of about 0.1 bars before steadily rising to 37 bars. The mixing curve also experiences no change in the gas pressures at start but later increases. The recorded values are lesser, between 0.1 and 17 bars, compared to the boiling processes. The titration process start with a linear increase in the gas pressures up to around 180 °C. The curve however shows a decline in the gas pressures between 180 °C and 220 °C.

OW-914 has its resulting gas pressures due to boiling ranging between 10 and 92 bars (Figure 5.6). The mixing graphs come in second with values ranging between 0 and 50 bars. The titration curves give almost a zero gradient trend between 100 °C and 200 °C. This is followed by a slight increase to about 5.0 bars at 300 °C. OW-915 just like OW-914 has its gas pressures due to boiling steadily increasing reaching a high of 85 bars (Figure 5.7). The mixing curve show a slight increase in the gas pressure with temperature, recording of values between 0 and 10 bars. The titration curve has almost similar trends to OW-724A. The curve start with evidence of an increase in gas pressures to a temperature of 170 °C, levels out to 210 °C before starting to increase to a high of about 5 bars.

The processes comparison curves (Figure 5.8) indicate boiling processes to be highest in magnitude in OW-914 followed by OW-915, OW-724A. OW-44 has the least amount of gas pressures generated. The mixing process gas evolution, on the other hand seems high in OW-914 followed by OW-724A then OW-915 and lastly OW-44. Titration processes just like the mixing ones are higher in OW-914. OW-915 comes in second followed by OW-44 then OW-724A.

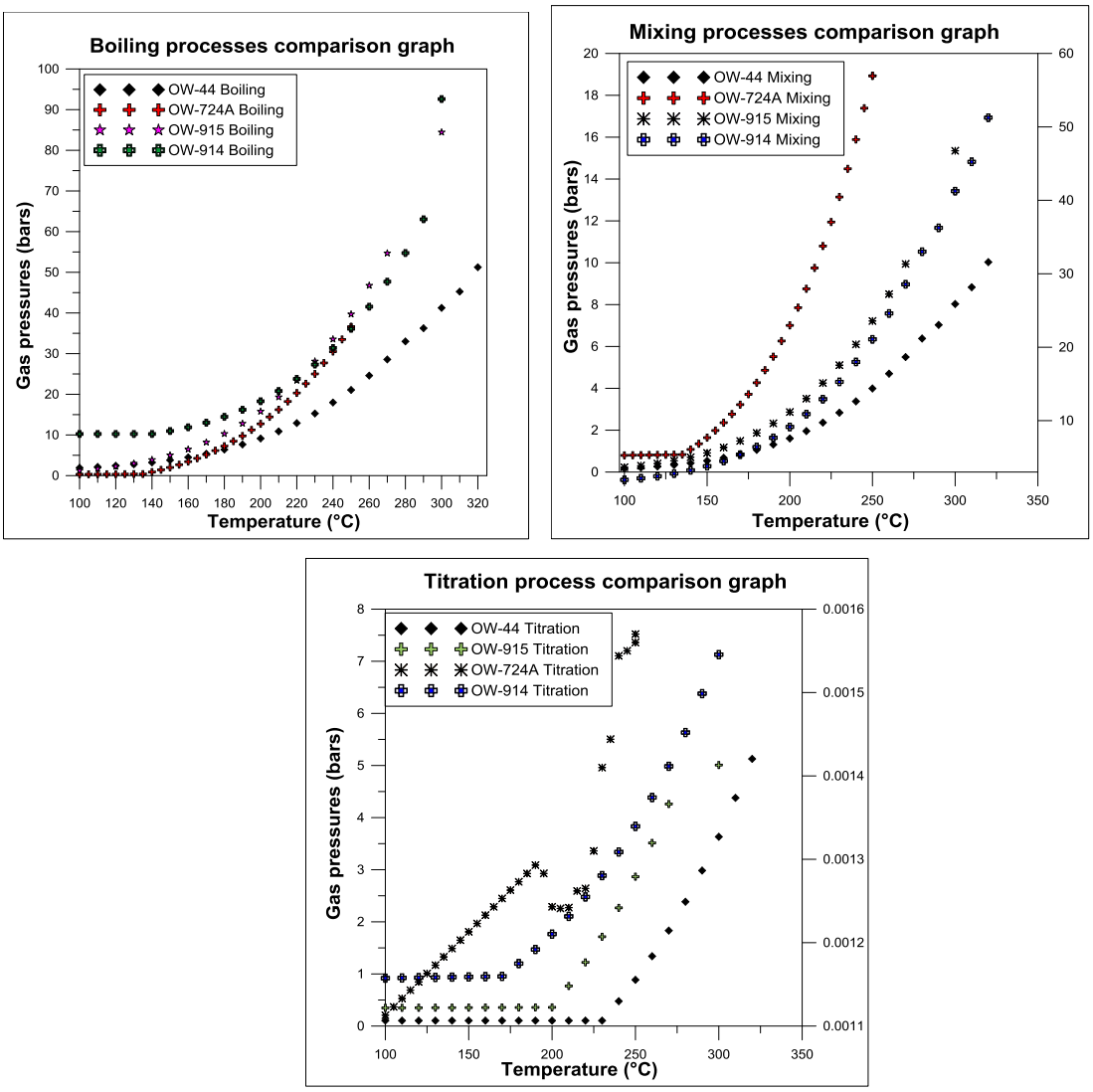

Figure 5.8: Reaction processes comparison graphs. The titration curve in OW-724A has been plotted on the secondary axis

5.1.3 Depth of gas breakout or bubble point

The measured pressures at the major feed zones give the highest values of 175 bars in OW-44 followed by OW-915 at 150 bars, OW-914 at 100 bars and lastly OW-724A at 90 bars (Table 5.5). Using steam tables, pressure of the liquid (P_{liquid}) then added to the pressure of the gas P_{gas} from CHIM, the totals ranged between 52 bars in OW-44 to 92 bars in the OW-914. From the results, it is identifiable that OW-914 has its total pressure close to the downhole measured one

indicating higher chances of gas break out at its major feed zone. OW-44 had the least chances, as its total pressure was way less, at 52 bars compared to 175 bars (measured).

Table 5.4: Showing a comparison between measured and calculated pressures in the main feed zones

Well name	Depth of major feed zone (m)	Measured pressure (bars)	Calculated liquid pressure (bars)	Calculated gas pressure (bars)	Total calculated pressure (bars)
OW-44	2250	175	0.105	52	52
OW-724A	1700	90	0.002	36	36
OW-914	1500	100	0.025	92	92
OW-915	2300	150	0.035	84	84

5.1.4 Results interpretation

5.1.4.1 The equilibrium state of the fluids

The current study and that of Arnórsson et al., (2010) agree that the H_2 and H_2S gas concentrations are low in the Olkaria geothermal field. This is confirmed by minor values ranging between -2 to -3.5 moles/kg (Figure 5.1, 5.2 and 5.3) indicating that the aquifer vapor fraction is insignificant. Arnórsson et al., (2010) attributes these low concentrations to steam loss resulting from the boiling of fluid flowing into these wells. OW-724A plotting way above the mineral assemblage curves in the H_2 whereas OW-914 plots way below in the H_2S graph. According to Arnórsson et al., (2010), non-equilibrium distributions of gas species in a high temperature field like Olkaria arises from processes like boiling, condensation and mixing.

The CO_2 plot indicates that the calculated aquifer fluid CO_2 concentrations are in equilibrium with mineral assemblages as in the case of OW-914 and OW-915. OW-44, apart from being in non-equilibrium with the mineral assemblages has the least concentration (Figure 5.3). According to Arnórsson et al., (2010), the low CO_2 values as in OW-44 are as a result of insufficient supply thus revealing that the aquifer fluid CO_2 concentration is externally controlled

that is, the flux into the geothermal fluid is either from a degassing magma or rocks or fumaroles or both. This is opposite with the case of OW-724A which plots above the equilibrium curves. This is an indication that the non-equilibrium in OW-724A maybe arising from a process of volcanic degassing below these areas with minor gas loss compared to OW-44.

5.1.4.2 Gas concentrations and the reservoir processes in the wells

The results point to gas evolution being due to boiling (Figure 5.4, 5.5, 5.6 and 5.7). Simsek et al. (2009) while studying the Kizildere geothermal field, Turkey stated that the increase in gases is as a result of elevated enthalpy resulting from the flow or gravity segregation of water and steam where the steam flows preferentially to the well leaving behind water or enhanced vaporization boiling where there is flow of heat from the rock to the fluid. The former describes a scenario where there is boiling in the area around the well while the latter is whenever the water has cooled by adiabatic boiling as a result of the pressure drop leading to generation of steam and gas (Simsek et al., 2009). From the graph, it is notable that the intensity of the processes increases with temperatures in the considered wells. This is so as temperatures act as catalysts for reactions leading to evolution of the gases (Haizlip et al., 2012).

The comparison in the magnitude of this processes in the wells indicate that the impacts of the processes are highest in OW-914 and lowest in OW-44 (Fig. 5.8). This trend in OW-914 is attributed to the high temperature values of about 325 °C such that chain reactions similar to those discussed in the mixing processes take place. This is further supported by the fact that this well has high injectivity capacity of about 315 lpm/bar, an indication of high permeability of the well. This acts to bring in fluids, that in turn react with the mineral assemblages in the aquifer rocks leading to generation of non-condensable gases.

OW-44 had amount of gas content despite the fact that it has high downhole temperatures of about 300°C and considerably high injectivity. Hazil et al. (2012) attributes this to loss of gas from the deep fluid due to degassing and near surface boiling. Besides that, NH_3, H_2 and H_2S can be removed from the steam formed through boiling by processes like wall-rock interactions and solution into steam condensate. Then depending on how far the well is from the recharge zone, gases in the reservoir fluid tend to enter the vapour phase whenever possible (Simsek et al., 2009). Therefore, when boiling sets in, the initial steam formed contains majority of the

dissolved gases thus the residual liquid is therefore highly depleted in dissolved gases and later stages of steam separation will contain increasingly lower concentrations of gases. Steam formed in the early stages of boiling is therefore characterized by higher gas content.

5.1.4.3 Depth of gas breakout or bubble point

This was meant to determine the potential impacts of the gases on the performance of the wells. The results (Table 5.4) indicate that likelihood of flashing is highest in OW-914 and least in OW-44. This therefore is an indication that OW-914 is likely to experience calcite scaling at its major feed zone at 1500m depth, considering the type of waters feeding the well. This finding agrees with a dynamic survey carried out in OW-914 well in 2014 (Figure 5.9). The results pointed to a calcite scaling potential in the depths between 1200 and 1800m. According to Akin et al. (2015) due to pressure drop, thermal fluids start to boiling and degassing of CO_2 as the fluids rise in a wellbore.

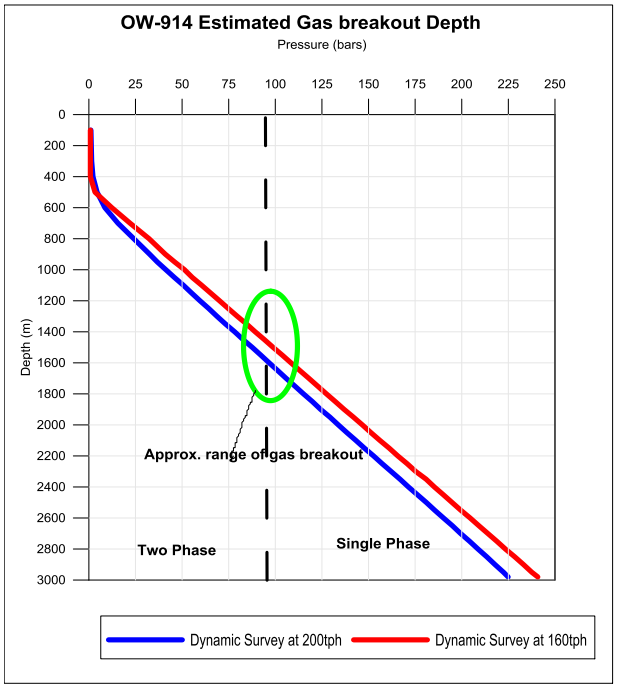

Figure 5.9: Estimated gas breakout depth in OW-914 from the dynamic surveys

When the initial gas bubbles are formed, CO_2 exsolution affects the pH together with the carbonate species leading to the thermal fluid becoming saturated with respect to calcite.

5.1.5 Possible reservoir management options

Continuous exploitation tends to increase the concentration of gases in geothermal reservoirs especially when depressurization occurs (Moya and Yock, 2005). In order to minimize this tendency, two reservoir management options were considered (Figure 5.10). First, a need for a prudent reinjection programme in the eastern sector (represented by well OW-44). The immediate response here would be the decrease in the enthalpy of the wells and gases evolution.

For wells around and with similar chemistry like OW-914, two options are applicable. First the management by operating the wells at lowest flow rates. According to Moya and Sanchez (2005) this will minimize chances of pressure drop that can lead to depressurization boiling. This will also lead to a lowered scaling point and or reduced numbers of work over. The second option will be to consider chemical inhibitors dosing. According to Haizlip et al., (2012) successful scale mitigation in the wellbore requires that the inhibitor is injected into the flowing well through capillary tubing at depths 10-50m below the estimated gas breakout depth preferably within the casing. The inhibitors act by inhibiting the growth of scale.

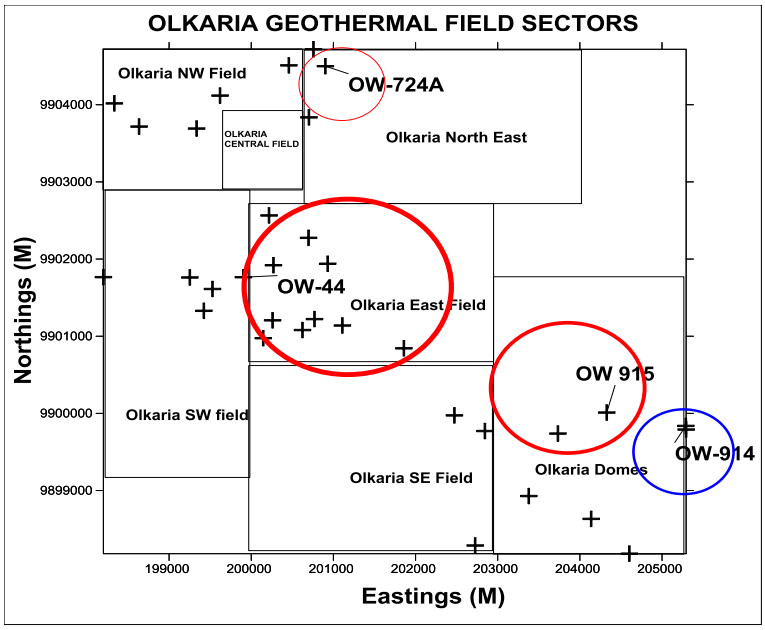

Figure 5.10: Management options for different parts of the field. Red eclipses for reinjection while the blue one is for reduced flow from wells and inhibition

Sub-chapter 5.2: Determination of the geothermal energy potential of the Olkaria field, Kenya based on geochemical data- a numerical model

The results of this study comprise of 3 sections which are initial state model, historical match and forecasting and are inform of time dependent curves. Spatial distribution maps for the various elements have also been included to provide a wider picture for chemical changes in the field at different stages. In order to avoid discontinuities in the plots, the study considered an overlap in the time periods by dividing the total time steps in to 3 portions i.e. 0-50000, 50000-63000 and 63000 -100000 time steps covering the initial states, historical matching and forecasting respectively.

5.2.1 Initial State Model

This was achieved after variations as described in section 4.1.1.1 which allowed a conductive and convective heating with upflow of 17.5 kg/s of brine at 340^{o}C in to the bottom of the well.

The match to the initial reservoir chloride in the main production horizon is shown in Fig. 5.11. In this figure, the chemistry of only four wells i.e. OW-5, OW-16, OW-18 and OW-19 was considered as they had data as from 1983 hence ease of correlation. It is evident that there is close correlation of the modeled (at the 5000 time step i.e. at the start of the initial model) and measured values of Chloride concentration (values in the text box). It is also notable that though there was reinjection in the field (Fig. 5.12), there was no significant change in the chemistry. The modeled pressures also agree with the measured draw down of 1 bar/year. This draw down together with the low reinjection rates is perhaps responsible for the minor decline in the concentration of the chloride values towards the end of the 0-5000 time step period.

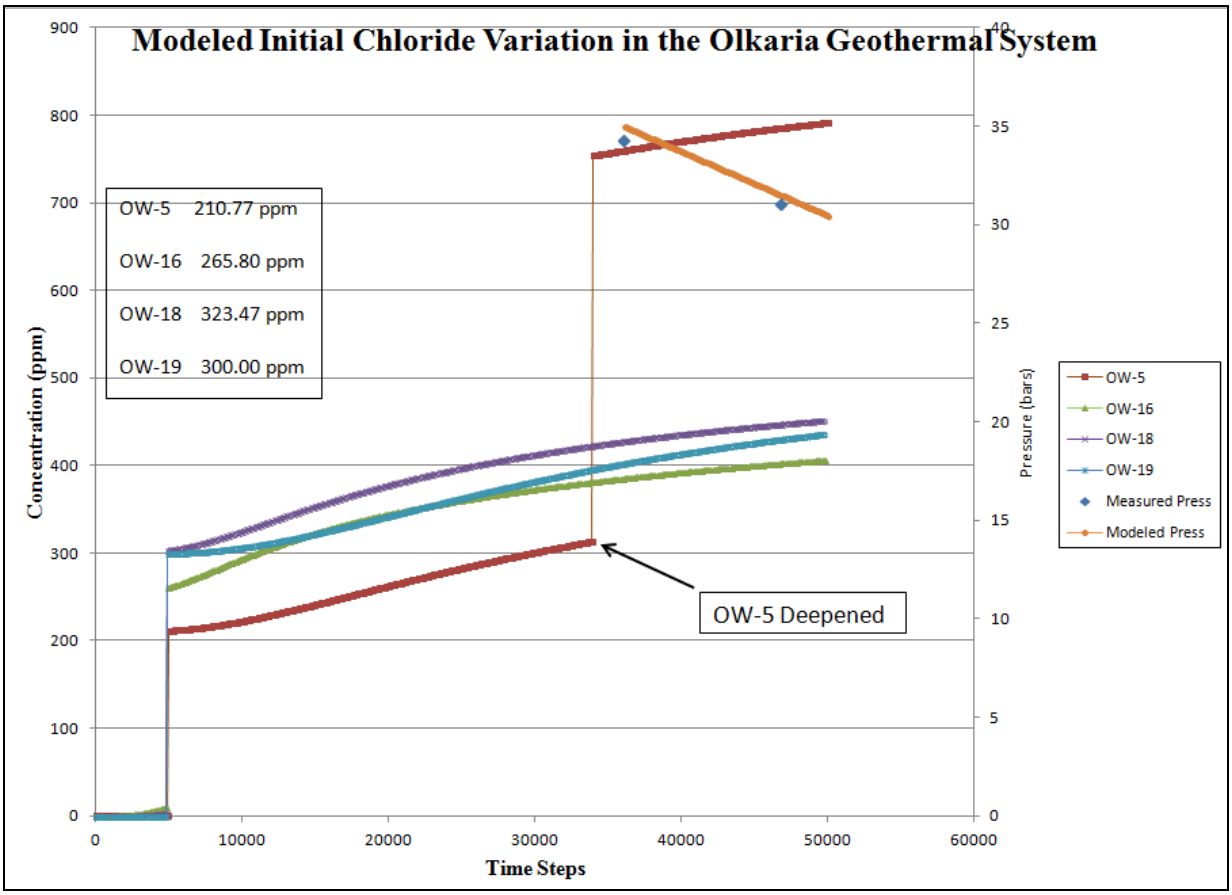

Figure 5.11: Comparison between Modeled Initial Chloride values. Timesteps in seconds.

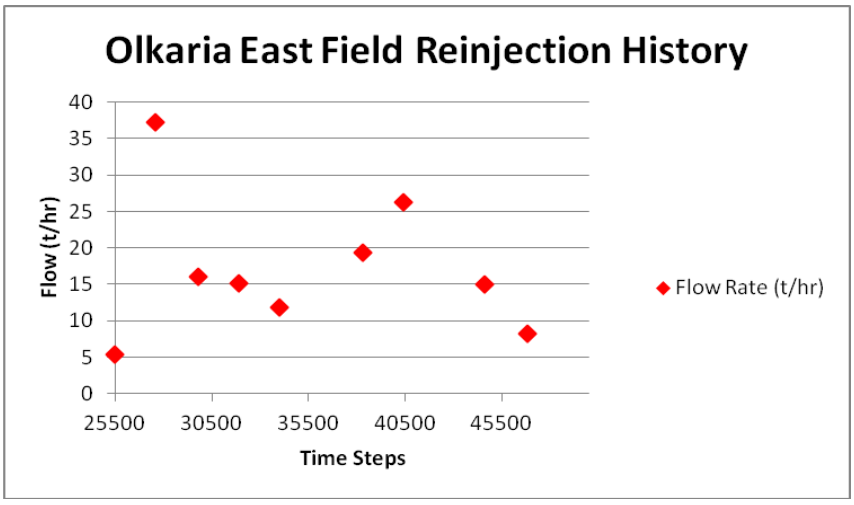

Figure 5.12: East production field reinjection history. Timesteps in seconds.

With individual wells variation, OW-5 have two regimes i.e. before deepening and after deepening (as shown on the graph). The chloride values before deepening were low at about 202 ppm but experienced a sharp increase to about 750 ppm thereafter. This is an indcation that the well OW-5 began tapping from deeper chloride rich aquifers after the deepening. Well OW-16 had the least concentration whose cause is to be clearer after evaluation of all the stages of modeling.

5.2.2 Historical Data Matching

The historical data matching considered modeled concentration of chloride, silica, reservoir temperature of wells OW-5, OW-11, OW-16, OW-19, OW-22 and OW-23 and pressure values. The Nitrogen gas values were also used to evaluate the possibility of atmospherically modified fluids finding their way in the production field. For comparison with the measured data, the study considered analyzed chemical values of all the wells within the East production field (EPF) in order to have a wider view of the field.

5.2.2.1 Reservoir Pressure Variation

The modeled pressure values indicate a linear decline in the reservoir pressure as shown in Fig. 5.11. These quite correctly agree with the measured pressure value in the identified monitoring well that estimates a 1bar/year draw down. This was attributed to minimal reinjection into the reservoir vis-a-vis the production rates and length.

5.2.2.2 Reservoir Temperature Variation

The chemical geothermometers were used to estimate the aquifer temperatures beyond the zone of secondary processes like boiling, cooling and mixing on the basic assumptions that the sampled fluids are representative of the undisturbed aquifers where local equilibrium conditions are achieved.

The model estimates reservoir temperatures of about 300^{o}C. Well OW-5 has high temperatures of about 320^{o}C due to the deepening effect as mentioned in the Initial state model. On the contrary, OW-22 had the lowest temperatures of less than 240^{o}C which are on the decline giving an indication of some cooling in the reservoir around the well (Fig. 5.13).

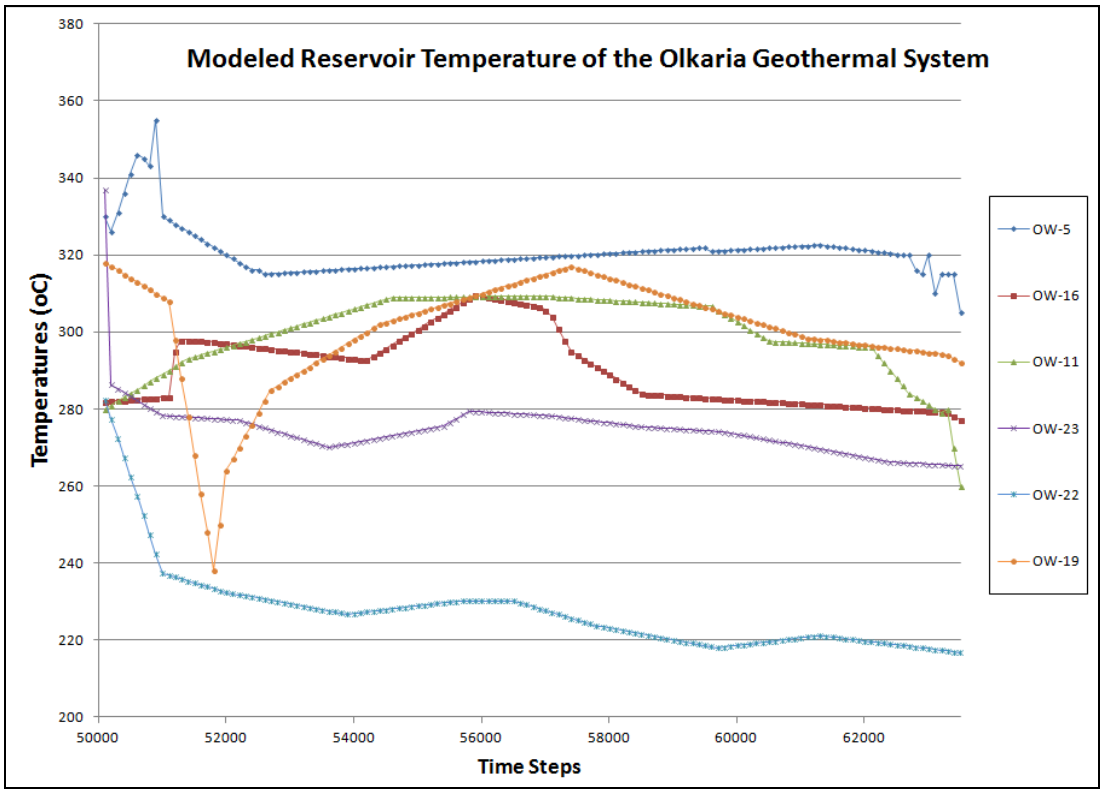

Figure 5.13: Modeled reservoir temperatures in the EPF. Timesteps in seconds.

These trends agree with the measured temperatures whose values clutter around 300^{o}C and show a gradual decline towards the end of 2013 (Fig. 5.14). The trends in individual wells give scenarios where the temperatures in the field rose gradually reaching a maximum in the 57000th time step before starting to decline. This was an indication of the fact that as production continued it led to pressure decline hence cooler fluids started entering the field of. It is also notable that the impact of pressure draw down is felt earlier in shallow wells compared to deeper wells as shown in the patterns of OW-11, OW-16, OW-22 and OW-23 which are 1300m deep compared to OW-5 which is 2200m deep.

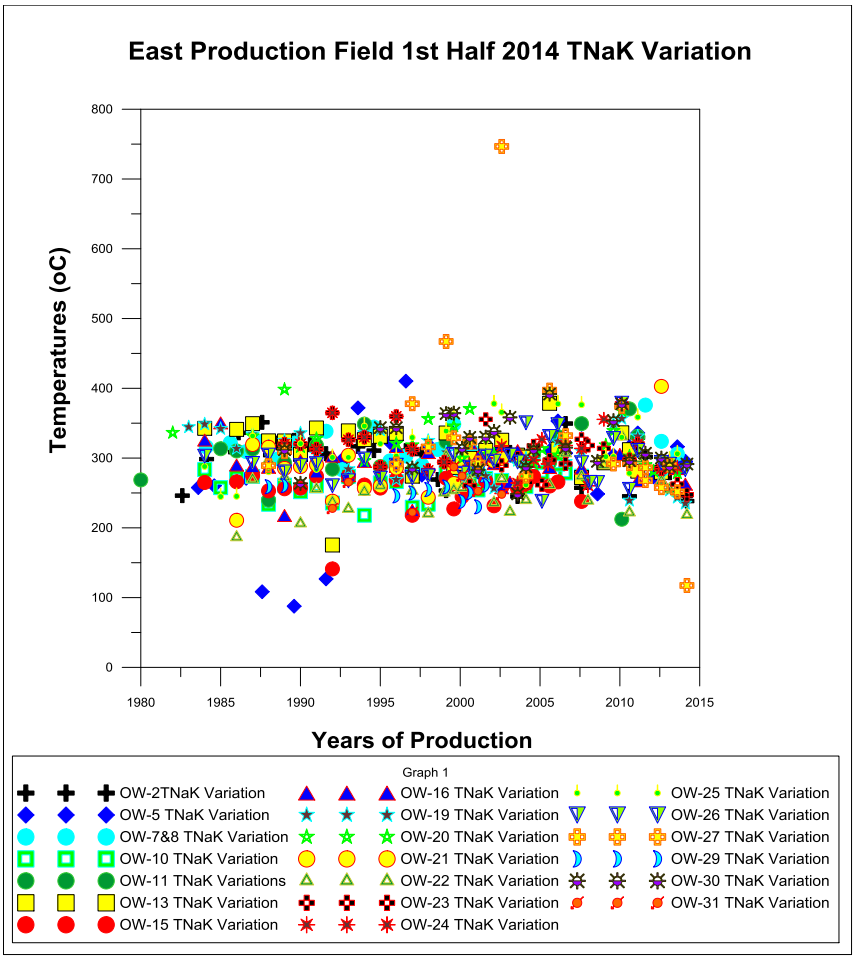

Figure 5.14: Measured reservoir temperatures in the EPF.

5.2.2.3 Reservoir Chloride Variation

The trend almost resembles the reservoir temperature one in a way, OW-5 has the highest values of chloride concentration and therefore thought to be tapping form deeper chloride rich reservoir (Fig. 5.15 and 5.16). The values then seem to decline SE wards through OW-16 through to OW-22 and OW-23 reaching lowest in OW-22. Also depicting the declining trend is OW-23 whose chloride concentration declined from about 700 ppm to 380 ppm. Such a trend could be an indication of dilution in the SE part of the EPF.

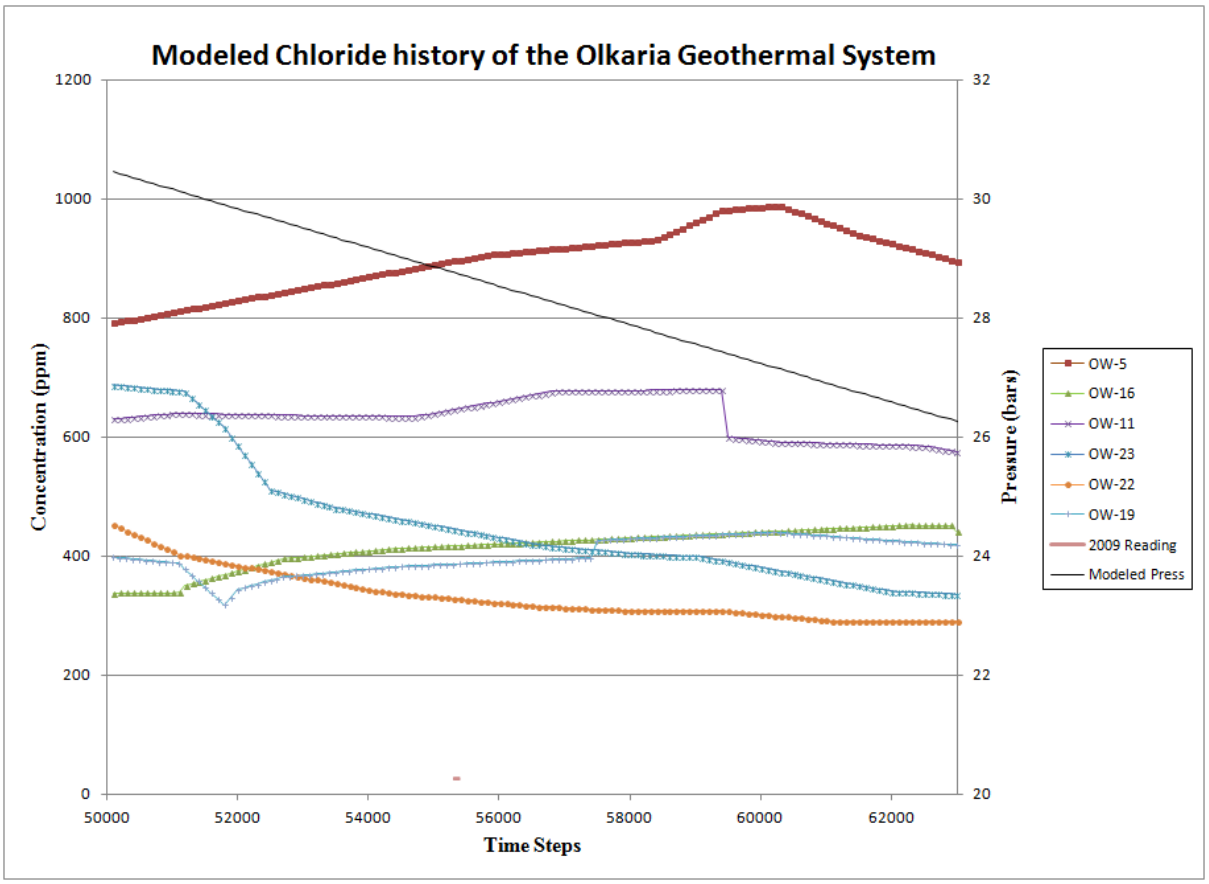

Figure 5.15: Modeled Chloride Concentrations in the EPF. Timesteps in seconds.

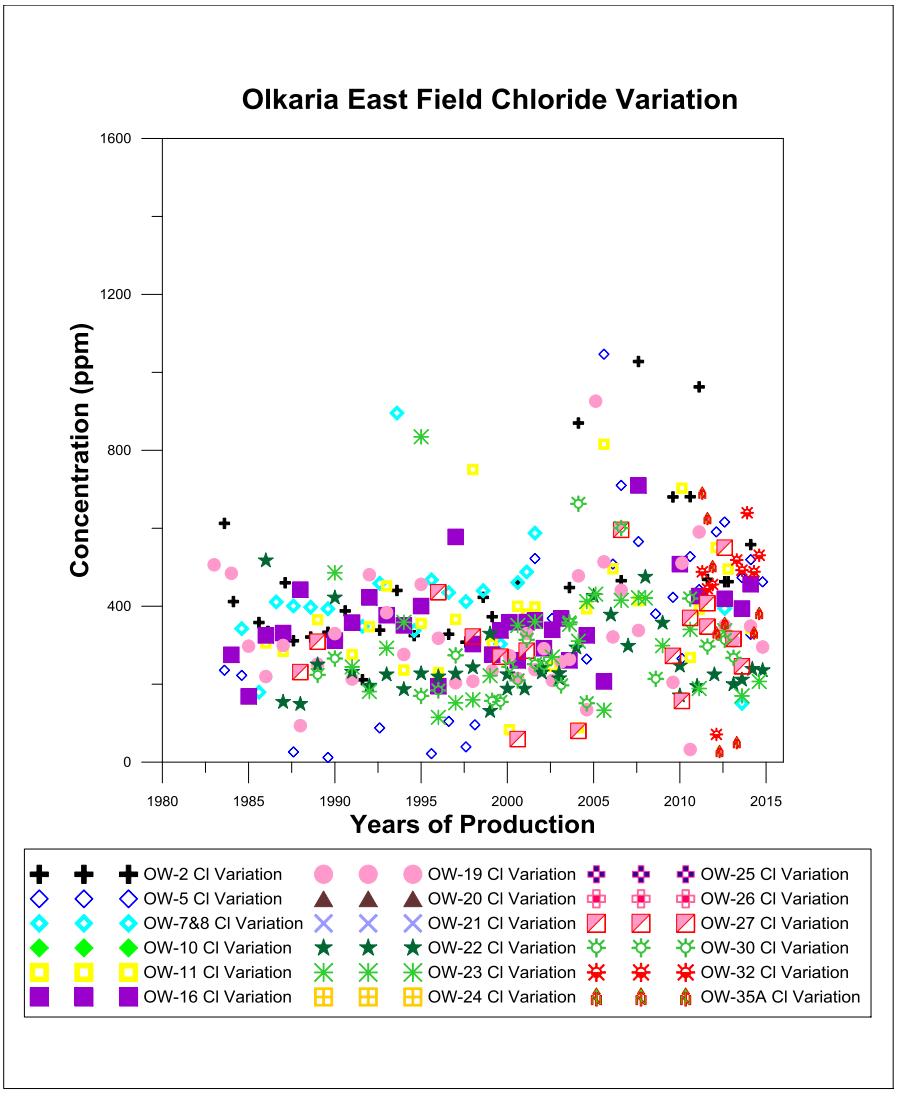

Figure 5.16 Measured Chloride Concentrations.

Overall, the shape and magnitude of the chloride concentrations predicted by the model closely match the conceptual model of the Olkaria EPF developed from various disciplines. Basically on the upflow areas which occur around the central part of the EPF (Fig.5.17) whereas the SE part acts as a recharge area through the young faults within the Olnjorrowa gorge.

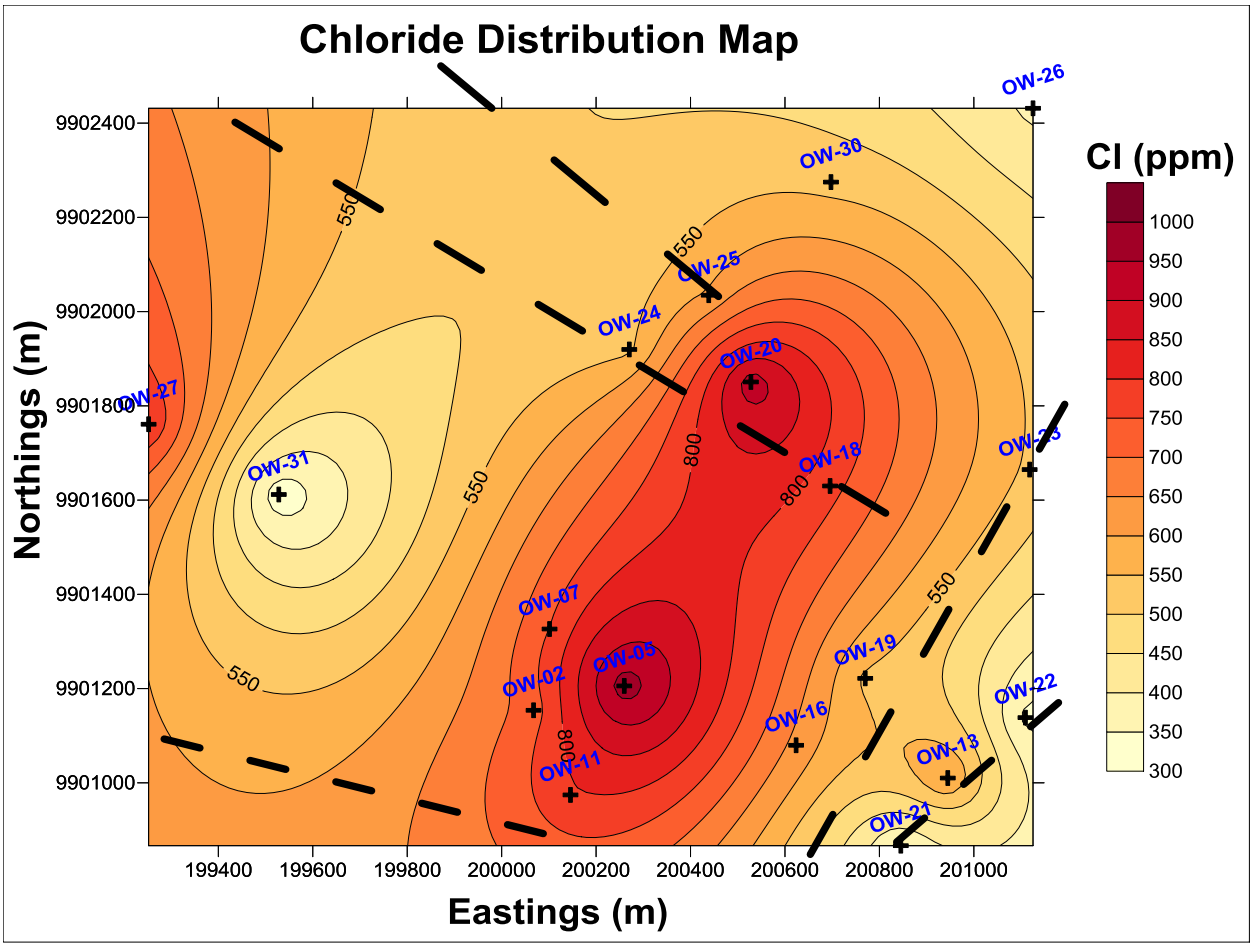

Figure 5.17: Reservoir Chloride Distribution Map at the initial state. The crosses indicate the location of the wells while the dashes indicate faults.

5.2.2.4 Reservoir Silica Variation

The variations give three regimes of A, B and C of concentration (Fig. 5.18 and 5.19). First is in the OW-5 whose values are high and on sharply increasing with values of above 700 ppm. This increase, as in the case of the chloride concentration, can be attributed to depressurization boiling especially in the central part of the EPF. The second regime has wells like OW-16, OW-11 and OW-19. These wells show a gradual but steady increase which was attributed to rising reservoir temperatures though at slower pace compared to those around OW-5. Lastly, OW-22 and OW-23 show declining trends, just as seen earlier, hence confirming the theory of dilution arising from declining pressures due to production hence allowing for entry of cooler waters on the periphery of the field.

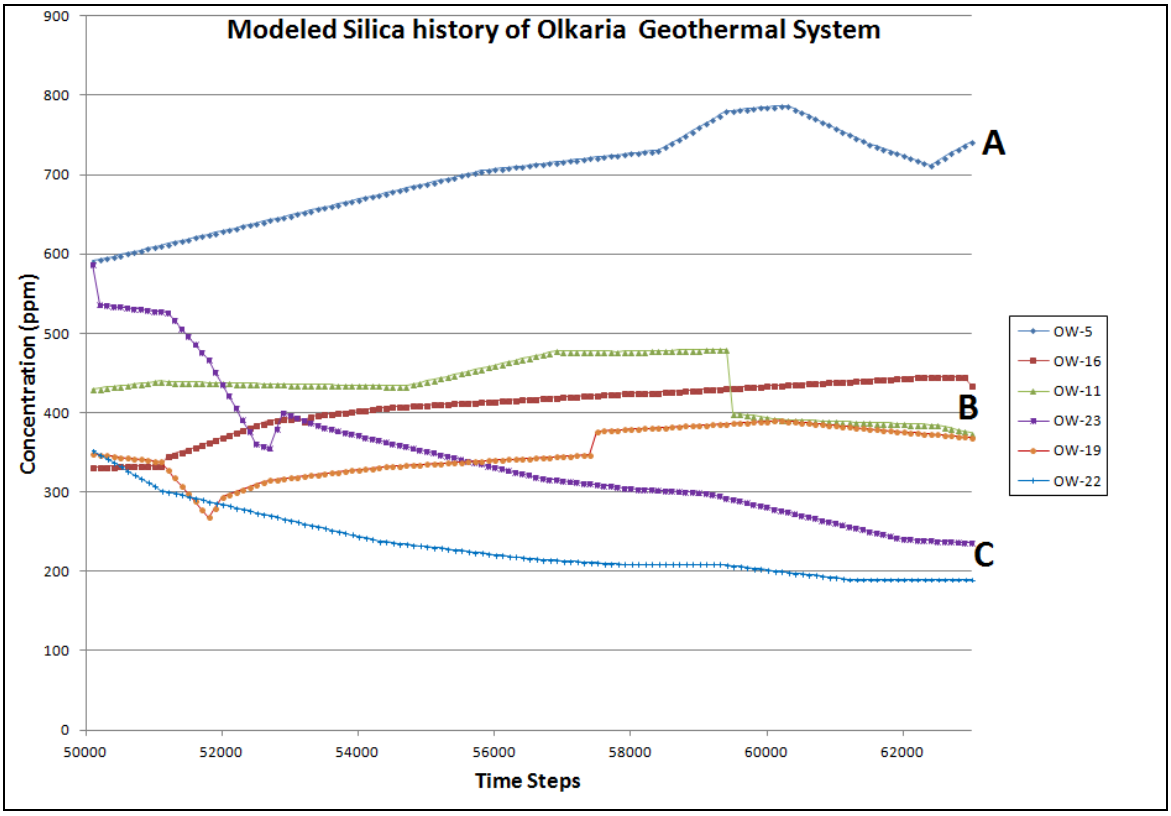

Figure 5.18 Modeled Silica Variations in the EPF. Timesteps in seconds.

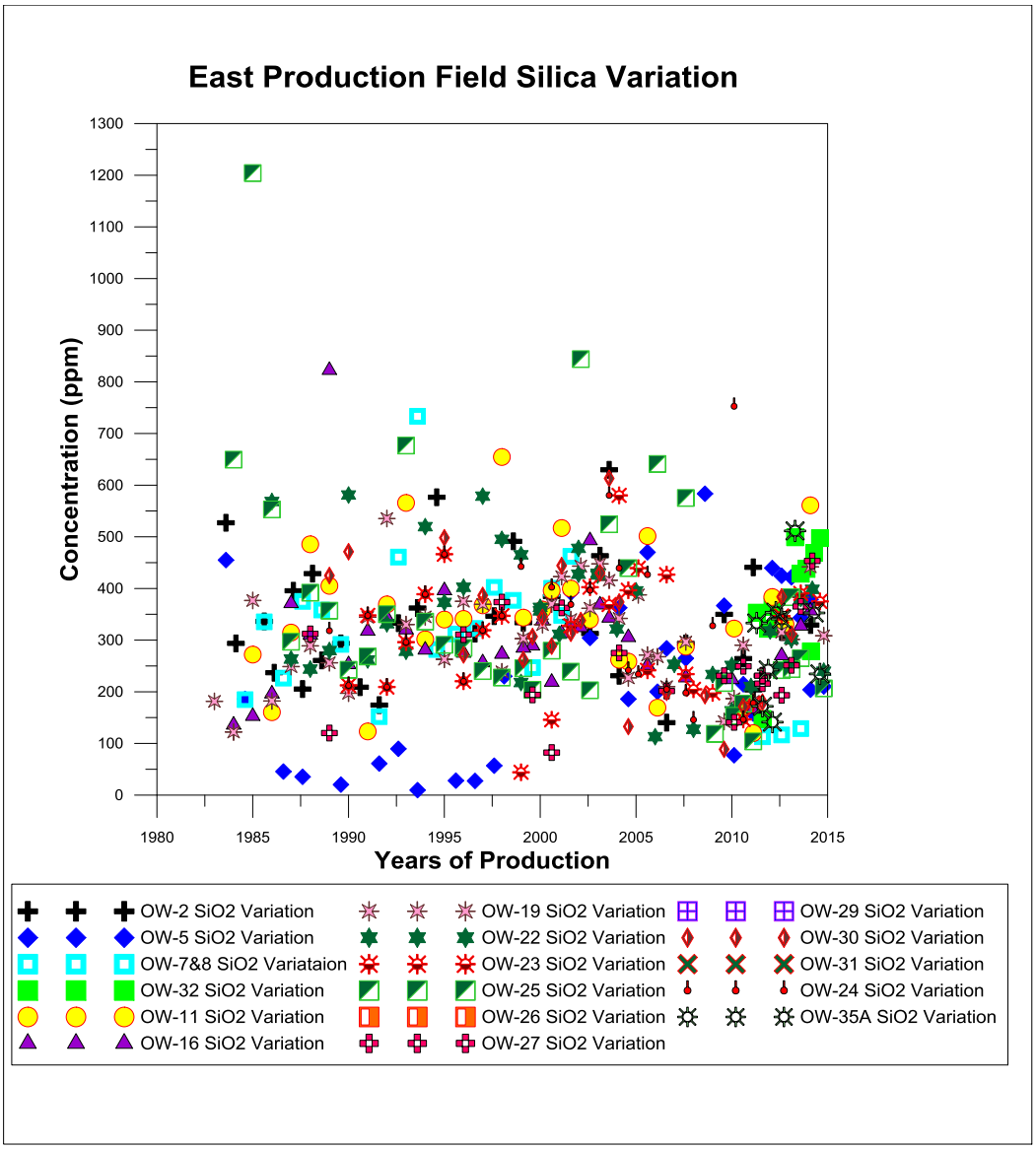

Figure 5.19: Measured Silica Variations in the EPF.

5.1.2.5 Reservoir Nitrogen Gas Variation

The nitrogen gas (N_2) was considered as the best indicator of incursion of atmospherically modified reservoir fluid mostly associated with dilution and cooling of geothermal reservoirs. OW-22 had the highest values followed by OW-23 (Fig.5.20 and 5.21). This therefore confirms an earlier interpretation that low solute concentrations and low temperatures are due to cooling and dilution by non-geothermal waters.

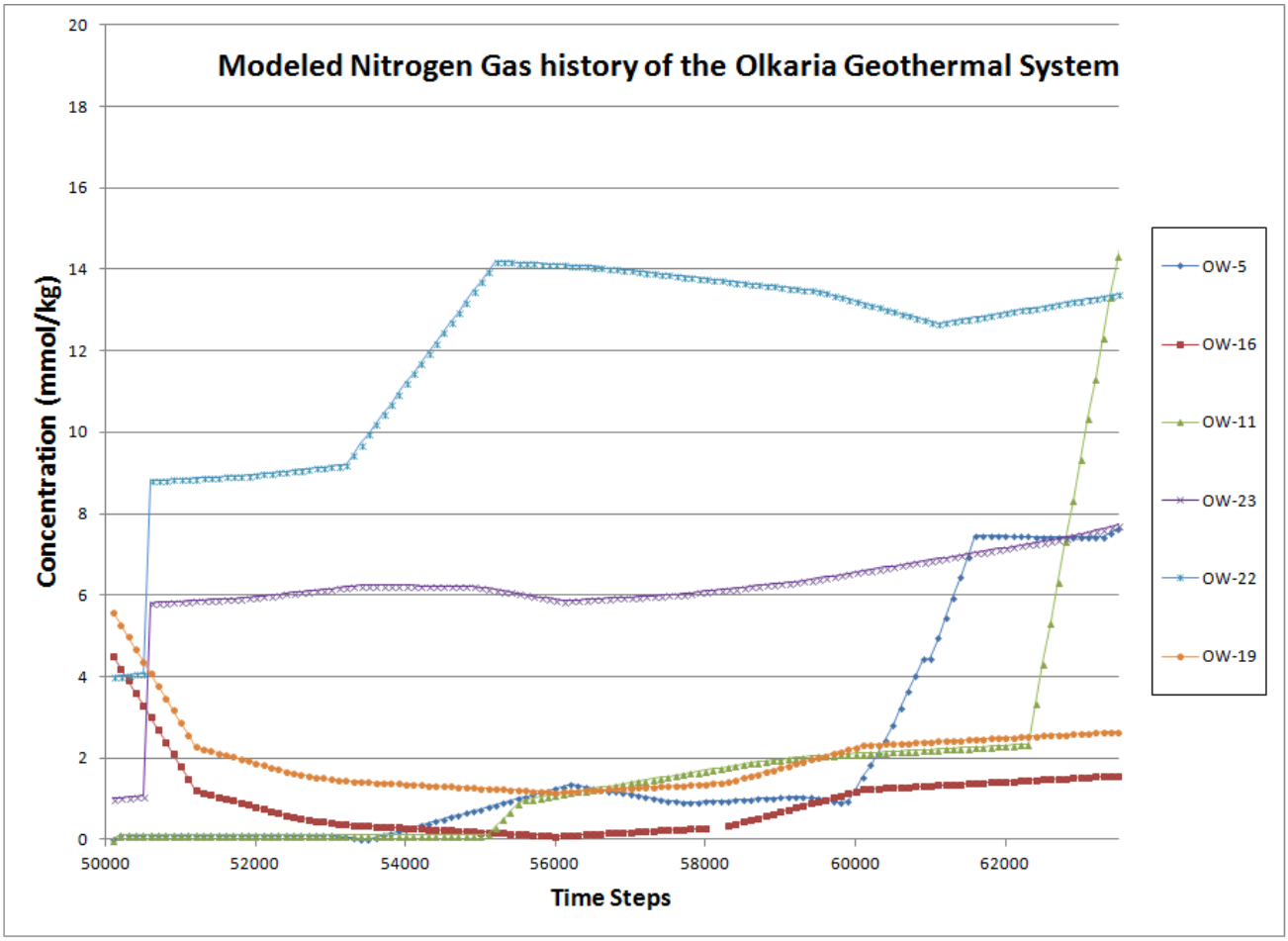

Figure 5.20: Modeled Nitrogen gas variation in the EPF. Timesteps in seconds.

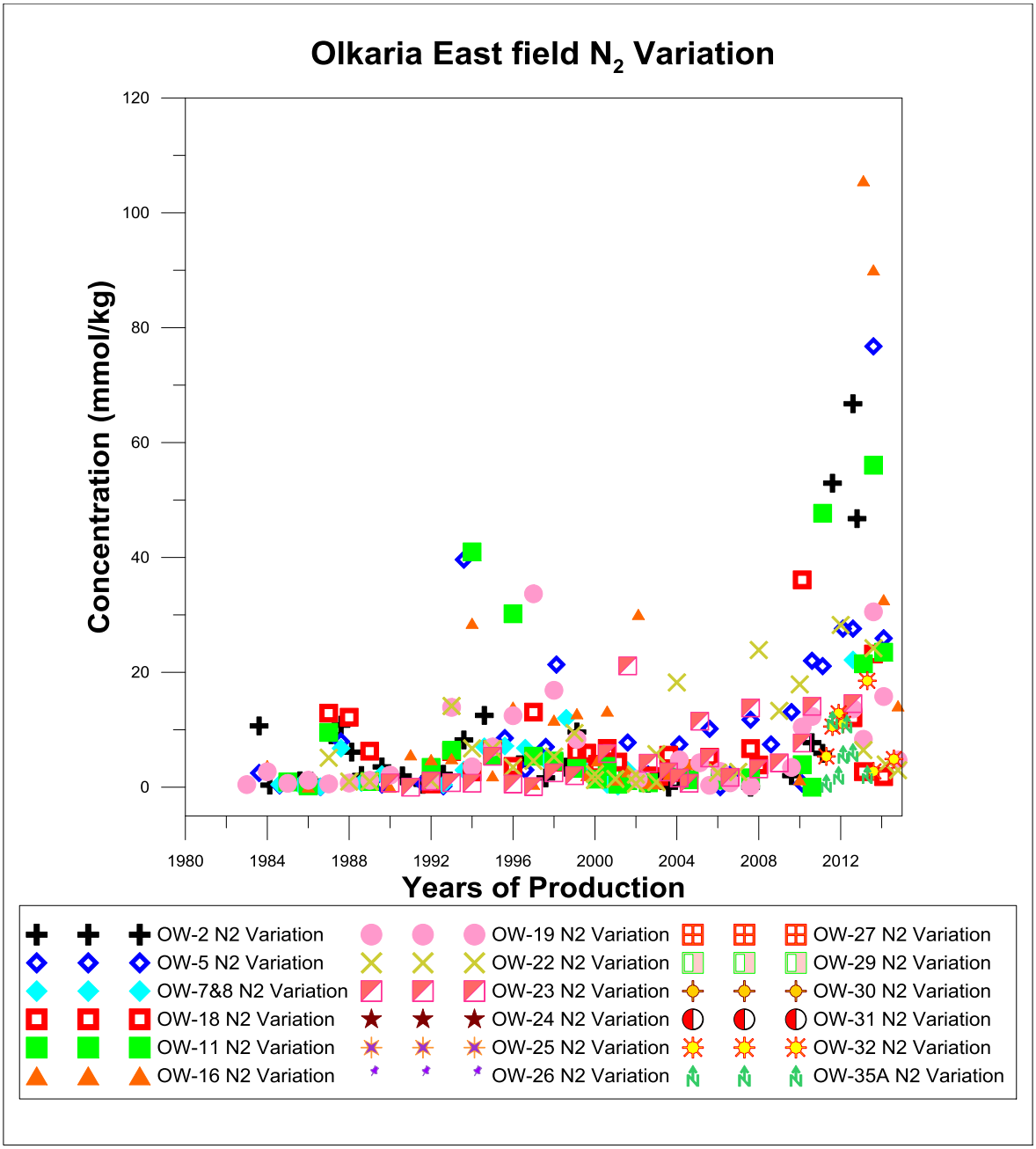

Figure 5.21: Measured Nitrogen gas variation in the EPF.

5.2.3 Forecasting

5.2.3.1 Chemical and temperature Variations in the Olkaria geothermal field without reinjection

5.2.3.1.1 Temperature Variations in the EPF without reinjection

The modeled temperatures give highest values in OW-5 at 300^{o}C whereas OW-22 and OW-16 had the least at 230^{o}C (Fig.5.22). With the existing conditions, OW-5 and OW-19 reach stable temperatures at 78000 time step that level out at 98000 time step and 90000 time step respectively. This therefore means that OW-5, without reinjection, will sustain production to 2028 compared to 2025 of OW-19. OW-16 reaches equilibrium temperatures earliest at 70000 time step whereas OW-22 has the shortest period of equilibrium temperatures.

These trends can be attributed to the fact that, wells on the SE part of the EPF are most affected by mixing and dilution processes leading to reduction in the solutes concentrations and temperatures. This is further augmented by drop in reservoir pressures due to minimal reinjection.

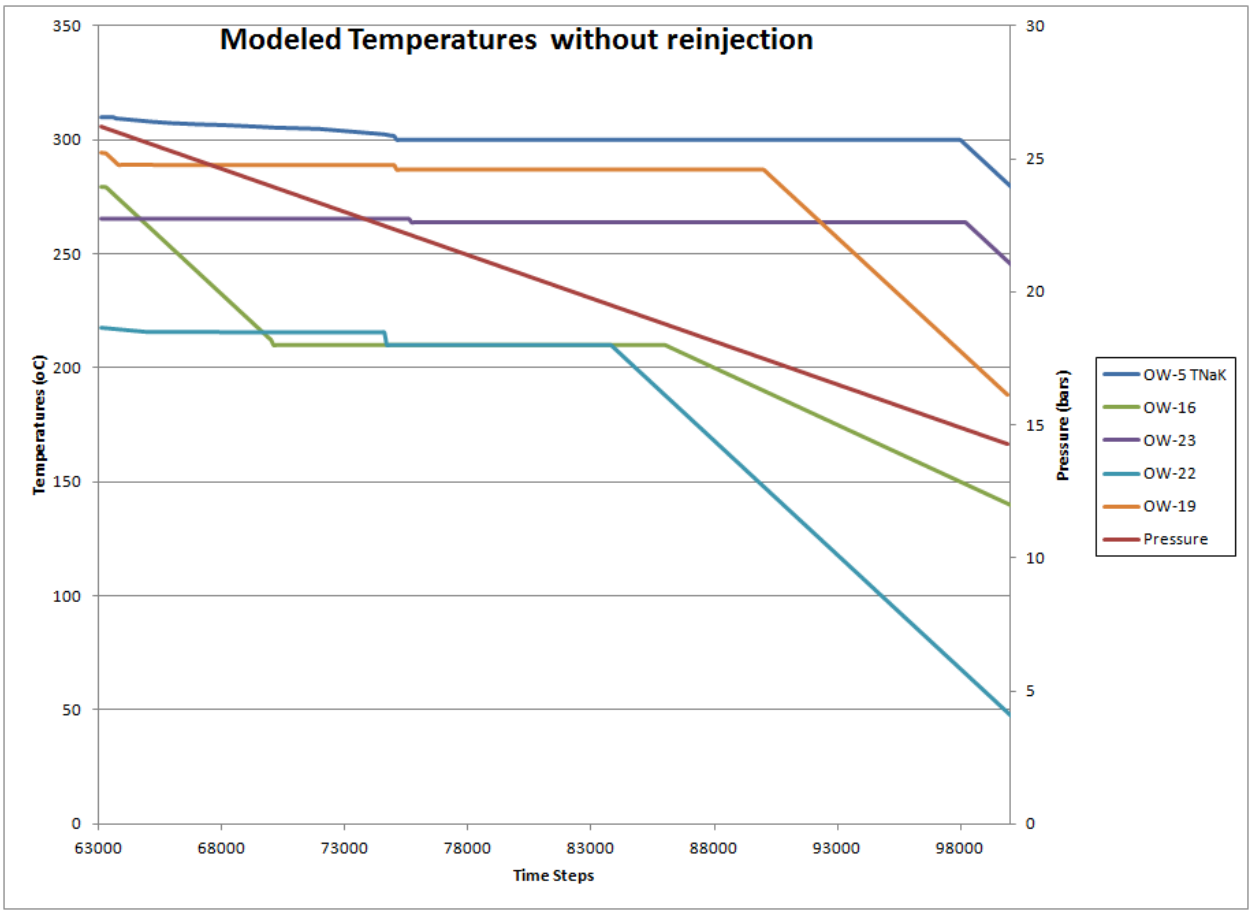

Figure 5.22: Modeled Temperatures for Shallow wells without reinjection.

The new deep wells have their temperatures forming an inverted U plot (Fig. 5.23) i.e. the temperatures sharply rise to the 78000 time step, stabilizes to around 83000 time step before starting to fall. OW-38 has the least temperatures followed by OW-37A and OW-39 respectively.

Overall, the effect of minimal reinjection is evident when the trends start falling sharply at the 83000th time step implying that, at the current rate of production deep wells will drastically reduce by 2022 as the reservoir would have experienced severe pressure drop.

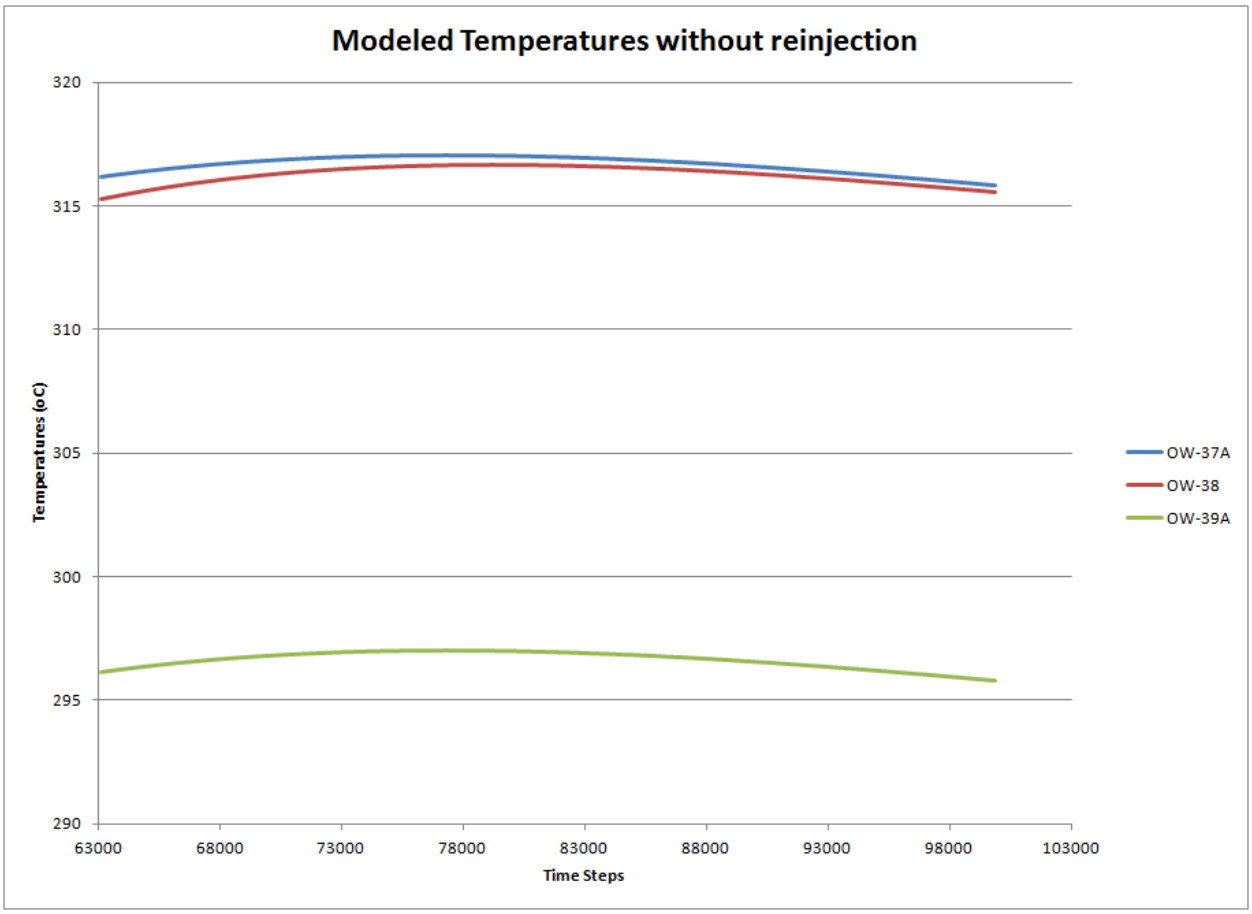

Figure 5.23: Modeled Temperatures for Deep wells without reinjection.

5.2.3.1.2 Sulfate Variations in the EPF without reinjection

The Sulfate trends show high values of 50ppm in OW-5 and reach equilibrium at the 75000th time step (Fig. 5.24). The other wells have values between 10 and 30ppm. OW-16 had its values steadily falling to zero. This is an indication that the well receives water with less oxygen in it compared to OW-19 which lies on its east (Fig.5.17). Besides that, the well tends to receive cool temperature waters hence minimal oxidation of H_2S to SO_4 arising from the condensation of steam.

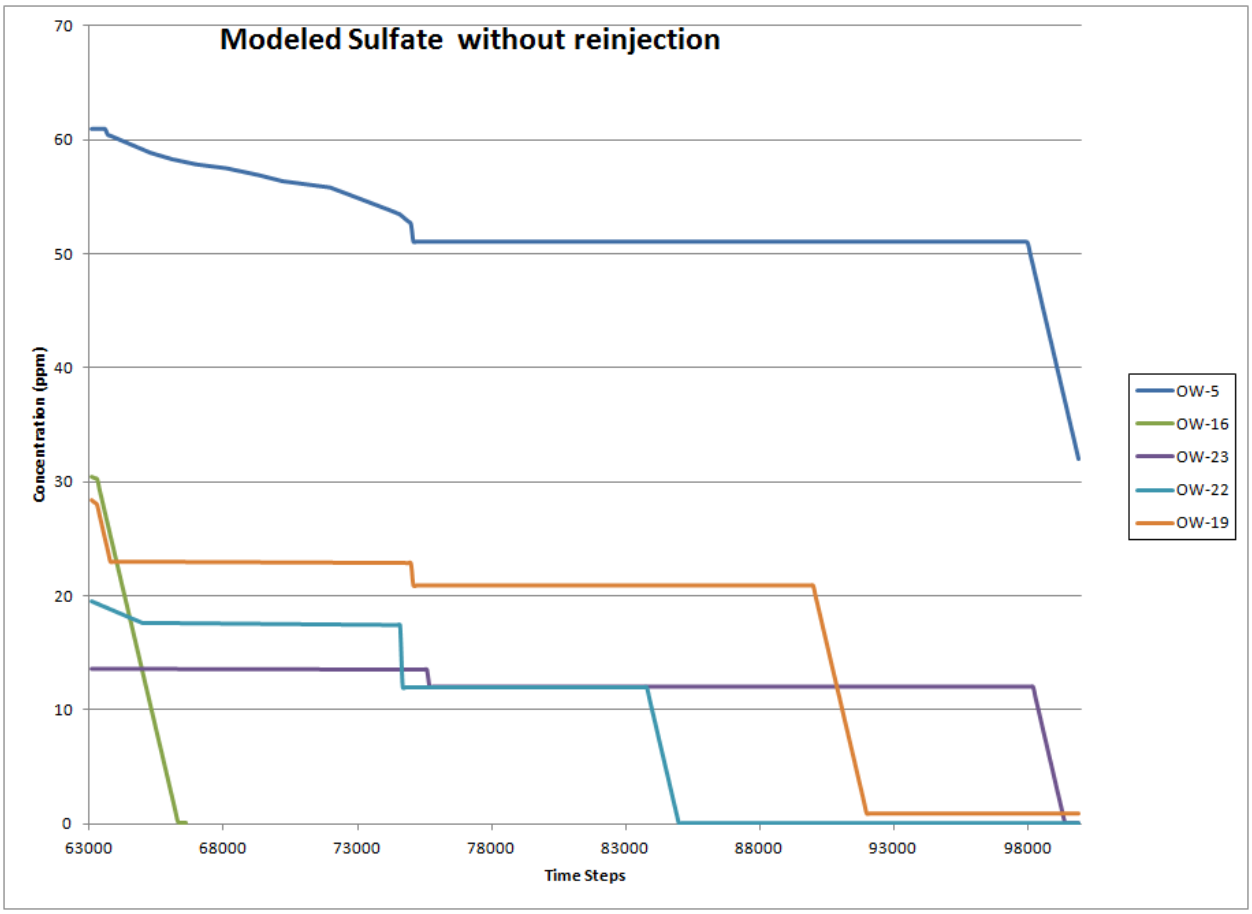

Figure 5.24: Modeled Sulfate for Shallow wells without reinjection.

The sulfates, in deep wells (OW-37A, OW-38 and OW-39) have the same trend as the modeled temperatures (Fig. 5.25). OW-38 has the least values followed by OW-37A and then OW-39A. This is as a result of oxidation of H_2S to SO_4 arising from the condensation of steam formed from the depressurization boiling.

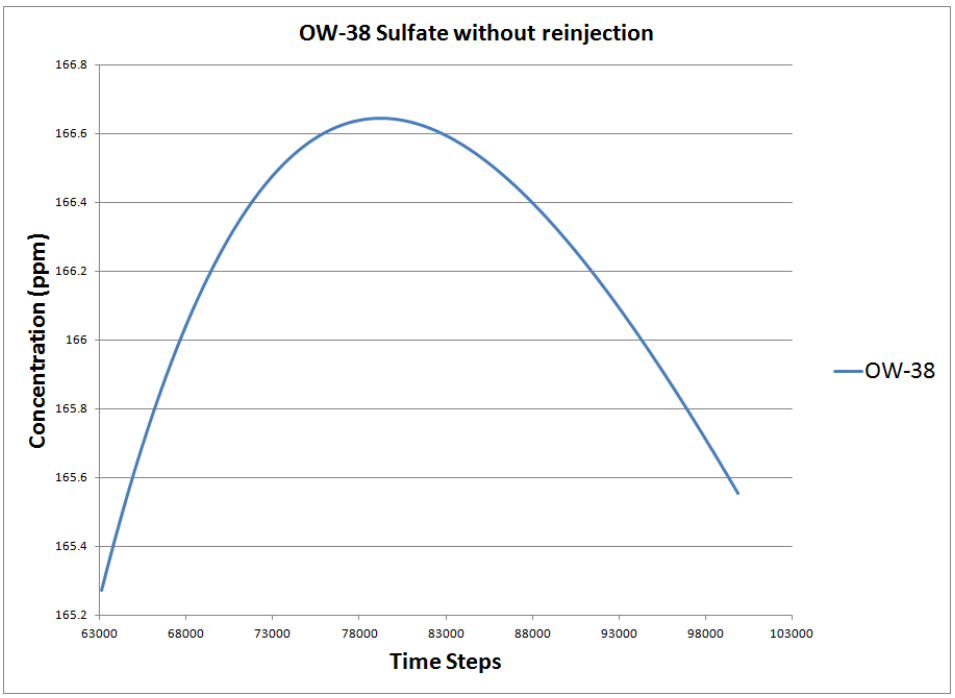

Figure 5.25a: OW-38 Modeled sulfate without reinjection

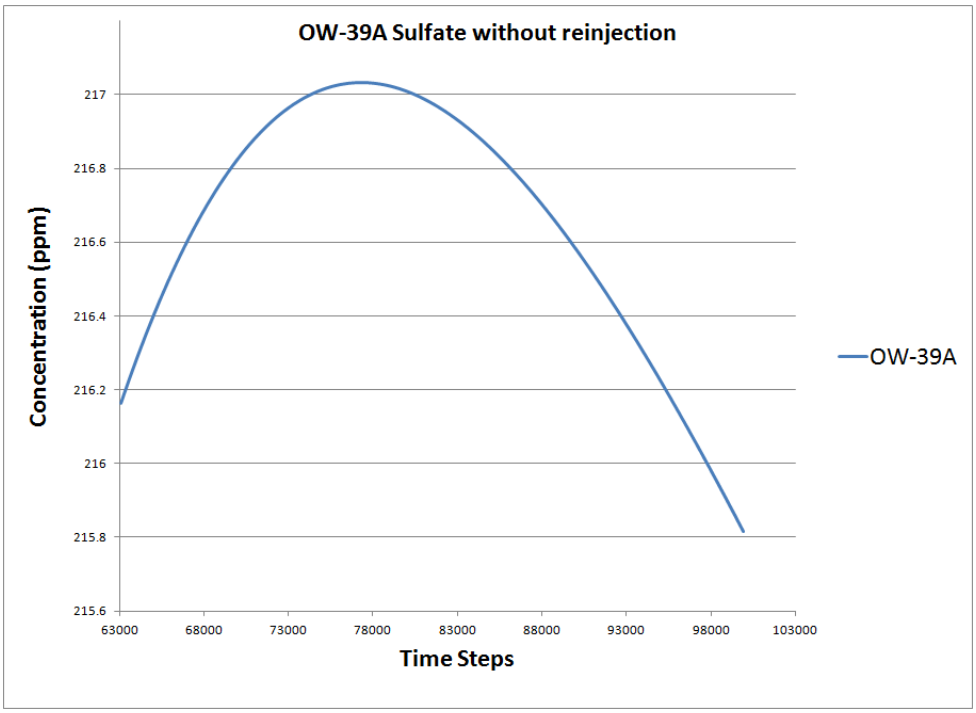

Figure 5.25b: OW-39A Modeled sulfate without reinjection

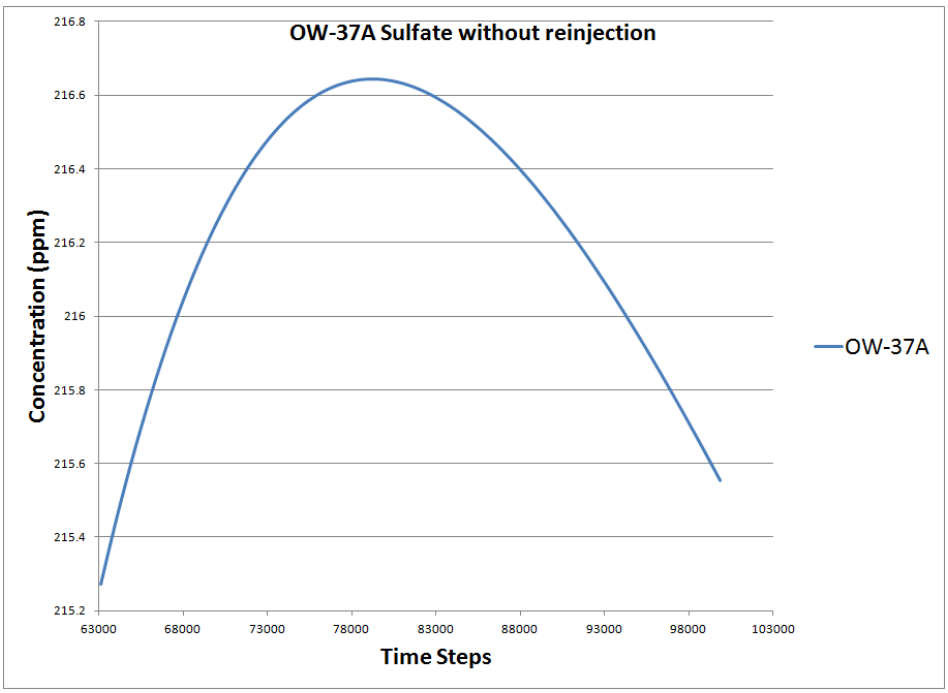

Figure 5.25c: OW-37A Modeled sulfate without reinjection

Figure 5.25: Modeled Sulfate for Deep wells in EPF without reinjection.

5.2.3.1.3 Silica Variations in the EPF without reinjection

The trend in the silica resemble that of the chloride (refer to section 5.2.4) in such a way, well OW-5 had the highest value for silica concentration (450ppm) that reached equilibrium at the 73000th time step. This is also indicative of increased chance of silica scaling in OW-5 followed by OW-19 with a silica concentration of 350ppm. The risk is much lower in OW-22 that has the least value for silica of 220ppm which reaches equilibrium between the 75000th and 83000th time step (Fig. 5.26).

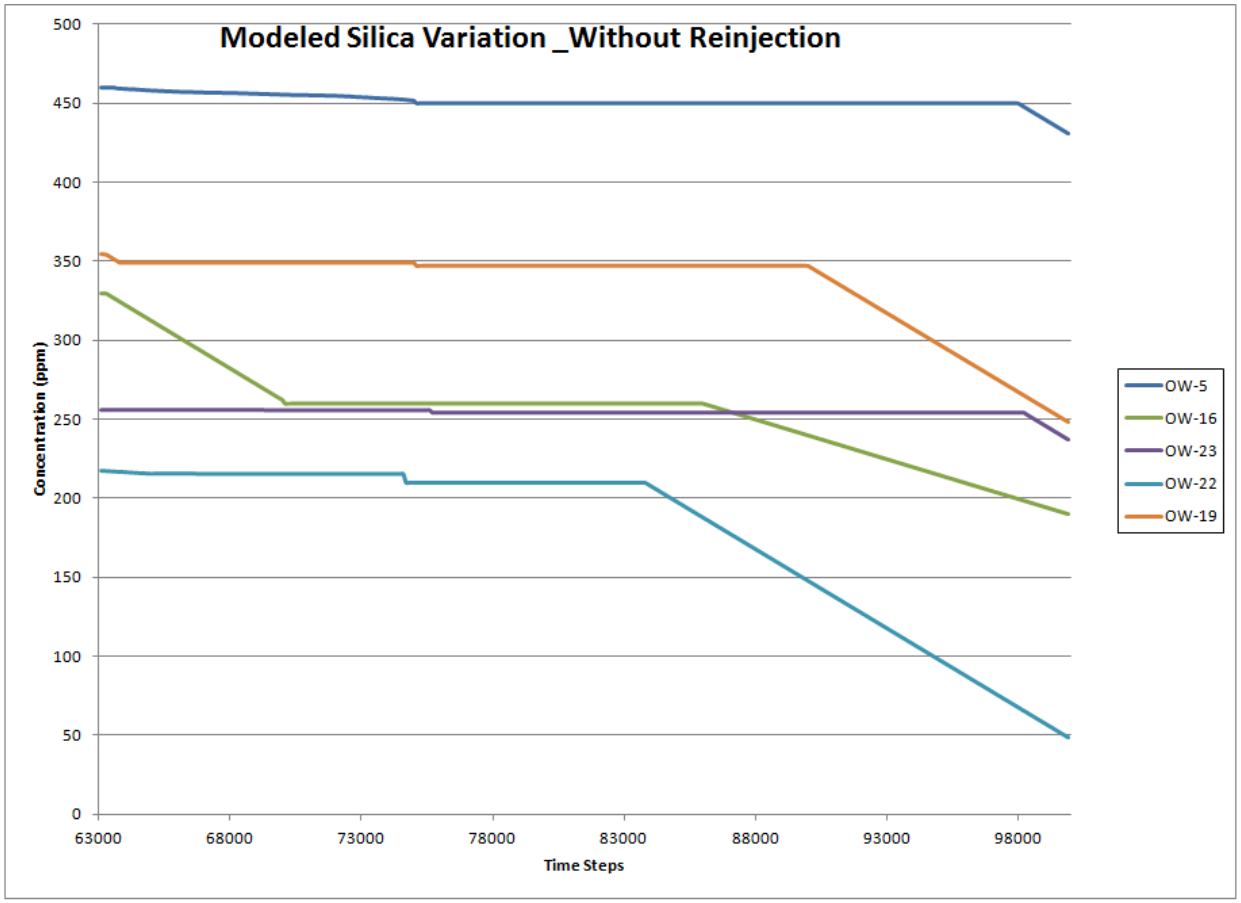

Figure 5.26: Modeled Silica for shallow wells in EPF without reinjection.

The inverted U shape is also seen in the trends of silica of deep wells (Fig. 5.27). This is attributed to depressurization boiling that leads to formation of steam with very low water content. The decline after the 88000th time step is thought to be partly arising from dilution by the steam condensate and incursion of cooler fluids due to reservoir pressure drop.

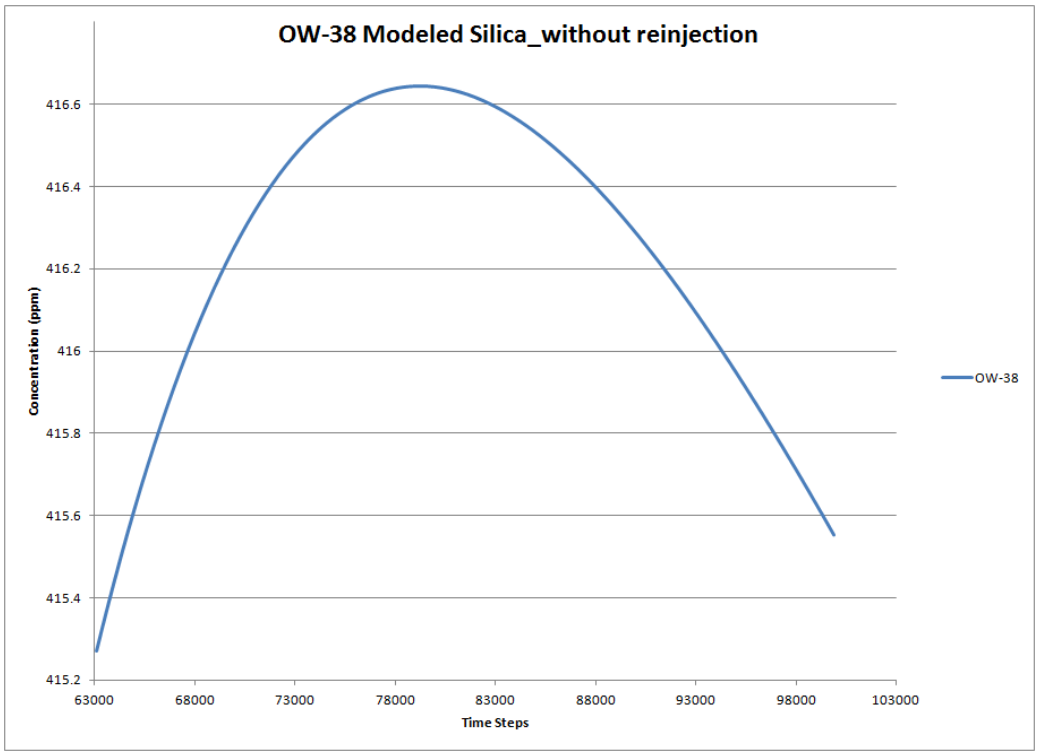

Figure 5.27a: OW-38 Modeled silica without reinjection

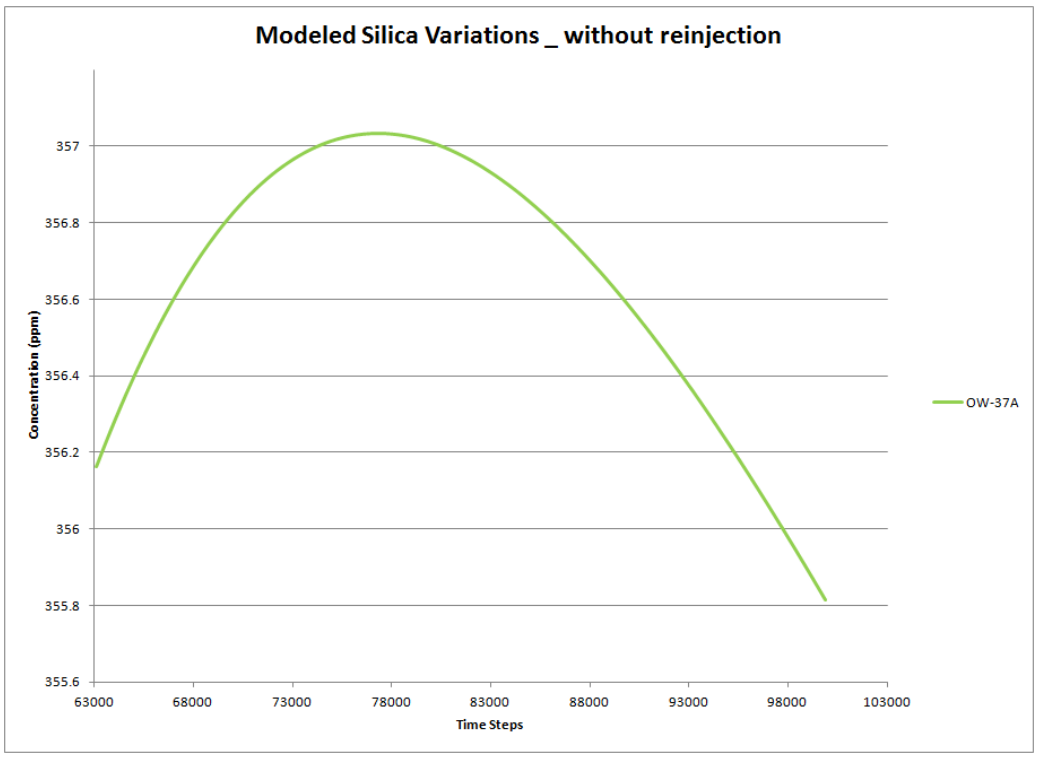

Figure 5.27b: OW-37A Modeled silica without reinjection

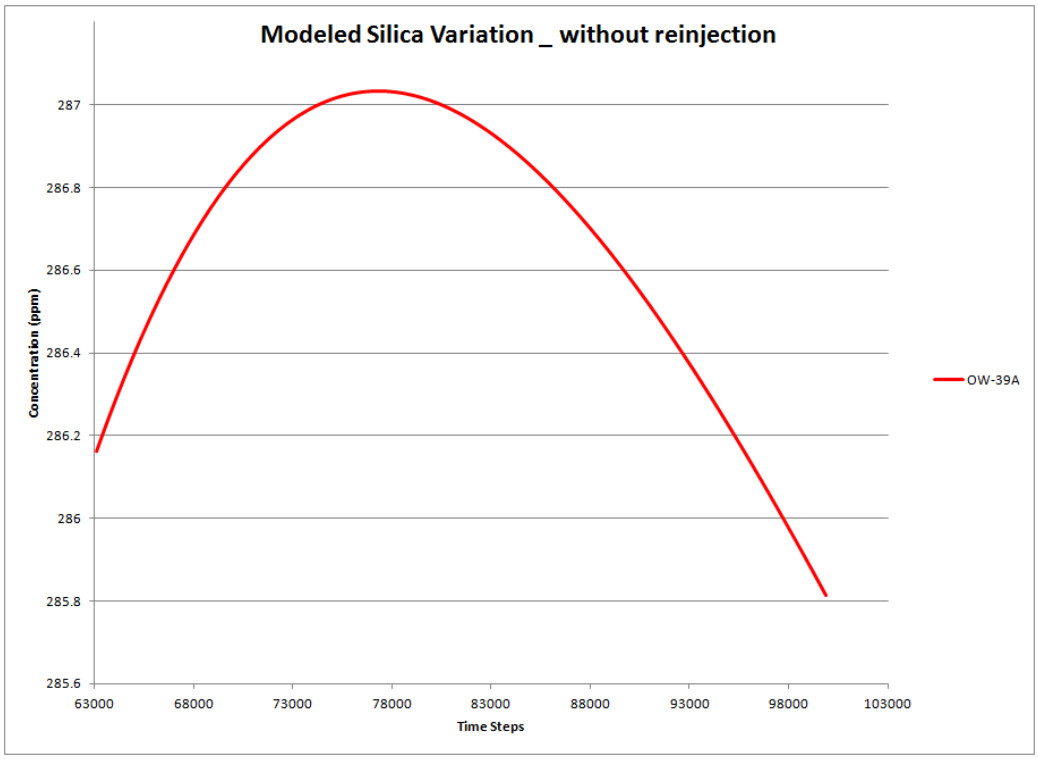

Figure 5.27c: OW-39A Modeled silica without reinjection

Figure 5.27: Modeled Silica for Deep wells in EPF without reinjection.

5.2.3.2 Chemical Variations in the EPF with reinjection

The study assumed an enclosed system in brine collection system in a manner that all the brine collected in generating approximately 170 Mw will be reinjected in designated reinjection wells i.e. OW-21, OW-13, OW-7 and OW-R5. Assuming an average steam conversion of 3t/Mw, then the 170 Mw will have 510t/hr of brine being reinjected.

5.2.3.2.1 Modeled Temperatures with reinjection

All the wells showed an increase in the temperatures to the 68000th time step except OW-16 (Fig.5.28). This is perhaps due to its proximity to the blocks for reinjection hence lower rate of temperatures recovery. The temperatures then level out to the end of the prediction period giving average values of about 300^{o}C.

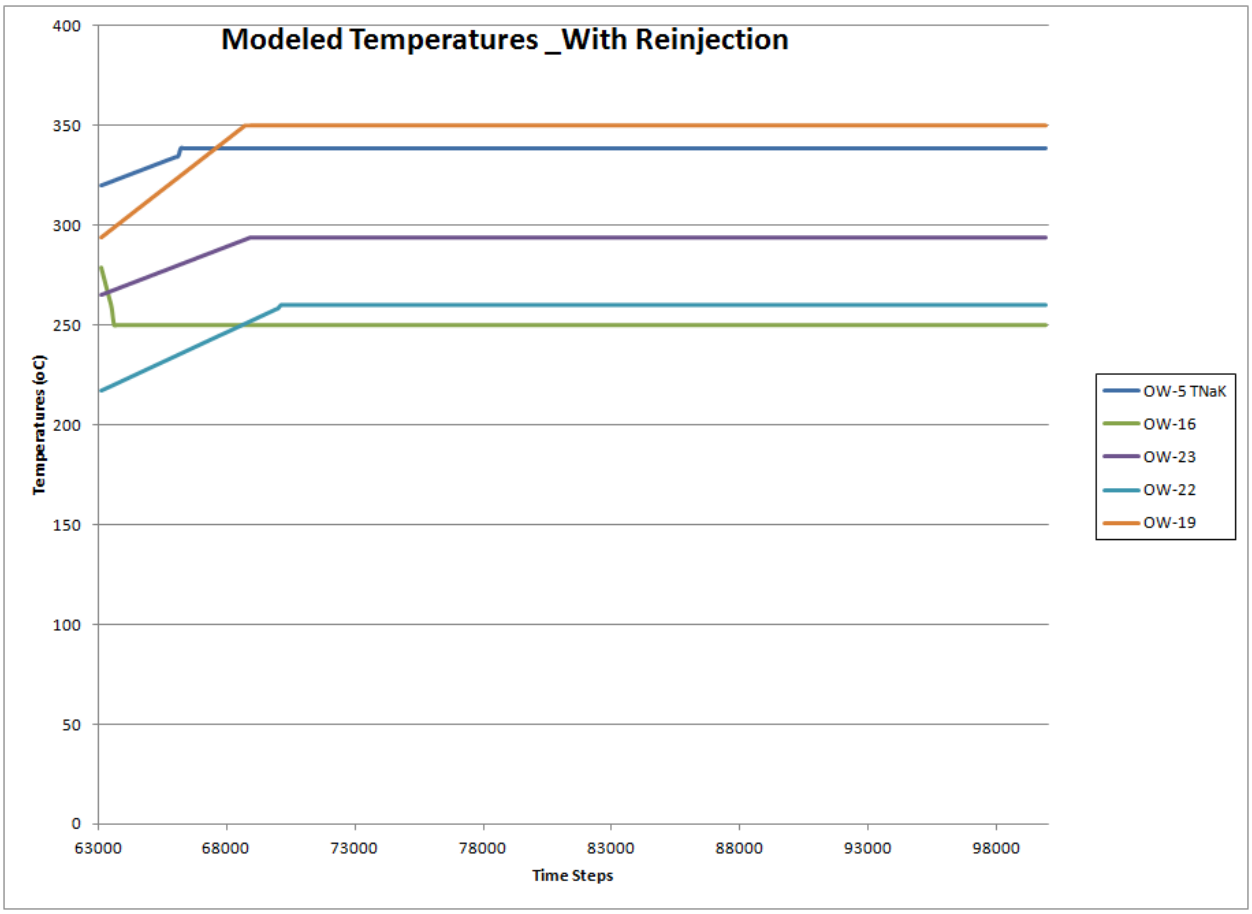

Figure 5.28: Modeled Reservoir temperatures for shallow wells in EPF with reinjection.

The deep wells also register average modeled temperatures of about 300^{o}C with the same trend as seen in the shallow wells (Fig 5.29). OW-38 located at the interpreted upflow zone of the EPF having the highest temperatures followed by OW-37A then OW-39A contrary to the wells without reinjection trend where OW-38 had the least temperatures. This phenomenon can be attributed to the fact that with adequate reinjection, the reservoir pressures will be maintained hence minimizing incursion of cooler waters together with cooling due to steam condensation.

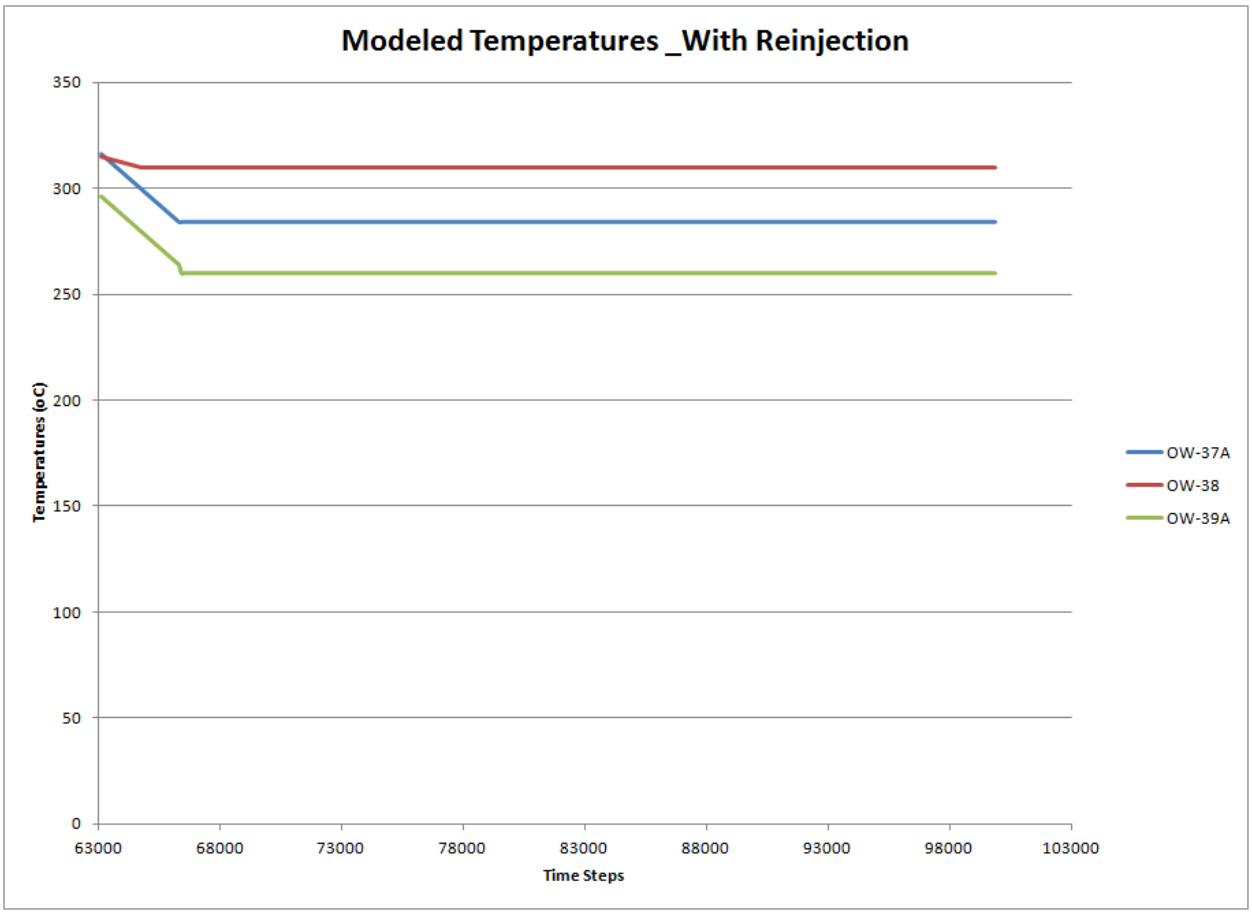

Figure 5.29: Modeled Reservoir temperatures for deep wells in EPF with reinjection.

5.2.3.2.2 Modeled Silica variations with reinjection

The trends resemble that of modeled temperatures in both shallow and deep wells (Fig.5.30 and Fig. 5.31) i.e. the shallow wells showed a slight increase whereas deep ones showed a decline to the 68000th time step before leveling out. This is indicative of the fact that shallow wells experience dilution arising from incursion of cool, non-geothermal waters arising from pressure drop.

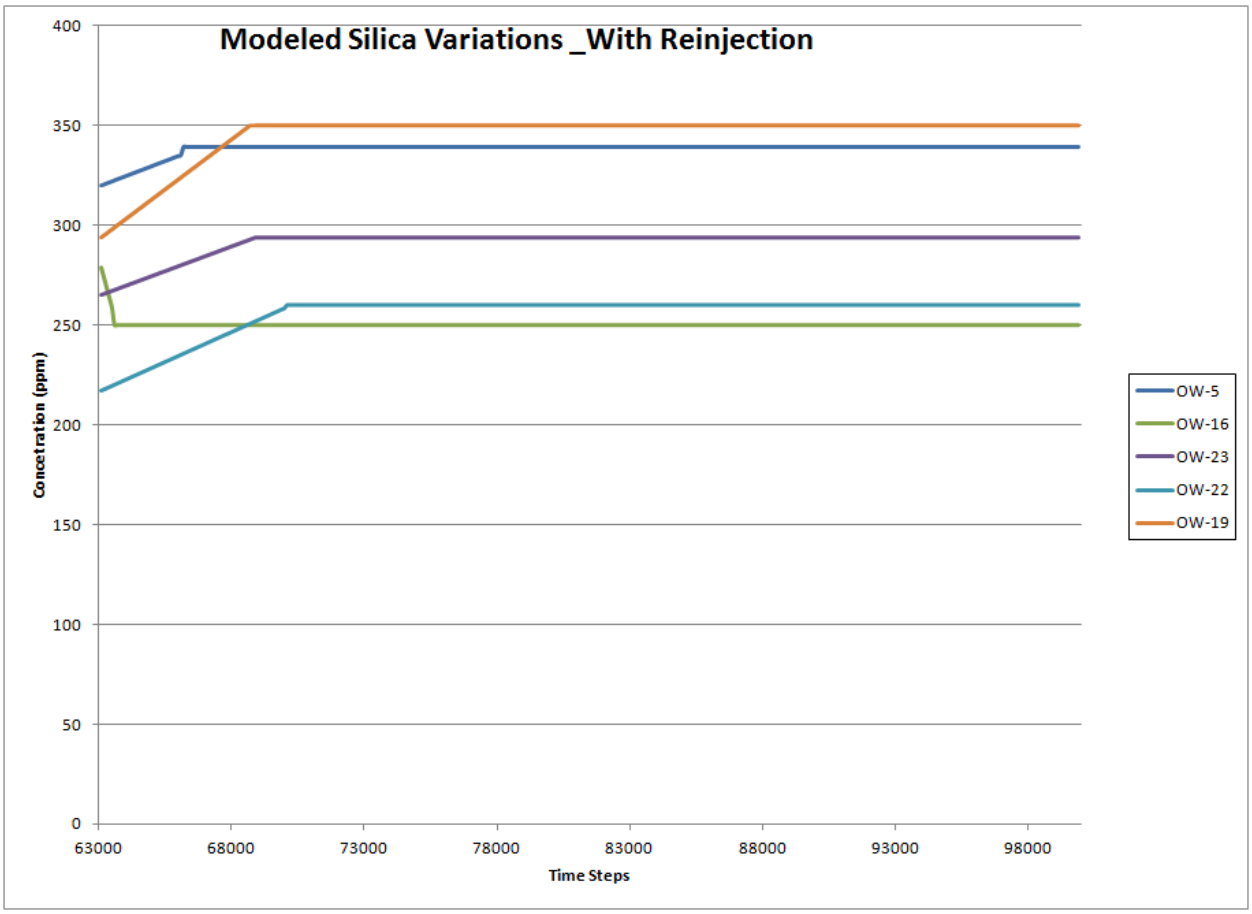

Figure 5.30: Modeled Silica for shallow wells in EPF with reinjection. Timesteps in seconds.

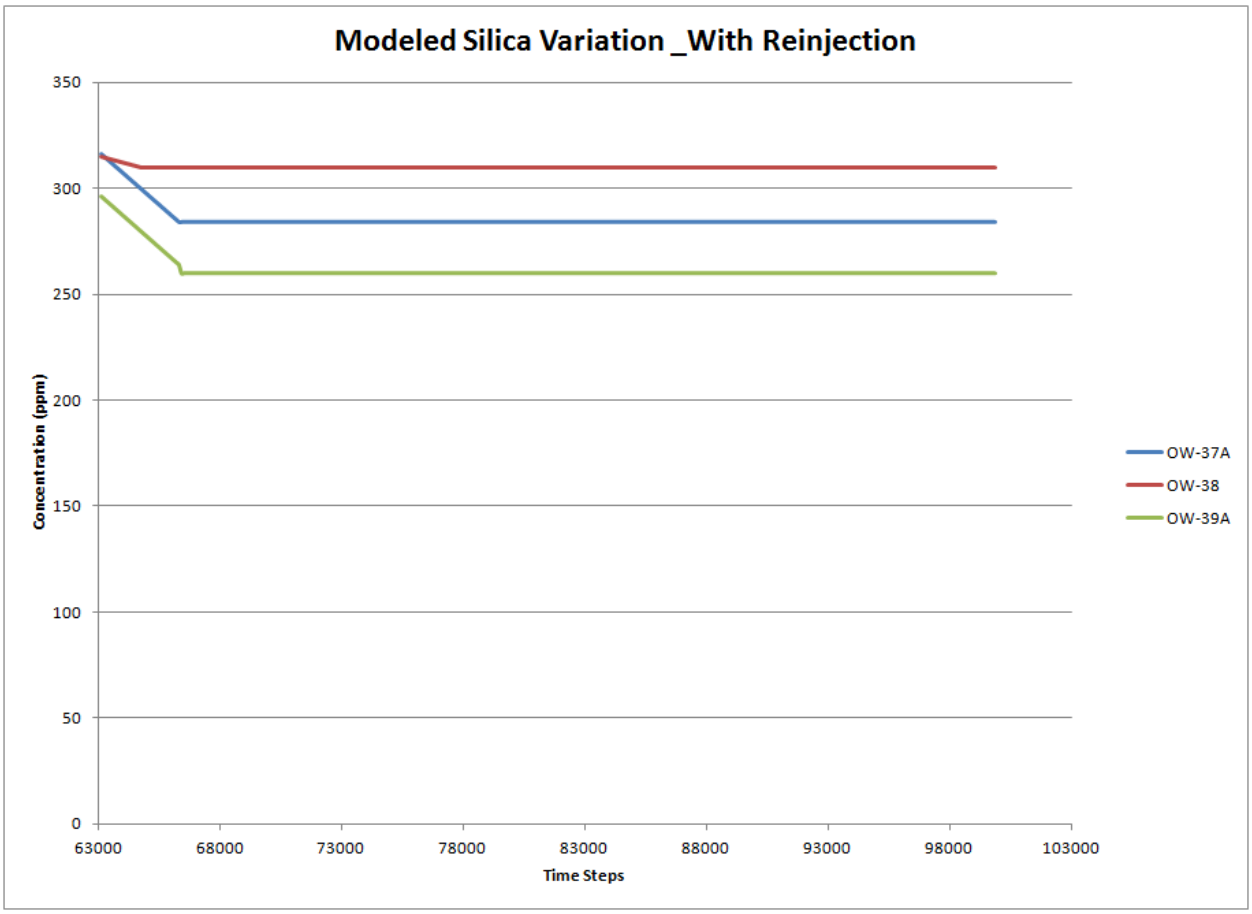

Figure 5.31: Modeled Silica for deep wells in EPF with reinjection. Timesteps in seconds.

5.2.3.2.3 Chemical Variations in the Domes Field without reinjection

The temperatures of the selected wells show a gradual decline (Fig. 5.32). OW-915A (located at the Domes upflow zone) had the highest temperatures between 325-310^{o}C whereas OW-907A had the least values between 290 -275^{o}C.

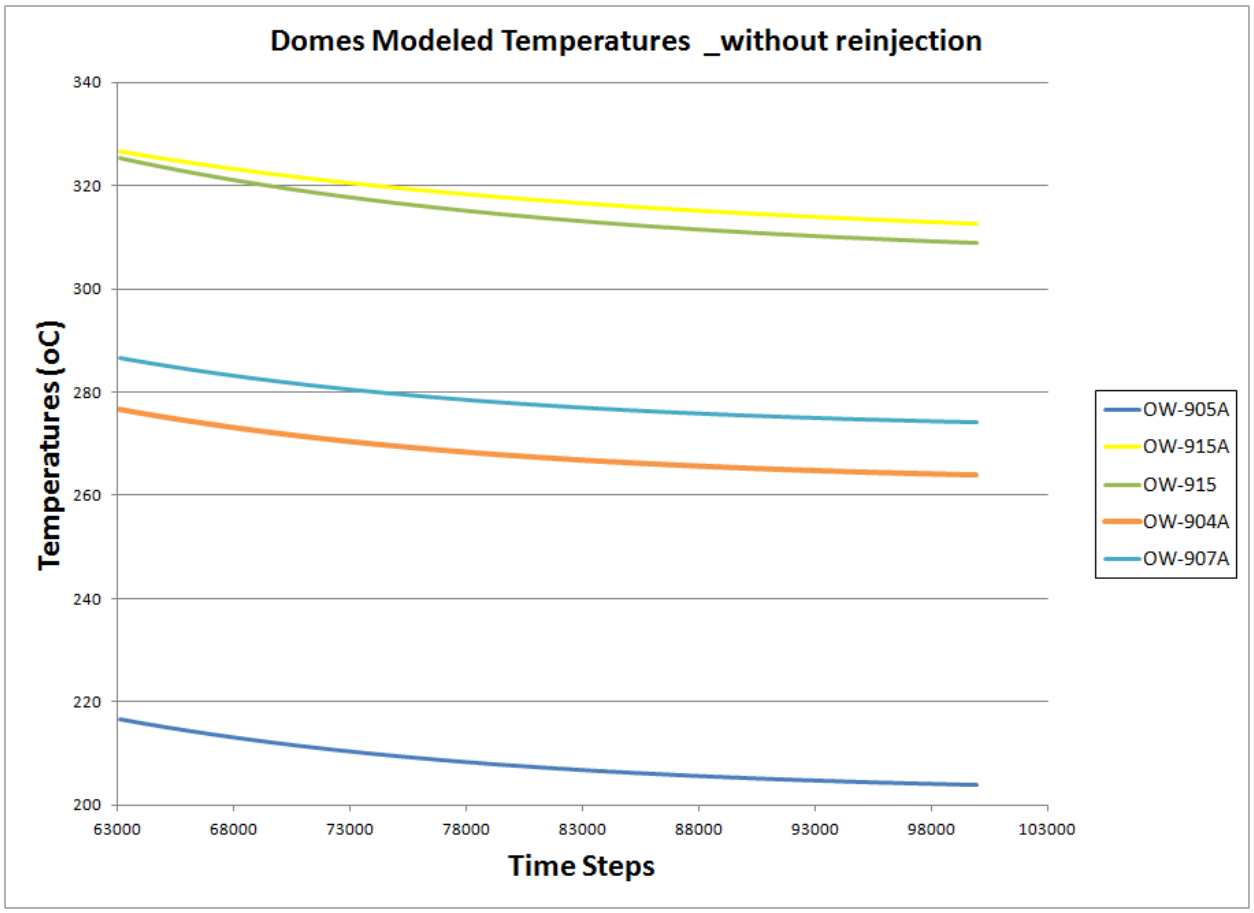

Figure 5.32: Modeled Temperatures for wells in the Domes without reinjection. Timesteps in seconds.

The sulfate graphs show the same trends for the wells in the upflow i.e. high values in OW-915A and OW-915 that gradually decline (Fig. 5.33). OW-905A and OW-907A which had lowest temperatures also have the lowest values of around 120 ppm.

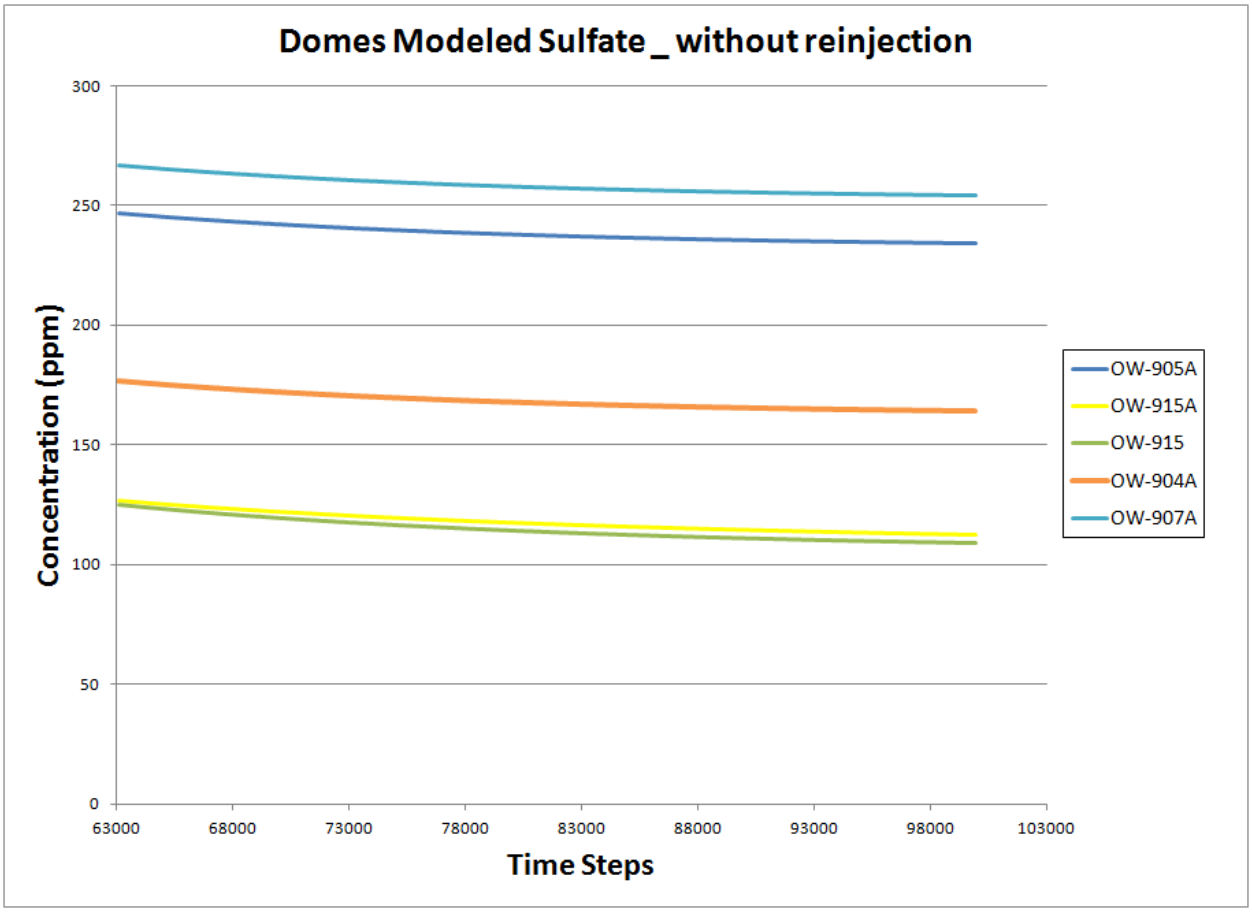

Figure 5.33: Modeled Sulfate for wells in the Domes without reinjection. Timesteps in seconds.

5.2.3.2.4 Chemical Variations in the Domes Field with reinjection

The temperatures average to about 300^{o}C. The individual well temperatures show a slight increase in OW-915, OW-915A and OW-907A. The well OW-905A has the least temperatures that showed a slight decline. This observation can be attributed to the recharge by the NW-SE trending faults (Fig.5.34).

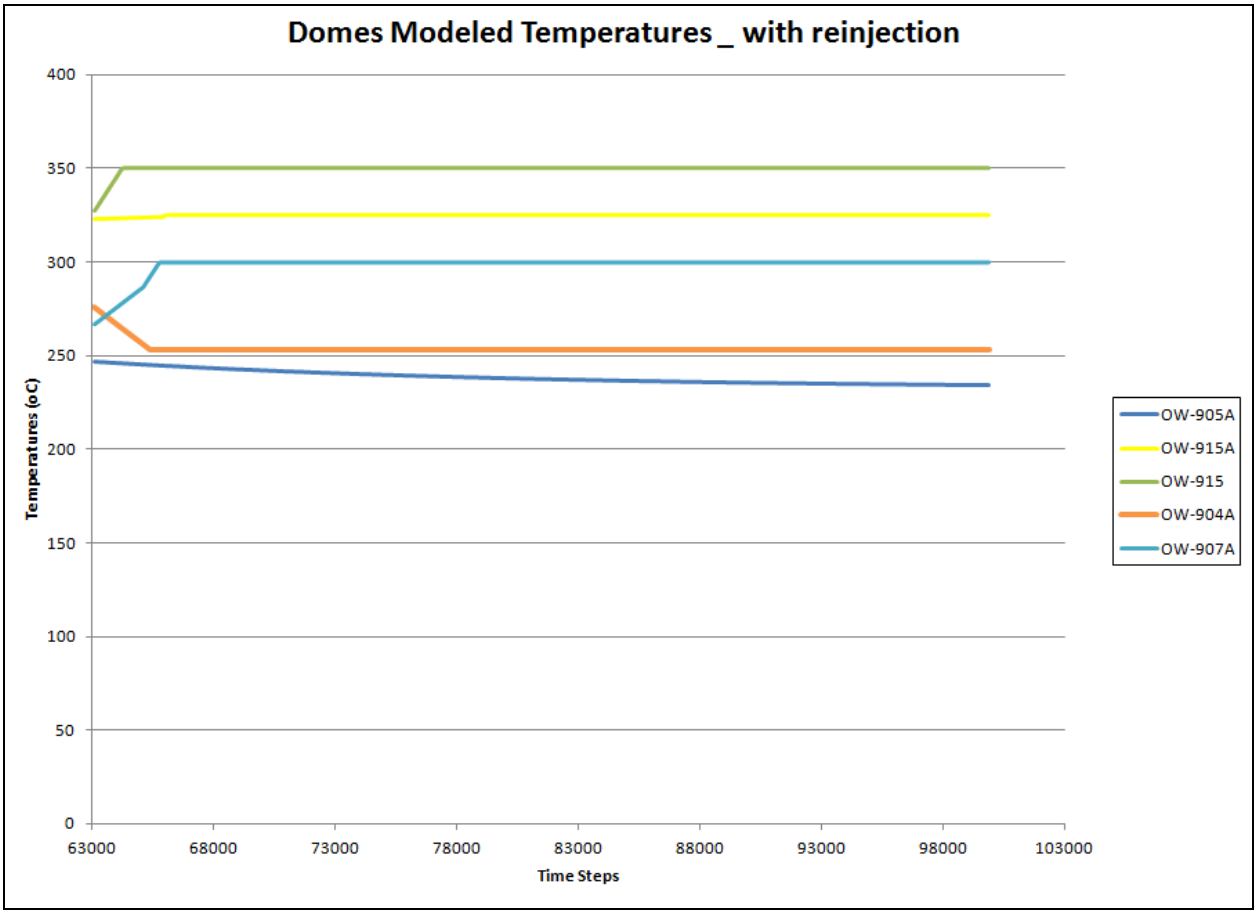

Figure 5.34: Modeled Temperatures for wells in the Domes with reinjection. Timesteps in seconds.

The sulfate concentration reaches equilibrium around the 67000th time step. The values are higher in OW-915A (165ppm) and least in OW-907A (90ppm) (Fig. 5.35). The increase in OW-915A can be due to the high temperatures in the reservoir around this well that is causing oxidation of the H_2S in the formed steam to SO_4.

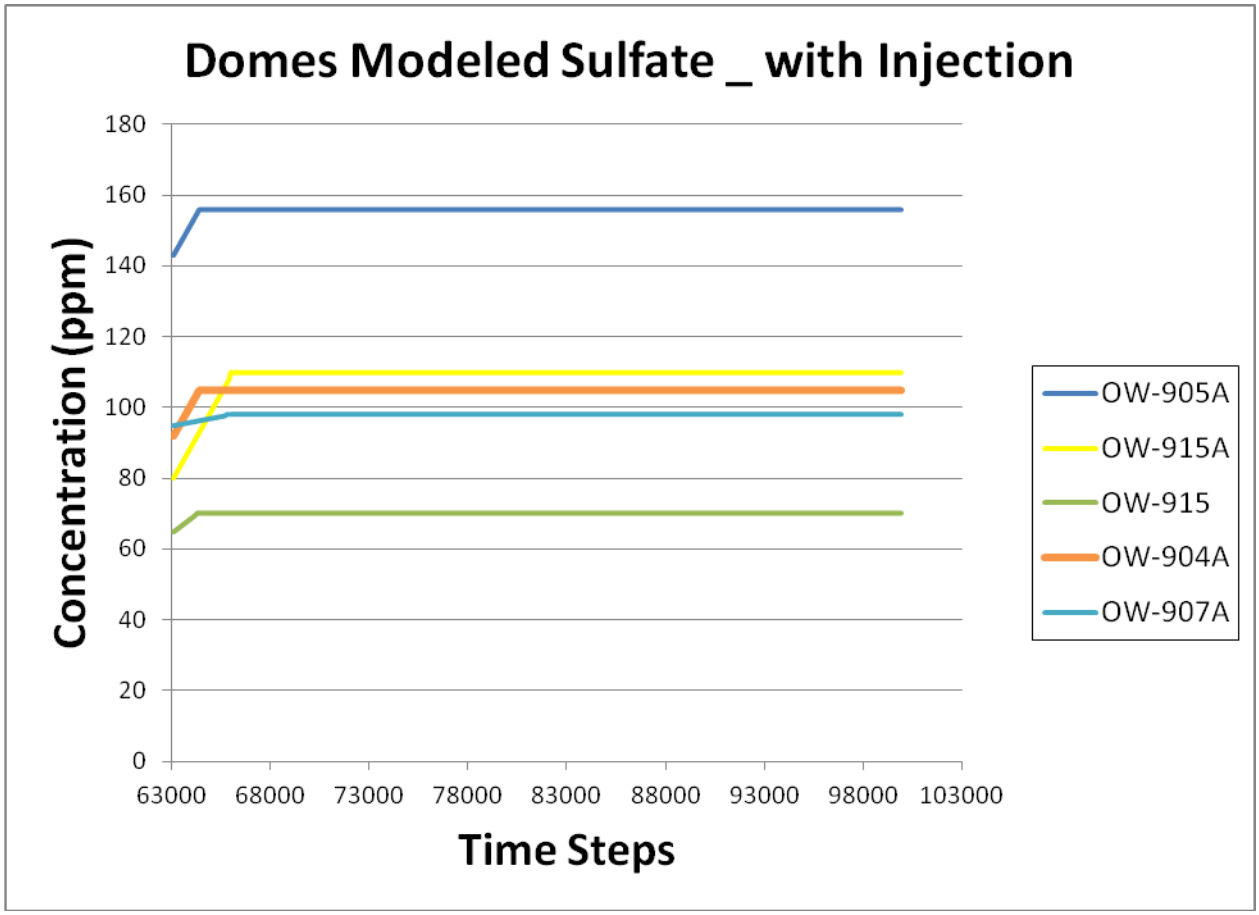

Figure 5.35: Modeled Temperature for wells in the Domes with reinjection.

5.2.4 Spatial Distribution Map of Chloride Concentration

The study also considered the presentation of the spatial distribution of the chloride content of the EPF at historical data matching and predictions with and without reinjection steps of modeling i.e. Fig. 5.36, 5.37 and Fig. 5.38 respectively. The end of historical matching map show high chloride concentration at the central part of the EPF but low values in areas on the periphery around OW-22, OW-23, OW-26 and OW-31. Compared to the initial state model, the trend have shown an increase at the central part of the EPF, perhaps a pointer towards the boiling effect as stated earlier. The SE area, on the other hand, still recorded lower values though higher than that of the initial model.

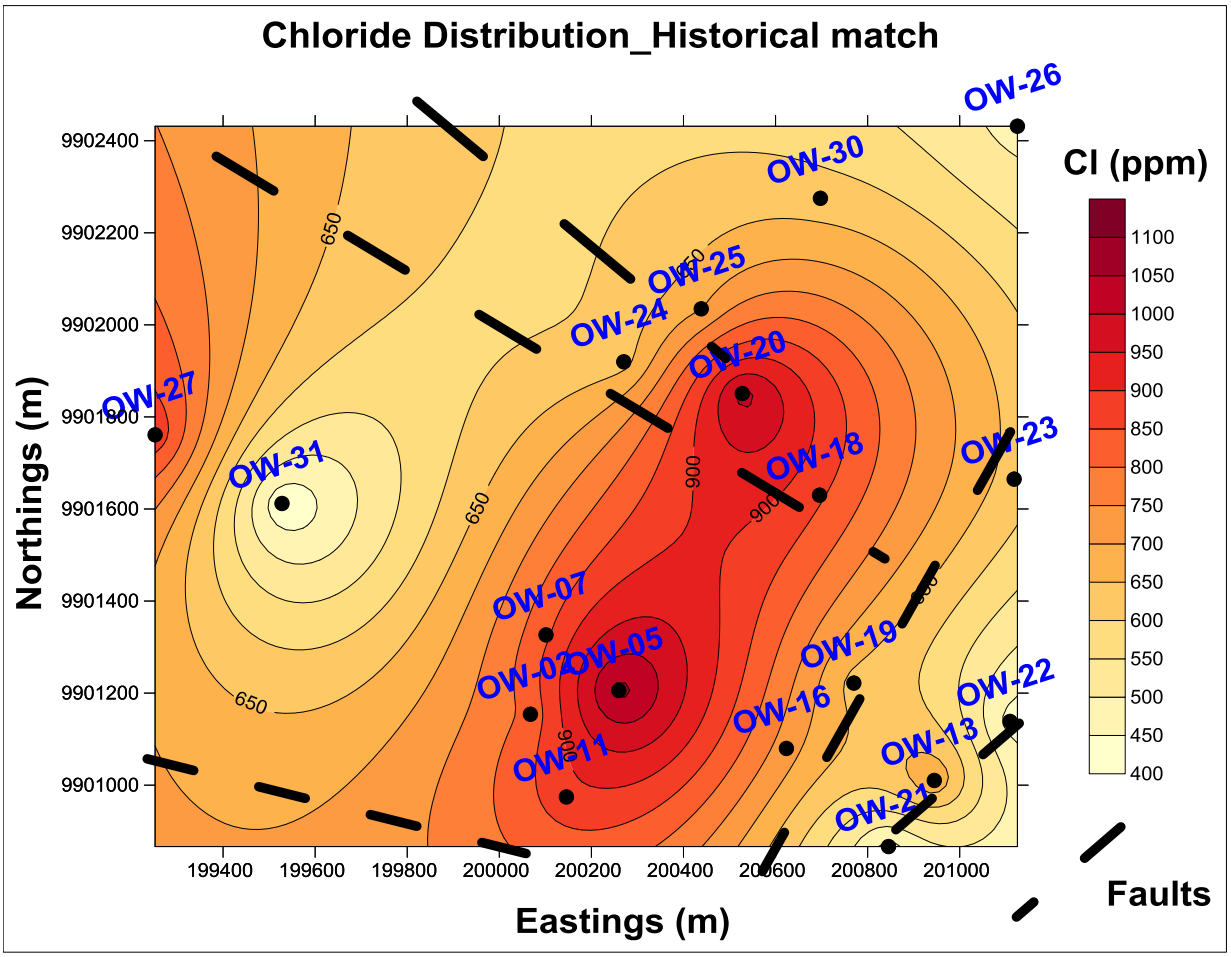

Figure 5.36: Chloride Spatial Distribution map for historical match.

The chloride spatial distribution map at the end of the prediction without injection gave a range of concentrations that lie between 50 – 1350ppm compared to 150 – 1650ppm for the prediction with reinjection map. The deference indicates that without reinjection, substantial amount of cooling resulting from the entry of non geothermal waters in the field.

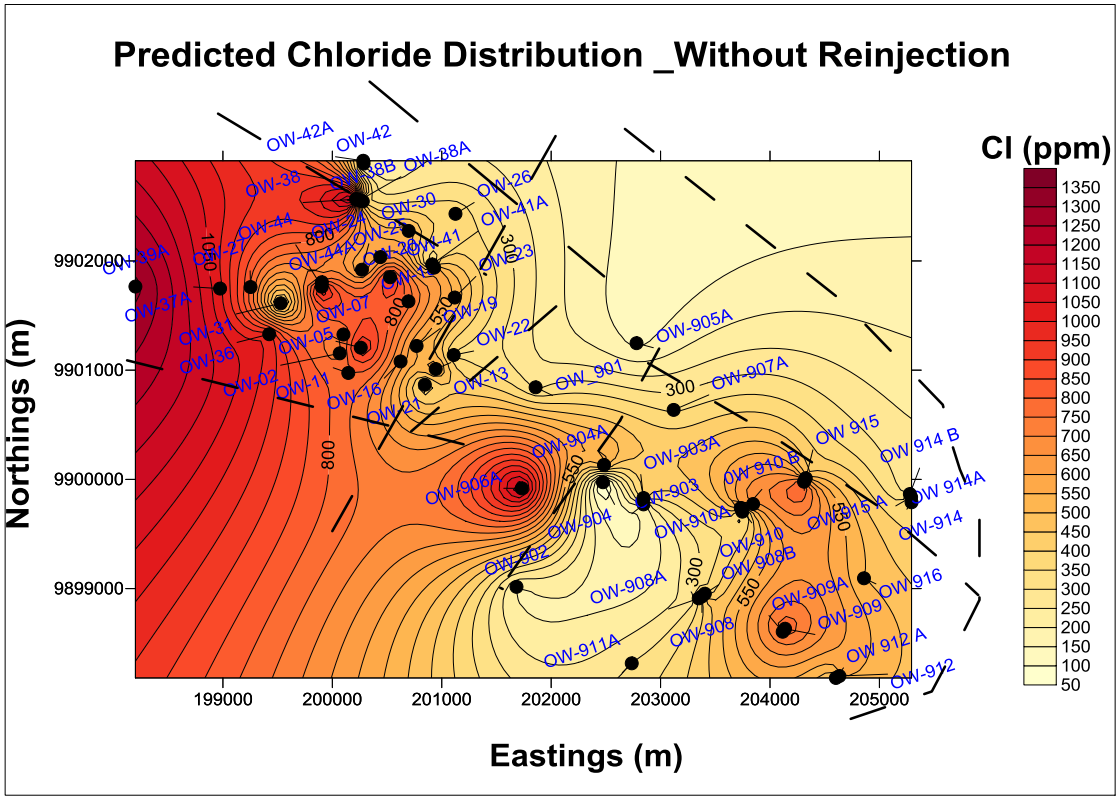

Figure 5.37: Chloride Spatial Distribution map without reinjection.

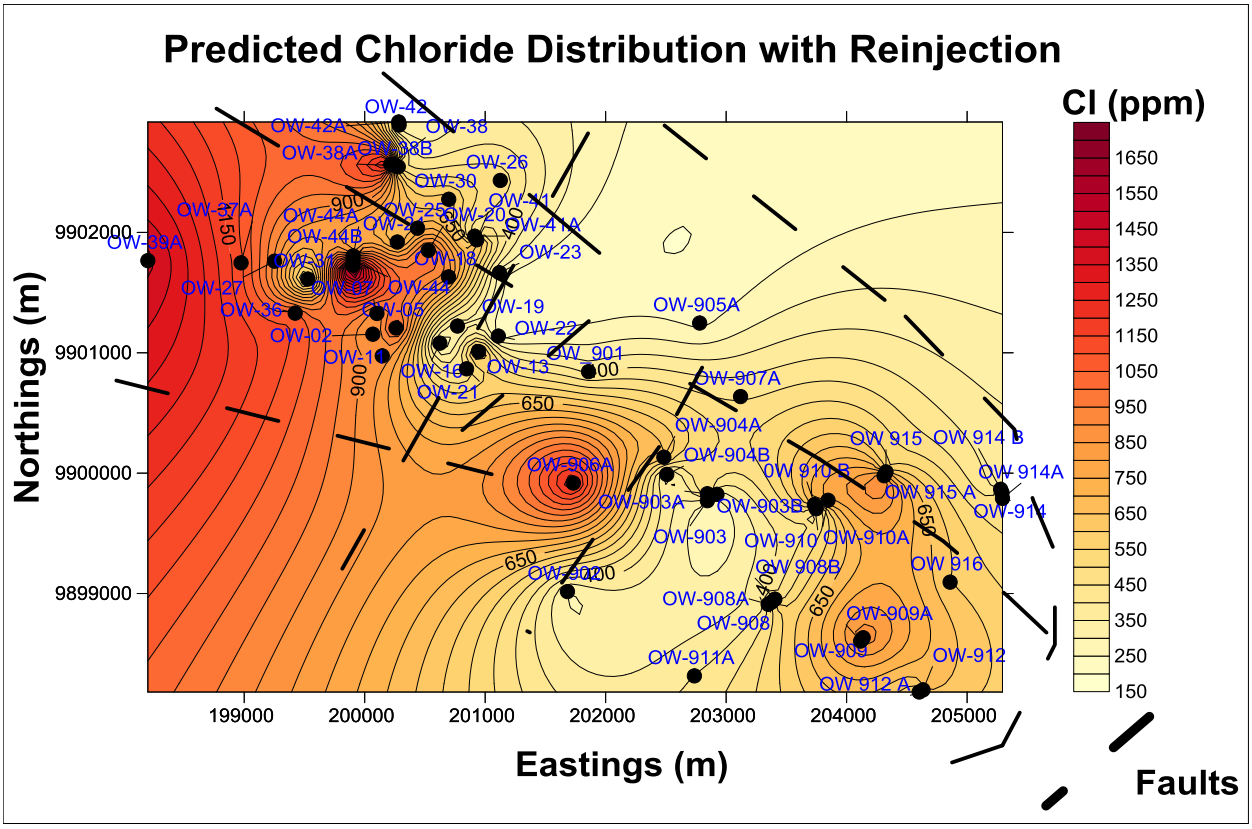

Figure 5.38: Chloride Spatial Distribution map with reinjection.

5.2.5 DISCUSSION

The geochemistry and by extension the potential of the Olkaria geothermal field has evolved overtime with reservoir pressures and temperatures being the major controlling factors as discussed below.

5.2.5.1 Reservoir Pressure Variation

Liquid and vapor may segregate in two-phase aquifers, leading to an increase in the vapor to liquid ratio of well discharges. Phase segregation results from the different flow properties of liquid/vapor resulting from difference in capillary pressure in a reservoir with varying relative permeability (Horne et al., 2000; Pruess, 2002; Li and Horne, 2004a and b). This permeability, which is provided for by faults in Olkaria field (Fig. 5.39) together with the pressure difference (Fig. 5.40), density and viscosity affect the mass flow rate of each phase. In this way, in the event of pressure difference, fluids will move from areas with high to low pressures.

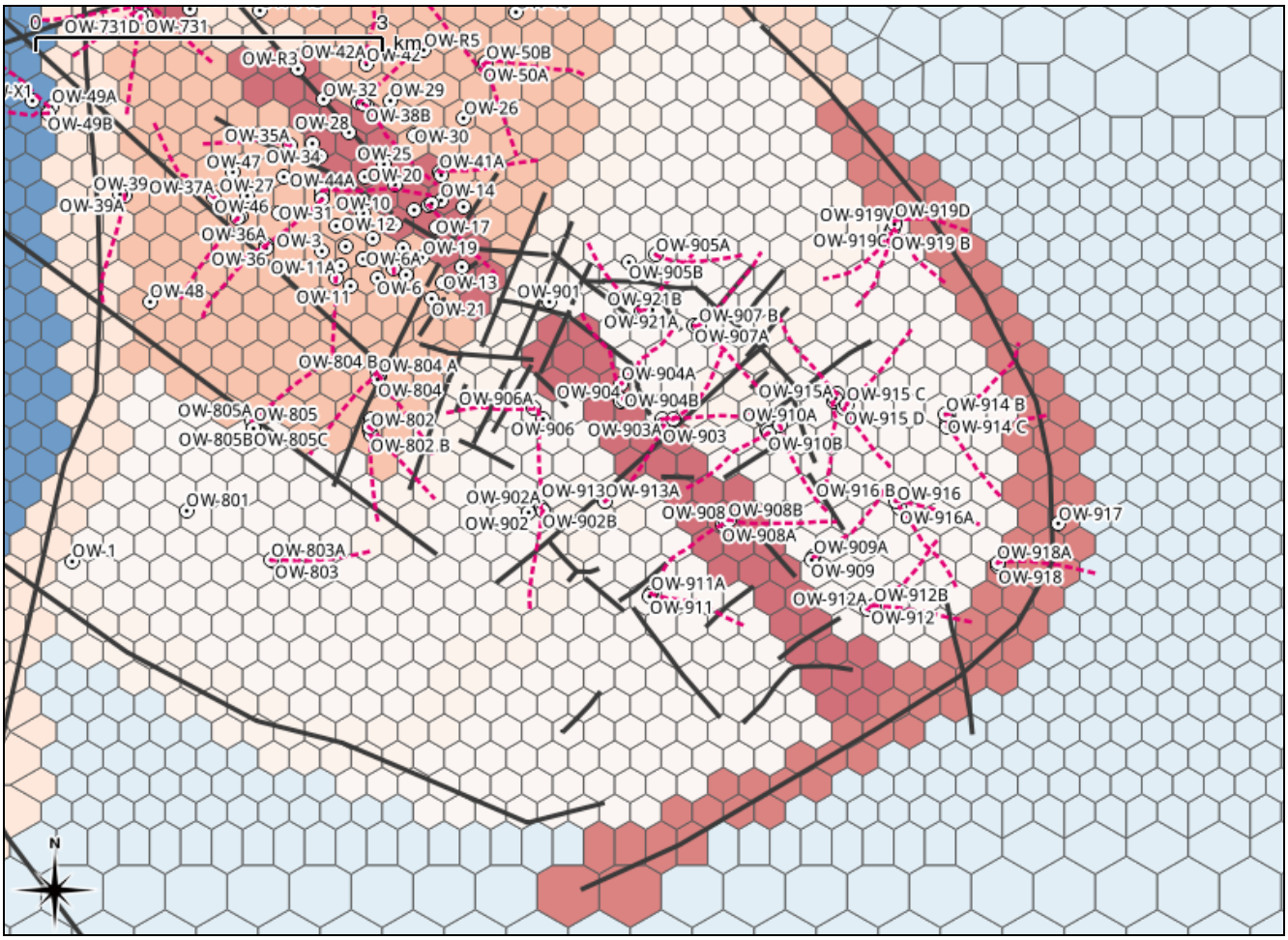

Figure 5.39: Modeled Permeability of the Olkaria geothermal field; red for high permeability, followed by pink colored then white. Blue represent lowest permeability (modified from Mannvit, 2011).

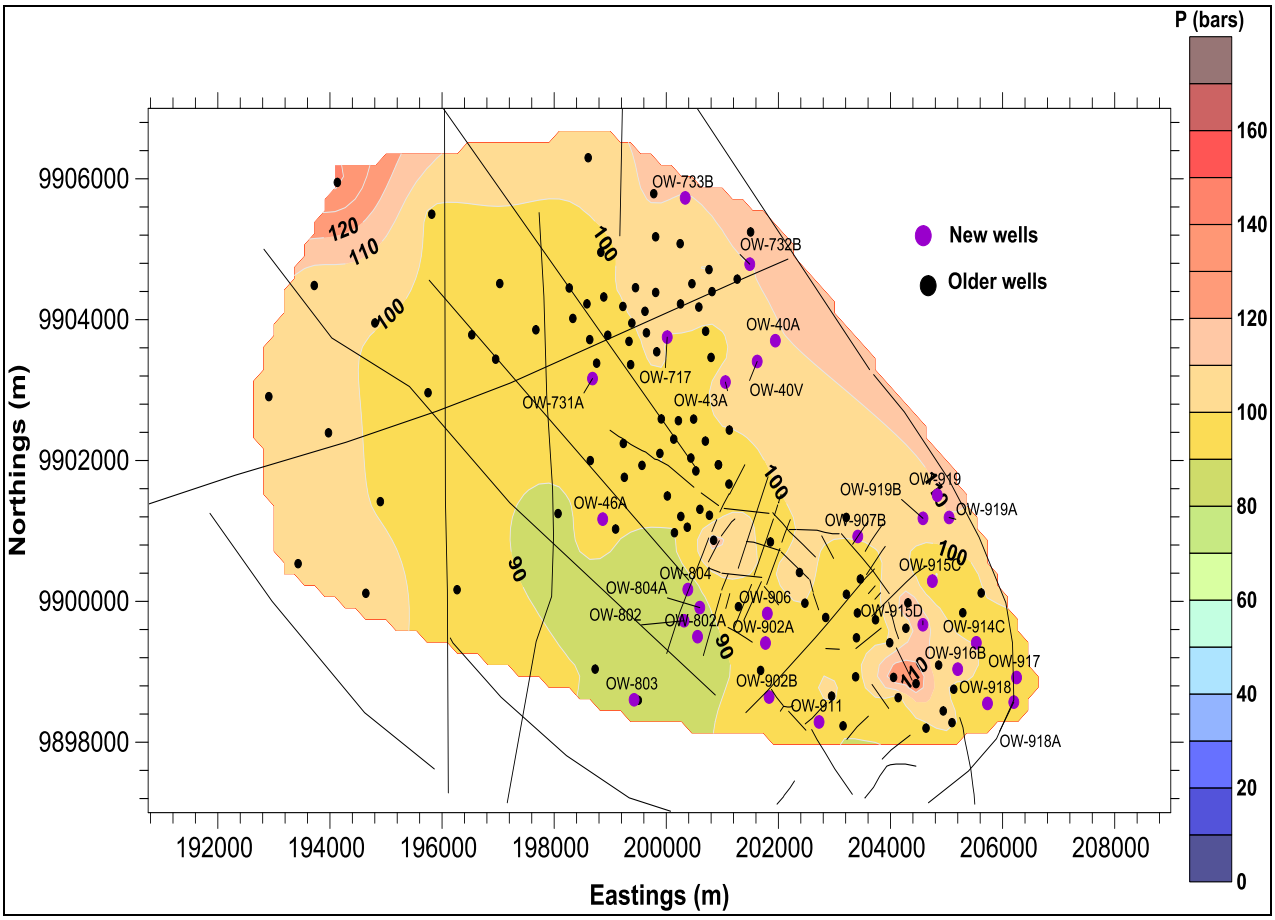

Figure 5.40: Measured Pressure variations for the Olkaria geothermal field.

The adhesive forces between mineral grain surfaces and fluid are the cause of capillary pressure. These forces are stronger for liquid than for vapor. In this way, the mobility of liquid is reduced relative to that for vapor.

Whenever a well intersects a two-phase aquifer (characteristic of the central part of the EPF) intensive depressurization boiling commences in the reservoir in the vicinity during discharge. The pressure drop produced by discharging the well, sometimes, is sufficiently large hence triggering start boiling in the aquifer even if the aquifer fluid was initially sub-boiling. In the course of intensive boiling, vapor may not only form by depressurization boiling, but also by conductive heat transfer from the rock to the fluid. The result of this boiling are lowered fluid temperature, creation of a temperature gradient between fluid and aquifer rock that results to conductive heat transfer from rock to fluid. The boiling point of an aqueous solution is

affected by its salinity and gas content (Bischoff and Rosenbauer, 1989) where dissolved gases lower it. Due to boiling and phase segregation in two-phase aquifers, the discharge enthalpy and solutes concentration of wells producing from liquid-dominated geothermal reservoirs is often higher than that of the initial aquifer fluid. This is the case in the central part of the EFP around OW-5.

On the other hand, wells on the boundaries of a geothermal system tend to receive cool waters which are less mineralized hence record low chemical elements concentration and temperatures as in areas on the SE of EPF around OW-22, OW-23, OW-16 and OW-19. Such areas may also have high pressure values due to hydrostatic pressure as in the case around the OW-919A in the Olkaria field.

5.2.5.2 Reservoir Pressure Decline and Mixing

Pressure decline during exploitation often leads to inflow of cold groundwater in the shallow part of the hydrothermal system which then mixes with the hot water. The is a process that is suspected to be causing low concentration of silica, chloride and temperature values in wells OW-22, OW-23 which are located to the SE of the EPF. To evaluate this further, mixing models were applied to evaluate the mixing ratios (Fig.5.41).

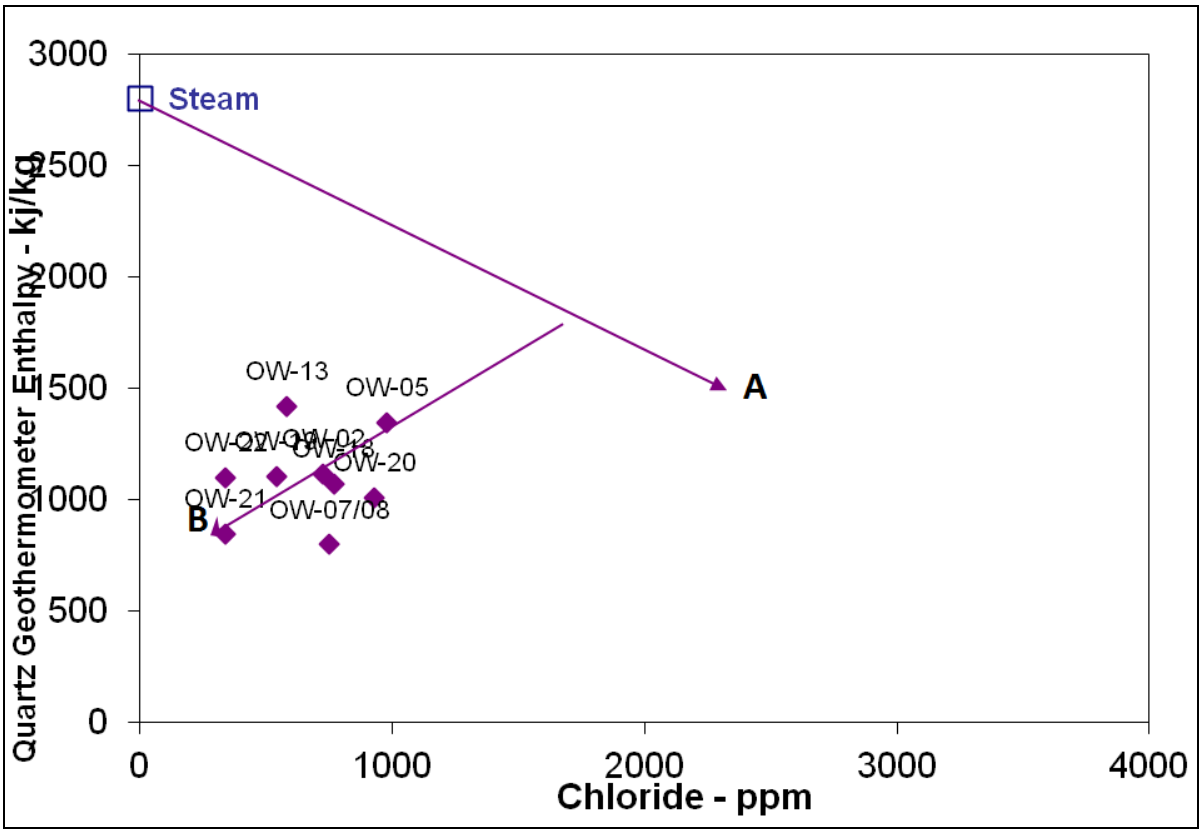

Figure 5.41: Mixing Model of the EPF.

The plot gives indications that OW-22 and OW-21 has undergone mixing that has led to the dilution of the reservoir fluids, OW-20 did undergo mixing but it is recovering as the reservoir heats up whereas OW-5 is tending towards boiling. This trend agrees with what has been seen in the elements concentrations and temperature values i.e. OW-5 located at the center of the EPF field had a steady increase that has been attributed to boiling due to depressurization while OW-22 and OW-23 has a consistent decline due to incursion of cooler fluids through the Olonjorowa gorge.

5.2.5.3 Aquifer fluid temperature

5.2.5.3.1 Mineral Equilibria and Fluid Temperature

The composition of geothermal fluid is highly controlled by temperature dependent reactions between the geothermal fluid and minerals (Giggenbach, 1980 and 1981). This is

besides other factors like pressure, rock type, permeability, fluid composition and duration of activity (Brown, 1978).

The chemistry of fluids in many geothermal fields worldwide is in near chemical equilibrium with secondary minerals for all major aqueous components except Cl and B (Arnórsson et. al., 1983 and Michard, 1991). Michard, (1991) further adds that before exploitation geothermal water may be in equilibrium with the alteration minerals such that with the incursion of cooler groundwater the reaction may deviate from equilibrium. This seems to be the case in the SE part of the EPF and East of Domes around OW-919, OW-907A and OW-905A and that need to be ascertained from the monitoring data.

5.2.5.3.2 Chemical Geothermometers

Chemical geothermometry refers to the use of fluid chemistry in the determination of geothermal reservoir temperature. The chemistry of the geothermal water is mostly controlled by chemical reactions between water and formed minerals (Truesdell and Fournier, 1977). The commonly used geothermometers are the silica geo-thermometers and the cation geothermometers. This study considered the cation geothermometers of Na-K as the silica geothermometers easily undergo equilibration and thus would not have given representative values of the reservoir temperatures.

5.2.5.3.3 Cation geothermometers

The Na-K geothermometer is based on temperature dependence of partitioning of sodium and potassium between the fluid and alkali feldspars as indicated in section 4.1.5.4.3 above. The main advantage of the Na/K geothermometer in geothermal exploration is that it is less affected by dilution and steam separation than other commonly used geothermometers (Arnórson et. al., 1982).

5.2.5.4 Reservoir Chloride Variation

Chloride (Cl), in many cases, is useful in determining mixing. That is if the chemistry of the thermal water has a different composition than the cooler water which it is to be mixed with. Cold groundwater often has lower chloride concentration than geothermal water. The infiltration

of non-geothermal water into a freshwater geothermal system is often easily traced. The inflow of cold freshwater into a geothermal system is often difficult to detect at an early stage.

Overall, chloride concentrations are variable between 200 to 1000ppm. The highest chloride concentration was around well OW-15 and low around wells OW-22, OW-23 and OW-31. This decline in the concentration is most probably due to dilution by the steam condensate. The southeast part of the field i.e. area around OW-19, OW- 22 and OW-23 had the lowest chloride concentrations which could suggest some dilution effects by the waters from the gorge in this part of reservoir.

5.2.5.5 Reservoir Sulfate Variation

Hydrogen sulfide (H_2S) is often present in geothermal water. Reduction in hydrogen sulfide content in geothermal water with time is thus an indication of dilution. This is a case where cold water is saturated with dissolved oxygen and it would react with hydrogen sulfide forming sulfate. But it should be notable that increase in sulfate is usually very low and is in most cases hardly seen in increasing sulfate.

The 2013 sulfate distribution map show high sulfate concentrations around wells OW-20 and OW-10. This is replicated in the 2014 monitoring. This confirms the cause of low pH as noted earlier i.e. could be attributed to the fact that the central part of the production field could be undergoing condensation of steam with oxidation of hydrogen sulfide gas. Low concentrations are evident around wells OW-22, OW-23 and OW-26. This is probably due to reduced boiling effects resulting from incursion of cold fluids in this part of the field as noted earlier with the Cl distribution.

5.2.5.6 Reservoir Nitrogen gas Variation

This monitoring also considered N_2 as it is the best indicator of incursion of atmospherically modified reservoir fluid. The 2014 graph shows a range between 5 and 80mmol/kg. High concentration is notable around OW-5 and OW-7&8 whereas very low concentrations were observed around OW-20, OW-24 and OW-15 (Fig. 5.21). According to Karingithi (2009) the occurrence of high nitrogen gas concentration in the central parts of the field is strange.

Considering that this has been notable since 2007, this trend can be attributed to the fact that the atmospherically modified fluids, probably from the gorge, have reached the central part of the field due to pressure drop.

CHAPTER 6

6.0 CONCLUSIONS AND RECCOMMENDATIONS

6.1 Conclusions

In conclusion, the study managed in estimating the potential of the Olkaria field based on the geochemical data and, therefore, achieved the set objectives as described below. The accuracy of the results is based on the fact that there is a close matching between the modeled and measured values during the historical data matching. For example, there is close correlation of the modeled (at the 5000 time step, i.e., at the start of the initial model) and measured values of Chloride concentration in wells before exploitation of the field began. The modeled pressures decline also agrees with the measured draw down of 1 bar/year.

a. Evaluation of the potential of the Olkaria- East and Olkaria-Domes fields

The study concludes that the potential of the fields is dependent on the reinjection strategy to be implemented. Without reinjection, for example, OW-5 will sustain production to 2028, 2025 for OW-19, OW-16 till around 2022 and lastly OW-22 in 2019. These trends can be attributed to the fact that, minimal reinjection translates to low pressure support for the field. When this occurs, the wells on the periphery of the field will tend to receive higher amounts of cooler fluids rendering them unproductive. Those at the center part of the field will experience depressurization boiling which will trigger changes like increase in the SiO_2 and SO_4 concentration which poses a risk of scaling and corrosion, respectively.

b. Evaluation of the future potential of deep drilled wells

With regard to well depths, the study concludes that deep drilled wells have the ability to sustain a given production regime for a longer period compared to shallow wells. This is as in the case of well OW-5 which had increased solute concentration from 300 ppm of chloride and reservoir temperatures from 200°C to 330°C upon deepening from 1500m to 2200m deep. This arises from the fact that deep wells tap from high temperature and pressure reservoirs that are suitable for geothermal resources. On the contrary, shallow wells tend to produce from shallow aquifers which have low chloride content and tend to deplete faster compared to those of deep wells.

c. Evaluation of the potential of scaling, dissolution and corrosion in the Olkaria- East and Olkaria-Domes fields

The silica scaling evaluation indicates that the wells have varying minimum separation temperatures. Deeper wells have the highest potential for scaling compared to the shallow ones as they have tapped from high temperature and silica content reservoirs. Non-condensable gases are also a key player in as far as calcite scaling is concerned. The results on the evaluation of a gas breakout potential in wells conclude that the risk is highest in wells on the SE of the Olkaria Domes, around OW-914 and least in OW-44. OW-914 is therefore likely to experience calcite scaling at its major feed zone that will lead to reduced productivity. This phenomenon is due to pressure drop leading to thermal fluids to start boiling and degassing of CO_2 as the fluids rise in a wellbore.

6.2 Recommendations

The recommendations are geared towards establishing a plan for long term reservoir monitoring and management which will ensure successful utilization. This will guarantee maintenance of the production schemes, avoidance of over-exploitation, foreseeing declining capacity of wells, avoidance of production problems like scaling and corrosion, minimization of cost, maximization of revenues and minimization of environmental effects. The study therefore recommends:

1. A study to determine the cause of measured high N_2 gas in the central part of the EPF especially in well OW-5 which is also a deeper well. This should be in an effort to isolate cases of wells with damaged casings which tend to allow surface waters in to the well.
2. Tracer dilution tests to be done to determine the connectivity of the reinjection wells. This is to ensure targeted reinjection that minimizes early breakthrough in to the producing reservoirs.
3. A study be done to evaluate the effects of the accelerated drilling on the chemical and physical properties of wells. This is in recognition that drilling operations pump large volumes of cooler waters in to the reservoir

7.0 REFERENCES

Akin, T., Guney, A., and Kargi, H. (2015) Modeling of calcite scaling and estimation of gas breakout depth in a geothermal well by using PHREEQC. *Proceedings of the Fortieth Workshop on Geothermal Reservoir Engineering, Stanford University, Stanford, CA, United States*, 8 pp.

Ambusso, W.J. and Ouma, P.A. (1991) Thermodynamic and permeability structure of Olkaria Northeast field: Olkaria fault. *Geothermal Resource Council Transactions,* **15**, 237-242.

Angcoy, E.C. (2010) Geochemical modeling of the high-temperature Mahanagdong Geothermal Field, Leyte, Philippines. University of Iceland, MSc thesis, UNU-GTP, Iceland, report 1, 71 pp.

Ármannsson, H. (2003) CO_2 emission from geothermal plants. *Proceedings of the International Conference on Multiple Integrated Uses of Geothermal Resources, Reykjavik, Iceland*, 56-62.

Ármannsson, H. and Ólafsson, M. (2006) Collection of geothermal fluids for chemical analysis. Iceland GeoSurvey-ÍSOR, Reykjavík, Report ISOR-**2006/016**, 17 pp.

Arnórson S., Sigurðsson S. and Svavarsson H. (1982) The chemistry of geothermal waters in Iceland. I. Calculation of aqueous speciation from 0° to 370°C. **Geochim. Cosmochim. Acta, 46,** 1513-1532.

Arnórsson S., Gunnlaugsson E. and Svavarsson H. (1983) The chemistry of geothermal waters in Iceland. II. Mineral equilibria and independent variables controlling water compositions. Geochim. Cosmochim. Acta, 47, 547-566.

Arnórsson, S., and Gunnlaugsson, E. (1985) New gas geothermometers for geothermal exploration – calibration and application, *Geochim. Cosmochim. Acta, 49,* 1307-1325.

Arnórsson, S., Angcoy, E.C., Bjarnason, J.Ö., Giroud, N., Gunnarsson, I., Kaasalainen, H., Karingithi, C., and Stefánsson, A. (2010) Gas chemistry of volcanic geothermal systems. *Proceedings of the World Geothermal Congress 2010, Bali, Indonesia*, 12 pp.

Arnórsson, S., Björnsson, S., Muna, Z.W., and Bwire-Ojiambo, S. (1990) The use of gas chemistry to evaluate boiling processes and initial steam fractions in geothermal reservoirs with an example from the Olkaria field, Kenya. *Geothermics,* **19**, 497-514.

Axelsson, G. (2008) The importance of geothermal injection. In: Fridleifsson, I.B., Holm, D.H.,Wang Kun and Zhang Baiming (eds.), Workshop for Decision Makers on Direct Heating Use of Geothermal Resources in Asia, Tianjin, China. *UNU-GTP, TBLRREM and TBGMED, CD*, 16 pp.

Baker, B.H. and Wohlenberg, J. (1971) Structural evolution of the Kenya Rift Valley. Nature, 229, 538-542.

Baker, B.H., Williams, L.A.J., Miller, J.A., and Fitch, F.J. (1971) Sequence and geochronology of the Kenya Rift volcanics. *Tectonophysics***, 11**, 191-215.

Bienkowski, R., Torres-Alvarado, I.S., and Hinderer, M. (2003) *Genese hochsaurer Fluide im Geothermalfeld von Los Humeros, Zentral-Mexiko*. Institut für Angewandte Geowissenschaften, Technische Universität Darmstadt, Diplomarbeit (MSc Thesis), 89 pp.

Bischoff J.L. and Rosenbauer R.J. (1989) Salinity variations in submarine hydrothermal systems by double diffusive convection. Journal of Geology, vol. 07. P 613 – 623.

Bodvarsson, G., and Witherspoon, P. (1989) Geothermal reservoir engineering, part I. *Geothermal Science and Technology,* **2(I)**, 1-68. Bureau of Standards, Springfield, VA.

Brown P. R. L., (1978). Hydrothermal alteration in active geothermal fields. Annual Review in Earth and Planetary Sciences, 6, 229-250.

Capasso, G., Alessandro, W.D. and Favara, R. (2001) Interaction between the deep fluids and the shallow groundwaters on Vulcano island (Italy). J. Volcanol. *Geotherm. Res.* **108**, 187–198.

Clarke, M.C.G., Woodhall, D.G., Allen, D., and Darling, G. (1990) Geological, volcanological and hydogeological controls of the occurrence of geothermal activity in the area surrounding Lake Naivasha, Kenya. Ministry of Energy report 95 pp.

D'Amore, F. and Arnórsson, S. (2000) Geothermometry. In: Arnórsson, S. (ed.), Isotopic and chemical techniques in geothermal exploration, development and use. *Sampling methods, data handling, and interpretation*. International Atomic Energy Agency, Vienna, 152-199.

Darling W. G., Allen D. J. and Armannsson H. (1990) Indirect detection of outflow from a Rift Valley Lake. Journal Hydrology 113, 297-305.

Edwards, A.L. (1972) A Computer Program for Transient and Steady State Temperature Distributions in Multidimensional Systems, National Technical Information Service.

Fernandez-Prini, R., Alvarez, J.L. and Harvey, A.H. (2003) Henry´s constants and vapor-liquid distribution constants for gaseous solutes in H_2O and D_2O at high temperatures. J. Phys. Chem. Ref. Data, 32 (2003), 903-916.

Fournier, R.O. (1999) Water geothermometers applied to geothermal energy. In: D'Amore, F. (editor), *Applications of geochemistry in geothermal reservoir development*. UNITAR/UNDP, Rome, Italy, 37-70.

Fournier, R.O. and Potter, R.W. (1982) A revised and expanded silica (quartz) geothermometer. *Geoth. Res. Council Bull.,11-10*, 3-12.

Gibb (Estern Africa) Ltd EHS (2003) Audits of Utilities in the Electric Power Sub-Sector, Geothermal Power Plants; Final Report; Electricity Regulatory Board.

Giggenbach, W. F. (1980) Geothermal gas equilibria. Geochim. Cosmochim. Acta, 44, 2021-2032.

Giggenbach, W. F. (1981) Geothermal mineral equilibria. Geochim. Cosmochim. Acta, 45, 393-410.

Giggenbach, W.F. (1991) Chemical techniques in geothermal exploration. In: D'Amore, F. (coordinator), *Application of geochemistry in geothermal reservoir development*. UNITAR/UNDP publication, Rome, 119-142.

Giroud, N., and Arnórsson, S. (2005) Estimation of long-term CO_2 and H_2S release during operation of geothermal power plants. *Proceedings of the World Geothermal Congress 2005, Antalya, Turkey,* 6 pp.

Gudmundsson, B.T., and Arnórsson, S. (2002) Geochemical monitoring of the Krafla and Námafjall geothermal areas, N-Iceland. *Geothermics, 31*, 195-243.

Haizlip, J.R., Guney, A., Tut Haklidir, F.S. and Garg, S.K. (2012) The impact of high non condensable gas concentrations on well performance – Kizildere geothermal reservoir, Turkey. *Proceedings of the Thirty-Seventh Workshop on Geothermal Reservoir Engineering, Stanford University, Stanford, CA, United States*, 6 pp.

Haukwa, C.B. (1984) Recent measurements within Olkaria East and west fields. Kenya Power Company internal report, 13 pp.

Holland, T.J.B. and Powell, R. (1998) An internally consistent thermodynamic dataset for phases of petrological interest. J. metamorphic Geol., 16, (1998), 309-343.

Horne R.N., Satik C., Mahiya G., Li K., Ambuso W., Tovar R., Wang C., and Nassori N. (2000) Steam-water relative permeability. Proceedings World Geothermal Congress 2000, Kyushu-Tohoku, Japan, 2609-2615.

Karingithi, C.W. (1993) Olkaria East production field geochemical report. Kenya Power Company, Ltd., internal report, 86 pp.

Karingithi, C.W. (1996) Olkaria East production field geochemical report. Kenya Power Company, Ltd., internal report 2, 124 pp.

Karingithi, C.W. (2000) Geochemical characteristics of the Greater Olkaria geothermal field, Kenya. Report 9 in: Geothermal Training in Iceland 2000. UNU-GTP, Iceland, 165-188.

Karingithi, C.W. (2002) Hydrothermal mineral buffers controlling reactive gases concentration in the Greater Olkaria geothermal system, Kenya. University of Iceland, MSc thesis, UNU-GTP, Iceland, report 2, 51 pp.

Karingithi, C.W. (2009) Chemical geothermometer for geothermal exploration. *Presented at "Short Course IV on Exploration for Geothermal Resources", UNU-GTP, KenGen and GDC, Lake Naivasha, Kenya*, 22 pp.

KenGen, (1999) Conceptualized model of the Olkaria geothermal field (compiled by Muchemi, G.G.) The Kenya Electricity Generating Company, Ltd, internal report, 46 pp.

Kenya Meteorological Department, (2012) The Outlook for the October-November-December (OND) 2012 Season and Review of Rainfall During the Long Rains(March to May) 2012 and June-July-August (JJA) 2012 Seasons.

Kenya Wildlife Service, (1992) Hell's Gate and Mt. Longonot National Parks / Suswa Ecosystem Management Plan (1991-1996). KWS Planning Department.

Kollikho, P. and Kubo, B. (2001) Olkaria geothermal gaseous emissions and their effects to the environment- A flower trail case study. KenGen Technical Proceedings, pp. 57-64.

Kubo, M.B. (2001) Environmental management at Olkaria geothermal project. Technical Seminar Proceedings, 2001. Kenya Electricity Generating Company Ltd., Kenya, p. 51-56.

Leach, T.M. and Muchemi G.G. (1987) Geology and hydrothermal alteration of the North and West exploration wells in the Olkaria geothermal field, Kenya. Proceedings of the 9th New Zealand Geothermal Workshop, Geothermal Institute, Auckland, 187-192.

Li K. and Horne R.N. (2004a) An analytical scaling method for spontaneous imbibitions in gas-water-rock systems. SPEJ, 9(3), 322-329.

Li K. and Horne R.N. (2004b) Experimental study of gas slippage in two-phase flow. SPEREE, 409-414.

Macdonald, R., Davies, G.R., Bliss, C.M., Leat, P.T., Bailey, D.K., and Smith, R.L. (1987) Geochemistry of high silica peralkaline rhyolites, Naivasha, Kenya rift valley. Journal of *Petrology*, **28**, 979-1008.

Mannvit, (2011) The Olkaria Optimization Study (Phase II) – Final reservoir analysis report. West Japan Engineering Consultants, Inc., 301 pp.

Martin M.N. (2010) Environmental and Socio-Economic Issues of Geothermal Development in Kenya, GeoSteam Services Ltd.

Mekuria, N., Gizaw, B., Teklu, A. and Gizaw, T. (1987), Geochemistry of the Aluto-Langano geothermal field, Ethiopia. Ethiopian Institute of Geological Surveys, Internal Report, 1-55.

Michard G. (1991) The physical chemistry of geothermal systems. In: F. D'Amore (co-ordinator) Application of Geochemistry in Geothermal Reservoir Development. UNITAR-UNDP Publication, Rome, 197-214.

Moller, N., Greenberg, J.P., Weare, J.H. (2004) Computer modelling for geothermal systems: predicting carbonate and silica scale formation, CO_2 breakout and H2S exchange. *Transport in PorousMedia Journal*, **33-1/2**, 173-204.

Mosley, P.N. (1993) Geological evolution of the late Proterozoic "Mozambique belt" of Kenya. *Tectonophysics*, **221**, 223-250.

Moya, P., and Sánchez, E. (2005) Non-condensable gases at the Miravalles geothermal field. *Proceedings of the Thirtieth Workshop on Geothermal Reservoir Engineering, Stanford University, Stanford, CA, United States*, 11 pp.

Moya, P., and Yock, A. (2005) First eleven years of exploitation at the Miravalles geothermal field. *Proceedings of the Thirtieth Workshop on Geothermal Reservoir Engineering, Stanford University, Stanford, CA, United States*, 8 pp.

Muchemi, G. G. (1992) Geology of the Olkaria North East field. KPC internal report, KenGen Unpublished. pp. 7-9.

Muna, Z.W. (1982) Chemistry of well discharges in the Olkaria geothermal field, Kenya. UNU G.T.P. Iceland, Report 8, 38 pp.

Mungania, J. (1992) Geology of the Olkaria geothermal complex. Kenya Power Company, Ltd, internal report, 38 pp.

Mungania, J. (1999) Geological report of well OW-714. Kenya Power Company internal report.

Narasimhan, T.N. and Witherspoon, P.A. (1976) An Integrated Finite Difference Method for Analyzing Fluid Flow in Porous Media, *Water Resource. Res.*, **Vol. 12**, No. 1, pp. 57 – 64.

Núñez, Q.M., Ocampo-Díaz, J.D., Moya-Acosta, S.L. (2005) Silica scaling as a predominant factor of the production in Cerro Prieto geothermal wells, Mexico. Proceedings of the World Geothermal Congress 2005, Anatalya, Turkey, CD, 5 pp.

Ofwona, C.O. (2010) Olkaria I reservoir response to 28 years of production. Proceedings World Geothermal Congress 2010, Bali, Indonesia, 25-29 April, 4 pp.

Ogoso-Odongo, M.E. (1986) Geology of Olkaria geothermal field. Geothermics, vol. 15, p741-748.

Ólafsson, M. (1988) *Sampling methods for geothermal fluids and gases.* Orkustofnun, Reykjavík, report OS-88041/JHD-06, 17 pp.

Omenda, P.A., (1994). The geological structure of the Olkaria west geothermal field, Kenya. Stanford Geothermal Reservoir Engineering Workshop, 19, 125-130.

Omenda, P.A., (1998). The geology and structural controls of the Olkaria geothermal system, Kenya.Geothermics, 27, 55-74.

Omenda, P.A., (2000). Anatectic origin for Comendite in Olkaria geothermal field, Kenya Rift; Geochemical evidence for syenitic protholith. *African Journal of Science and Technology*. Science and Engineering series, **1**, 39-47.

Opondo K.M. (2007) Corrosive species and scaling in wells at Olkaria and Reykjanes, Svartsengi and Nesjavellir, Iceland. University of Iceland, MSc thesis, UNU-GTP, Iceland, report 2, 76 pp.

Opondo K.M. (2008) Fluid characteristics of three exploration wells drilled at Olkaria Domes field, Kenya. Proceedings of the 33rd Workshop on Geothermal Reservoir Engineering, Stanford University,Stanford, California, 6 pp.

Opondo K.M. and Ofwona C.O. (2003) Report on the Possible Cause of the Unusual Silica Deposition in Well OW-34, Kenya Electricity Generating Company Ltd., internal report 20pp.

Osato K., Sato, T., White, S., Burnell, J., and Yokomoto, S. (1998) Development of an integrated geothermal reservoir modeling system (database & mapping system for reservoir modeling/simulation/management, pre-processor system and post-processor system). Proceedings, Twenty-third Workshopon Geothermal Reservoir Engineering, pp.26-28.

Ouma P. (2010) Geothermal exploration and development of the Olkaria geothermal field. Proceedings of Short Course V on Exploration for Geothermal Resources, UNU-GTP, GDC and KenGen, Lake Bogoria and Lake Naivasha, Kenya, October – November, 16pp.

Pang Z.H., and Ármannsson, H. (2006) Analytical procedures and quality assurance for Power Chem Technology, 7 pp.

Pruess K., (2002) Mathematical modeling of fluid flow and heat transfer in geothermal systems. UNU-GTP, Reykjavik, Iceland, Report to the Earth Science Division, Lawrence Berkeley National Laboratory, University of California.

Pruess K., Oldengurg C. And Moridis G. (1999) TOUGH2 User's Guide Version 2.0. LBNL-43134, Lawrence Berkeley Lab, Calif.

Pruess, K. (1991) "TOUGH2" – A General-purpose Numerical Simulator for Multiphase Fluid and Heat Flow. Report LBL-29400, Lawrence Berkeley Laboratory.

Reed, M.H., Spycher, N.F., and Palandri, J. (2012a) *SOLVEQ-XPT: A computer program for computing aqueous-mineral-gas equilibria*. University of Oregon, Department of Geological Sciences, Eugene, OR, United States, 43 pp.

Reed, M.H., Spycher, N.F., and Palandri, J. (2012b) *Users guide for CHIM-XPT: A program for computing reaction processes in aqueous-mineral-gas systems and MINTAB guide (Ver 2.43).* University of Oregon, Department of Geological Sciences, Eugene, OR, United States, 73 pp.

Robie, R.A. and Hemingway, B.S. (1995) Thermodynamic properties of minerals and related substances at 298.15 K and 1 bar (105 Pascals) pressures and at higher temperatures. U.S. Geol. Surv. Bull., 2131 (1995).

Rural Focus Ltd, (2002) Lake Naivasha Water Resource Management ProgrammeWater Status Report; Lake Naivasha Growers Group, 2002.

Sato,T., Ohsato, K.,White, S.P., Burnell, J.G., Yokomoto, S. (1998) Development of an Integrated Geothermal Reservoir Modeling System for the Modeling Study using TOUGH2, Proceedings: TOUGH2 Workshop 1998, Report LBNL-14995, Lawrence Berkeley National Laboratory, 47–52.

Shackleton, R. M. (1986) Precambrian collision tectonics in Africa. In: Coward, M.P., and Ries, A.C.(eds.). *Collision Tectonics.* Geol. Soc. Spec. Publ. **No. 19**, 329-349.

Sikes H. L. (1935) Notes on the hydrology of Lake Naivasha. Journal East Africa Uganda Natural History Society 13, 74-89.

Simiyu, S.M. (2010) Status of geothermal exploration in Kenya and future plans for its' development. Proceedings world geothermal congress 2010 Bali, Indonesia, 25-29 April 2010.

Simiyu, S.M. and Keller, G.R. (1997) An integrated analysis of lithospheric structure across the East African plateau based on gravity anomalies and recent seismic studies. In: Structure and dynamic processes in the lithosphere of the Afro-Arabian rift system. Fuchs, K., Altherr, R., Müller, B., and Prodehl, C. (eds.), *Tectonophysics*, **278,** 291-313.

Simiyu, S.M., Omenda, P.A., Keller, G.R., and Anthony, E.Y. (1995) Geophysical and geological evidence for the occurrence of shallow magmatic intrusions in the Naivasha sub-basin of the Kenya rift. AGU Fall 1995 meeting abst., F657, no. V21A-12.

Simsek, S., Parlaktuna, M., and Akın, S. (2009) *Data gathering and evaluation of Kizildere geothermal field*. Report for Zorlu Energy, 13 pp.

Smith, M. and Mosley, P. (1993) Crustal heterogeneity and basement influence on the development of the Kenya rift, East Africa. *Tectonics,* **Vol. 12**, 591-606.

Sombroek, W. G., Braun, H.M.H and Pour, B.J.A. van der (1982) Exploratory Soil Map and Agro- climatic Zone Map of Kenya; Exploratory Soil Survey Report No. E1, Kenya Soil Survey.

Stapleton, M. (2002). Scaling and corrosion in geothermal operation. GeoChemical Services - Nesjavellir, Iceland. University of Iceland, MSc thesis, UNU-GTP, Iceland, report 2, 76 pp.

Stefánsson, A., and Arnórsson, S. (2000) Feldspar saturation state in natural waters. *Geochim. Cosmochim. Acta,* **47**,567-577.

Teklemariam, M. (2000) Chemical and thermal changes in the Aluto-Langano geothermal field, Iceland GeoSurvey-ÍSOR, Reykjavík, report ISOR-2006/016, 17 pp.

Thorarinsson, F., and Bjorgvinsdottir, B. (1980) Kraa-Namafjall: Groundwater level (Tech. Rep. No. FTh-BB-80/01 (in Icelandic)). Orkustofnun Jardhitadeild.

Tianfu X., Sonnenthal E., Spycher N. and Liange Z. (2014) TOUGHREACT V3.0-OMP Reference Manual: A Parallel Simulation Program for Non-Isothermal Multiphase Geochemical Reactive Transport.

Tole, M.P., Ármannsson, H., Pang Z.H., and Arnórsson, S. (1993) Fluid/mineral equilibrium calculations for geothermal fluids and chemical geothermometry. *Geothermics*, **22**, 17-37.

Truesdell A. H. and Fournier R. O., (1977) Procedure for estimating the temperature of a hot water component in mixed water using a plot of dissolved silica vs. enthalpy. J. Res. U.S. Geological Survey, 5, 49-52.

Truesdell, A.H., Janik, C.J., Goff, F.E., Shevenell, L.A., Trujillo, P.E. Jr., Counce, D.A., Kennedy, B.M. and Paredes, J.R. (1987) The origin of thermal waters of Honduras and puzzling variations in spring chemistries. Proceedings 9th New Zealand Geothermal Workshop, Auckland, NZ, 79-88.

Vienna, (2005) *Use of isotope techniques to trace the origin of acidic fluids in geothermal systems*. IAEA, Vienna, 204 pp

Wambugu, J.M. (1995) Geochemical update of Olkaria West geothermal field. Kenya Power Company, Ltd., internal report, 40 pp.

Wanyonyi E. (2014) Status Report on Steam Production and Reservoir Assessment of Olkaria East Field (First Half of 2014) KenGen Internal Report.

Wessel, P., and Smith, W. (2010) The Generic Mapping Tools version 4.5.2, Technical reference and cookbook [Computer software manual].

West-JEC, (2009) The Olkaria Optimization Study (Phase II) – Final reservoir analysis report. West Japan Engineering Consultants, Inc., 301 pp.

Wetang'ula G.N. and Snorrason, S.S. (2005) Evaluation of trace element levels and their ecotoxicological relevance in geothermal wastewater of Olkaria East Field, Kenya. World Geothermal Congress.

White S.P., Burnell, J.G., Ohsato, K., Sato, T. (2003) GeoCad, a pre and postprocessor for TOUGH2, Proceedings: TOUGH Symposium 2003, Lawrence Berkeley National Laboratory.

Xiang R.Z., Guo Z.L., Ying D.W., Ren W., Zhi W. and Ping J.Z. (2000) The assessment report of geothermal resources in Liangxiang. Beijing Institute of Geological Engineering, China, report, 82 pp.

APPENDICES

Appendix 1: Programme code

Set Up Grid Code

Setup Grid

```
Private void SetUpGrid ()
        {

            int totalblocks = BlocksLength * BlocksWidth * BlocksDepth;
            int blocksinlayer=BlocksLength * BlocksWidth;

            int Blayernum;

            SetBlockDimensions();

            for (int n = 0; n < totalblocks; n++)
            {
                var fr = new FlowRate();
                var blk = new Block();
                blk.blockNum = n;

                Blayernum = n % blocksinlayer;


                blk.length = Blength;
                blk.width = Bwidth;
                blk.height = Bheight;
                blk.volume = blk.length * blk.width * blk.height;

               // sext the y distance

                blk.blocky = Bwidth / 2 + Bwidth * (Blayernum / BlocksLength);
                blk.blockx = Blength / 2 + Blength * (n % BlocksLength);
                blk.blocz = Bheight / 2 + Bheight * (n / blocksinlayer);

                // set block pressure
                blk.pressure  = 35.0 + Bheight * (n / blocksinlayer)/10;
                blk.permeabilityH =  Math.Pow(10, 2);
                blk.permeabilityV = blk.permeabilityH / 10.0;
                blk.porosity = 0.08;
                blk.ChlConc = 0.0;
                blk.diffusivity = Math.Pow(10, -2);

                //if (n % (BlocksLength * BlocksWidth / 2) == BlocksLength * BlocksWidth
              * BlocksDepth / 2) blk.source = -1000.0;
                // sets fluid source

                if (n==19)
                {
```

```
                     blk.ChlConc = 0.1;
                    blk.source = 10000.0;
                }
                    else if(n==41)
                {

                    blk.source = -10000.0;
                }
                else blk.source = 0.0;

                //set front block
                if ((n+1) % BlocksLength == 0) blk.blockFront = -1;
                else blk.blockFront = n + 1;

                //set rear block
                if (n % BlocksLength == 0) blk.blockRear = -2;
                else blk.blockRear = n - 1;

                //set left block
                if (n % blocksinlayer >= (blocksinlayer-BlocksLength)) blk.blockLeft =-3;
                else blk.blockLeft = n + BlocksLength;

                //set right block
                if (n % blocksinlayer < BlocksLength) blk.blockRight  = -4;
                else blk.blockRight = n - BlocksLength;

                //set Top block
                if (n <blocksinlayer) blk.blockUp  = -5;
                else blk.blockUp = n - blocksinlayer;

                //set botom block
                if (n >=(totalblocks- blocksinlayer) ) blk.blockDown = -5;
                else blk.blockDown = n + blocksinlayer;

                fr.front  = fr.left =fr.rear =fr.right = 0.0;

                Flow.Add(fr);
                GridBlocks.Add(blk);
                UpGridBlocks.Add(blk);

            }

        }

    }
}
```

Set up Pressure Code

```
   private void SetUpPressureFile()
        {
            StreamWriter file = new StreamWriter("D:\\Ruth\\PressureInfo.txt");// CREATE
PRESSURE FILE

            file.Write("Time,");// WRITE COLUMN HEAD
```

```
            for (int n = 0; n < BlocksLength * BlocksWidth * BlocksDepth; n++)
            {
                file.Write("BlockNum{0},", n);
            }
            file.Write("\n");

            file.Write("{0},", 0);
            for (int n = 0; n < BlocksLength * BlocksWidth * BlocksDepth; n++)
            {
                file.Write("{0},", GridBlocks[n].pressure);// INITIAL PRESSURE
            }
            file.Write("\n");
            file.Close();


        }
```

Computing for Pressure

```
  private void ComputePressure()
    {

        for (int n = 0; n < BlocksLength * BlocksWidth * BlocksDepth; n++)
        {

            //front block
            if(GridBlocks [n].blockFront >0)
                UpGridBlocks[n].pressure += (GridBlocks[n].permeabilityH /(GridBlocks
[n].porosity * GridBlocks[n].length ) ) * (GridBlocks[GridBlocks[n].blockFront].pressure
- GridBlocks[n].pressure);
            //REAR block
            if (GridBlocks[n].blockRear  > 0)
                UpGridBlocks[n].pressure += (GridBlocks[n].permeabilityH /
(GridBlocks[n].porosity * GridBlocks[n].length )) *
(GridBlocks[GridBlocks[n].blockRear].pressure - GridBlocks[n].pressure);

            if (GridBlocks[n].blockRight  > 0)
                UpGridBlocks[n].pressure += (GridBlocks[n].permeabilityH /
(GridBlocks[n].porosity * GridBlocks[n].width )) *
(GridBlocks[GridBlocks[n].blockRight].pressure - GridBlocks[n].pressure);

            if (GridBlocks[n].blockLeft  > 0)
                UpGridBlocks[n].pressure += (GridBlocks[n].permeabilityH /
(GridBlocks[n].porosity * GridBlocks[n].width )) *
(GridBlocks[GridBlocks[n].blockLeft].pressure - GridBlocks[n].pressure);

            UpGridBlocks[n].pressure += GridBlocks[n].source /
(GridBlocks[n].porosity*GridBlocks[n].volume);

           // UpGridBlocks[n].pressure = GridBlocks[n].pressure;
        }

        for (int n = 0; n < BlocksLength * BlocksWidth * BlocksDepth; n++)
```

```
            GridBlocks[n].pressure = UpGridBlocks[n].pressure;

    }
```

Setting Up Flow rates

```
   private void SetuPFlowRateFile()
        {
            StreamWriter file = new StreamWriter("D:\\Ruth\\FlowData.txt");// CREATE
PRESSURE FILE

            file.Write("Time,");// WRITE COLUMN HEAD

            for (int n = 0; n < BlocksLength * BlocksWidth * BlocksDepth; n++)
            {
                file.Write("BlockNum{0}, Front, Rear, Left, Right,", n);
            }
            file.Write("\n");

            file.Close();

        }
        private void SetFlowRateFile( int num)
        {
            StreamWriter file = new StreamWriter("D:\\Ruth\\FlowData.txt",true);// CREATE
PRESSURE FILE

            file.Write("Time{0},", num);// WRITE COLUMN HEAD

           /* for (int n = 0; n < BlocksLength * BlocksWidth * BlocksDepth; n++)
            {
                file.Write("BlockNum {0}, Front, Rear, Left, Right,", n);
            }
            file.Write("\n");

            file.Write("{0},", 0);
            */
            for (int n = 0; n < BlocksLength * BlocksWidth * BlocksDepth; n++)
            {
                file.Write("{0},{1},{2},{3},{4},", n, Flow[n].front, Flow[n].rear,
Flow[n].left, Flow[n].right);// INITIAL flow rate
            }
            file.Write("\n");

            file .Close ();

        }
```

Computing Flow Rates

```
        private void ComputeFlowrate()
        {
            for (int n = 0; n < BlocksLength * BlocksWidth * BlocksDepth; n++)
            {

                //front block
                if (GridBlocks[n].blockFront > 0)
                    Flow[n].front = (GridBlocks[n].permeabilityH /
(GridBlocks[n].porosity * GridBlocks[n].width)) *
(GridBlocks[GridBlocks[n].blockFront].pressure - GridBlocks[n].pressure);
                //REAR block
                if (GridBlocks[n].blockRear > 0)
                    Flow[n].rear = (GridBlocks[n].permeabilityH / (GridBlocks[n].porosity
* GridBlocks[n].width)) * (GridBlocks[GridBlocks[n].blockRear].pressure -
GridBlocks[n].pressure);

                if (GridBlocks[n].blockRight > 0)
                    Flow[n].right = (GridBlocks[n].permeabilityH /
(GridBlocks[n].porosity * GridBlocks[n].width)) *
(GridBlocks[GridBlocks[n].blockRight].pressure - GridBlocks[n].pressure);

                if (GridBlocks[n].blockLeft > 0)
                    Flow [n].left = (GridBlocks[n].permeabilityH /
(GridBlocks[n].porosity * GridBlocks[n].width)) *
(GridBlocks[GridBlocks[n].blockLeft].pressure - GridBlocks[n].pressure);
            }

        }
```

Elements Concentration Computation

```
private void SetUpChlorideFile()
        {
            StreamWriter file = new StreamWriter("D:\\Ruth\\ChlorideInfo.txt");// CREATE
PRESSURE FILE

            file.Write("Time,");// WRITE COLUMN HEAD

            for (int n = 0; n < BlocksLength * BlocksWidth * BlocksDepth; n++)
            {
                file.Write("BlockNum{0},", n);
            }
            file.Write("\n");

            file.Write("{0},", 0);
            for (int n = 0; n < BlocksLength * BlocksWidth * BlocksDepth; n++)
            {
                file.Write("{0},", GridBlocks[n].ChlConc );// INITIAL PRESSURE
            }
            file.Write("\n");
            file.Close();

        }
        private void SaveChloride(int n)
```

```
        {
            StreamWriter file = new StreamWriter("D:\\Ruth\\ChlorideInfo.txt", true);//
CREATE PRESSURE FILE


            file.Write("{0},", n);

            for (int m = 0; m < BlocksLength * BlocksWidth * BlocksDepth; m++)
            {
                file.Write("{0},", GridBlocks[m].ChlConc );
            }
            file.Write("\n");


            file.Close();

        }
```

Computing Chloride Concentration in the fluids

```
private void ComputeChloride()
        {

            for (int n = 0; n < BlocksLength * BlocksWidth * BlocksDepth; n++)
            {
                UpGridBlocks[n].ChlConc = GridBlocks[n].ChlConc;
```

Diffusivity

```
              //Diffusivity


                //front block
                if (GridBlocks[n].blockFront > 0)
                    UpGridBlocks[n].ChlConc += (GridBlocks[n].diffusivity /
(GridBlocks[n].porosity * GridBlocks[n].length)) *
(GridBlocks[GridBlocks[n].blockFront].ChlConc - GridBlocks[n].ChlConc);
                //REAR block
                if (GridBlocks[n].blockRear > 0)
                    UpGridBlocks[n].ChlConc += (GridBlocks[n].diffusivity /
(GridBlocks[n].porosity * GridBlocks[n].length)) *
(GridBlocks[GridBlocks[n].blockRear].ChlConc - GridBlocks[n].ChlConc);

                if (GridBlocks[n].blockRight > 0)
                    UpGridBlocks[n].ChlConc += (GridBlocks[n].diffusivity /
(GridBlocks[n].porosity * GridBlocks[n].width)) *
(GridBlocks[GridBlocks[n].blockRight].ChlConc - GridBlocks[n].ChlConc);

                if (GridBlocks[n].blockLeft > 0)
                    UpGridBlocks[n].ChlConc += (GridBlocks[n].diffusivity /
(GridBlocks[n].porosity * GridBlocks[n].width)) *
(GridBlocks[GridBlocks[n].blockLeft].ChlConc - GridBlocks[n].ChlConc);
```

Advection

```
//Advection
                if (GridBlocks[n].blockFront > 0)
                {
                    if (GridBlocks[GridBlocks[n].blockFront].ChlConc >
GridBlocks[n].ChlConc)
                        UpGridBlocks[n].ChlConc -= Flow[n].front *
(GridBlocks[GridBlocks[n].blockFront].ChlConc - GridBlocks[n].ChlConc) /
((GridBlocks[n].porosity * GridBlocks[n].length));
                    else UpGridBlocks[n].ChlConc += Flow[n].front *
(GridBlocks[GridBlocks[n].blockFront].ChlConc - GridBlocks[n].ChlConc) /
((GridBlocks[n].porosity * GridBlocks[n].length));
                }
                    //REAR block
                if (GridBlocks[n].blockRear > 0)
                {
                    if (GridBlocks[GridBlocks[n].blockRear ].ChlConc >
GridBlocks[n].ChlConc)
                        UpGridBlocks[n].ChlConc -= Flow[n].rear  *
(GridBlocks[GridBlocks[n].blockRear ].ChlConc - GridBlocks[n].ChlConc) /
((GridBlocks[n].porosity * GridBlocks[n].length));
                    else UpGridBlocks[n].ChlConc += Flow[n].rear  *
(GridBlocks[GridBlocks[n].blockRear ].ChlConc - GridBlocks[n].ChlConc) /
((GridBlocks[n].porosity * GridBlocks[n].length));
                }


                if (GridBlocks[n].blockRight > 0)
                {
                    if (GridBlocks[GridBlocks[n].blockRight ].ChlConc >
GridBlocks[n].ChlConc)
                        UpGridBlocks[n].ChlConc -= Flow[n].right  *
(GridBlocks[GridBlocks[n].blockRight ].ChlConc - GridBlocks[n].ChlConc) /
((GridBlocks[n].porosity * GridBlocks[n].length));
                    else UpGridBlocks[n].ChlConc += Flow[n].right  *
(GridBlocks[GridBlocks[n].blockRight ].ChlConc - GridBlocks[n].ChlConc) /
((GridBlocks[n].porosity * GridBlocks[n].length));
                }

                if (GridBlocks[n].blockLeft > 0)
                {
                    if (GridBlocks[GridBlocks[n].blockLeft ].ChlConc >
GridBlocks[n].ChlConc)
                        UpGridBlocks[n].ChlConc -= Flow[n].left  *
(GridBlocks[GridBlocks[n].blockLeft ].ChlConc - GridBlocks[n].ChlConc) /
((GridBlocks[n].porosity * GridBlocks[n].length));
                    else UpGridBlocks[n].ChlConc += Flow[n].left  *
(GridBlocks[GridBlocks[n].blockLeft ].ChlConc - GridBlocks[n].ChlConc) /
((GridBlocks[n].porosity * GridBlocks[n].length));
                }


            }
```

```
            for (int n = 0; n < BlocksLength * BlocksWidth * BlocksDepth; n++)
                GridBlocks[n].ChlConc = UpGridBlocks[n].ChlConc;
        }
```

Chloride Computation

```
private void SaveChloride(int n)
        {
            StreamWriter file = new StreamWriter("D:\\Ruth\\ChlorideInfo.txt", true);//
CREATE PRESSURE FILE


            file.Write("{0},", n);

            for (int m = 0; m < BlocksLength * BlocksWidth * BlocksDepth; m++)
            {
                file.Write("{0},", GridBlocks[m].ChlConc );
            }
            file.Write("\n");


            file.Close();
        }

        private void Solver()
        {
            for (int n = 0; n < 100000; n++)
           {
                ComputePressure();
               ComputeFlowrate();
                ComputeChloride();
                if(n<500 || (n%100==0))
                {
                SavePressure(n);
                SetFlowRateFile(n);
                SaveChloride(n);
                }
            }
        }
```

Appendix 2: Analysis procedures during chemical analysis

PARAMETER	METHOD APPLIED
pH	pH meter
Hydrogen sulfide	Titrimetry using ditiozone indicator
Carbon dioxide	Titrimetry with HCl from pH 8.3 – 3.8
Chloride	Mohr tiration using siver nitrate
Floride	Ion selective electrode
Sulfate	Turbidometric method using spectrometer
Silica	Spectrophometric method using molybdosilicate method
Cations	Atomic absorption spectrometer
Residual gases	Gas chromatography

Appendix 3: Wamalwa R.N., Waswa A.K., Nyamai C.N., Mulwa, J. and Ambusso W.J. (2016) Evaluation of the Factors Controlling Concentration of Non-Condensable Gases and Their Possible Impact on the Performance of Geothermal Systems: Case Study of Olkaria Wells in the Kenyan Rift Valley. *International Journal of Geosciences, 7, 257-279.*

Appendix 4: Wamalwa, R.N., Nyamai, C.M., Ambusso, W.J., Mulwa, J. and Waswa, A.K. (2016) Structural Controls on the Geochemistry and Output of the Wells in the Olkaria Geothermal Field of the Kenyan Rift Valley. *International Journal of Geosciences, 7, 1299-1309.*